UNIVERSITÀ DI SIENA 1240

DIPARTIMENTO DI MEDICINA MOLECOLARE E DELLO SVILUPPO

Dottorato in Medicina Molecolare

XXXVI° Ciclo

Coordinatore: Prof. Vincenzo Sorrentino

Enhancing Insight into Human Endometrial Biology through advanced 3D Cellular Models

Settore scientifico disciplinare: BIO 13

Candidata
Francesca Paola Luongo

Firma digitale della candidata

Supervisore
Prof.ssa Alice Luddi

Co-supervisore
Prof.ssa Paola Piomboni
Università di Siena

A.A 2022-2023

TABLE OF CONTENT

INTRODUCTION

CHAPTER 1 THE ENDOMETRIUM: A UNIQUE TISSUE

The human body has a limited number of structures able to respond to different kinds of injuring events preferably by regeneration. These include the endometrium, the internal mucous layer of the uterus reaching 10–15 mm thickness in adult healthy women (**Figure 1**). The human endometrium is a highly dynamic tissue that is cyclically shed, repaired, regenerated, and remodeled, primarily under the orchestration of estrogen and progesterone, in preparation for embryo implantation. Humans are among the very few species that menstruate and that, consequently, are equipped with unique cellular and molecular mechanisms controlling these cyclic processes. Many reproductive pathologies are specific to menstruating species, and studies in animal models rarely translate to humans. Abnormal remodeling and regeneration of the human endometrium leads to a range of reproductive complications. Unlike other organs, the endometrium does not have a single, constant function from birth to death. The endometrium serves as a 'fertile ground' for the implantation of an embryo and the development of a highly invasive placenta. These processes are achieved by an orderly sequence of development and transformation within each menstrual cycle, under the influence of the ovarian steroid hormones (Evans *et al.*, 2016). The endometrial cells become terminally differentiated during each menstrual cycle; in the absence of conception, tissue shedding and regeneration for subsequent fertile cycles occurs. In menstruating species, decidualization is spontaneous, rather than guided by the presence of the embryo (Eremichev *et al.*, 2021) the blastocyst can implant during a limited period between days 20 and 24 of a normal 28-day menstrual cycle(Achache and Revel, 2006).

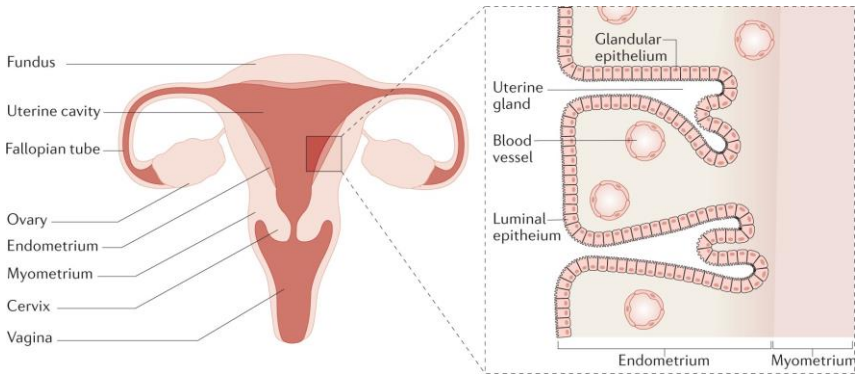

Figure 1: Schematic of human Uterine anatomy. The endometrium is the inner lining of the uterus (Makker *et al.*, 2021).

1.1 Endometrial Cell composition

The endometrium is made up of glandular and luminal epithelia that are derived from mesoderm and are supported by a connective tissue stroma and basement membrane (**Figure 2**). The human endometrium can be divided into two main areas based on histology. First, there are glands that stretch from the epithelial surface to the endometrium/myometrium junction in the upper two-third stratum functionalis layer (**Figure 1**). During each monthly menstruation, this portion of the endometrium loses (Classen-Linke *et al.*, 1996a). The adult endometrium is a complex tissue that not only consists of stromal, luminal and glandular epithelial cells but also includes endothelial and vascular smooth muscle cells, as well as a complex network of leukocytes populations (Deryabin *et al.*, 2020). During the menstrual cycle, the endometrium undergoes remodeling, shedding and regeneration, all of which are driven by substantial gene expression changes in the underlying cellular hierarchy. In the proliferative (or follicular) phase both the endometrial glands and stroma proliferate in response to the rising estrogen levels of ovarian follicle origin. The thickness of the endometrium increases, glands become increasingly tortuous and are lined by a tall, pseudostratified columnar epithelium. The cytologic appearance of proliferative glands is very "active," and characterized by a moderately high nuclear/cytoplasmic ratio, abundant mitotic activity, and prominent nucleoli (**Figure 2 and 3**).

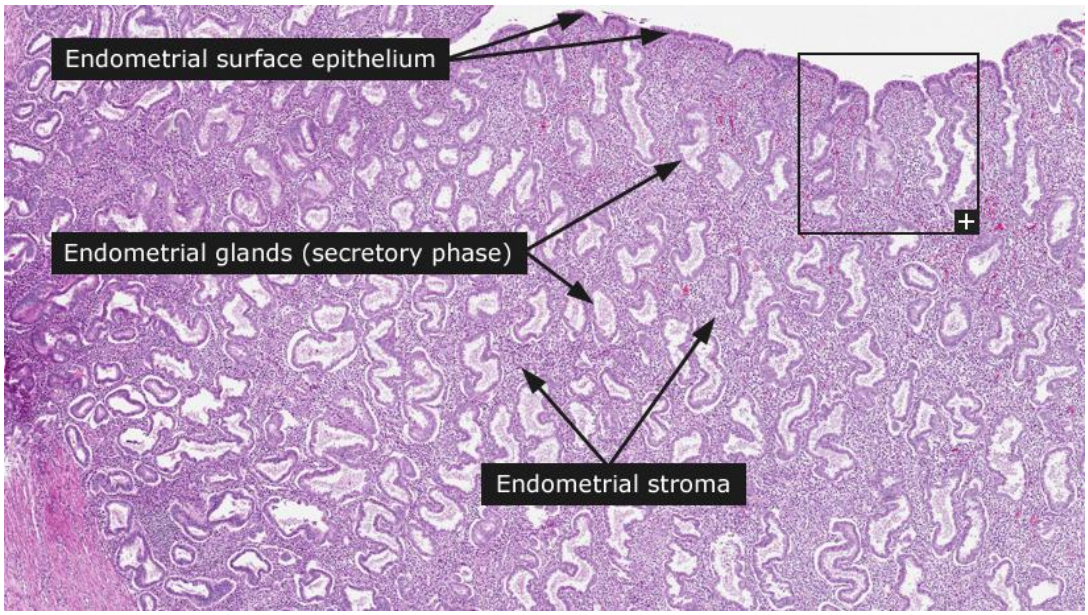

Figure 2: Histology of normal endometrium. The inner layer of the uterus is constituted by a lining epithelium, distinguished in glandular and luminal epithelium, and a stromal compartment. Source: Human Protein Atlas *https://www.proteinatlas.org/learn/dictionary/normal/endometrium*

The progesterone surge of ovulation ends the proliferative phase, and the endometrium moves into the secretory (or luteal) phase. Under normal conditions, the secretory phase is 14 days length, and the endometrium moves through an orderly sequence of morphologic changes. Under the influence of local autocrine factors, the secretory endometrium disintegrates and collapses. The resultant menstrual endometrium is characterized by cellular whorls of endometrial stroma exhibiting nuclear debris ("blue balls"), often with overlying, draping epithelium. Endometrial epithelial cells proliferate in close relationship with the production of predominantly ovarian estrogens, complemented by conversion to estrogen from adrenal androgens. Estrogens also induce a complex neoangiogenesis with the determination of an intricate network of endometrial microvessels destined cyclically to break down along with the rest of the endometrium (Mandalà, 2020). Endometrial stromal cells instead respond very poorly to estrogen stimulation. The imbalance in estrogen production, demonstrated in significant proportions in women with adrenal hyperfunction, in some of those with polycystic ovarian syndrome (PCOS) (Rosenfield and Ehrmann, 2016), and in some obese women, is often associated to an altered endometrial proliferation and reduced embryo implantation (Lv *et al.*, 2022). Progesterone during the ovarian cycle is mainly synthesized by estrogen-secreting granulosa cells of the ovary, concomitant with ovulation and in relation to Luteinizing Hormone (LH) surge (Niswender *et al.*, 2000).

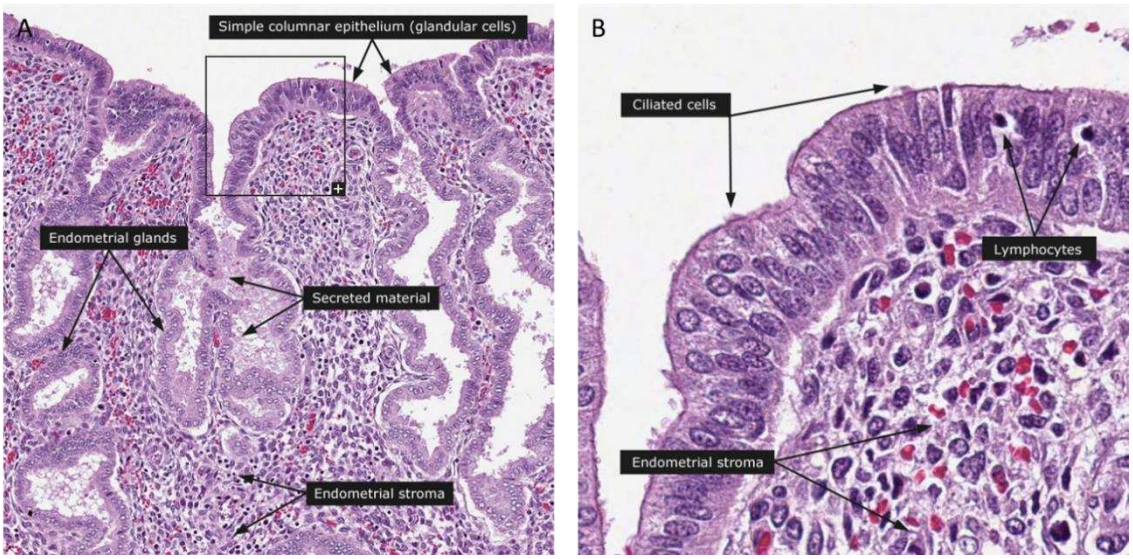

Figure 3: (A) The simple columnar epithelium is made up of two types of cells ciliated and secreted cells. The connective tissue, rich in cells and poor in collagen fibers contains the uterine glands. (B) Immune cells are also present in the endometrium. Source: Human Protein Atlas *https://www.proteinatlas.org/learn/dictionary/normal/endometrium*

Progesterone acts on the endometrium by an anti-proliferative estrogen antagonistic effect (Li *et al.*, 2011) and an adequate preparation of the endometrium for embryo implantation through:

a) specific effects on stromal cells (decidualization);

b) structural and secretory modifications of luminal and glandular epithelial cells;

c) structural and flow modification effects on the endometrial microcirculation;

d) reduction of contractile activity on the endometrium, inhibitory action of maternal embryotoxicity toward the embryonic trophoblast (Herrler, Von Rango and Beier, 2003).

During endometrial priming, progesterone thickens endometrium by the proliferation of its epithelial cells, the increase in the volume of its stromal cells (from stellate to globular and round shape), the edematous imbibition of the extracellular matrix, and a dramatic modification of endometrial microcirculation. This latter consists of an increase in the vessel caliber and the formation of true venous lakes, resulting in increased oozing of fluid on the surface of the uterine cavity and a predisposition to rapid, enveloping vascularization of the embryo immediately after its invasion process of the endometrium itself (Vinketova, Mourdjeva and Oreshkova, 2016). These structural changes are accompanied by a complex and intricate production of factors, predominantly protein or glycoprotein, produced by epithelial, stromal, and transudate-derived cells from the extracellular matrix that come to make up the natural culture medium that accommodates, in the lumen of the uterine cavity, the embryos for about three days prior to implantation, thereby conditioning their success and the onset of pregnancy. Decidualization is initiated by progesterone in stromal cells adjacent to blood vessels, and in vascular mesenchymal stem cells. These cells undergo mesenchymal–epithelial transition (MET) to become rounded, secretory cells expressing the decidual markers prolactin and insulin-like growth factor-binding protein. Decidual cells secrete factors (such as hormones, cytokines, chemokines, lipids and noncoding RNAs) that act synergistically or additively to create a wave of decidualization throughout the endometrium (Evans *et al.*, 2016) (**Figure 4**).

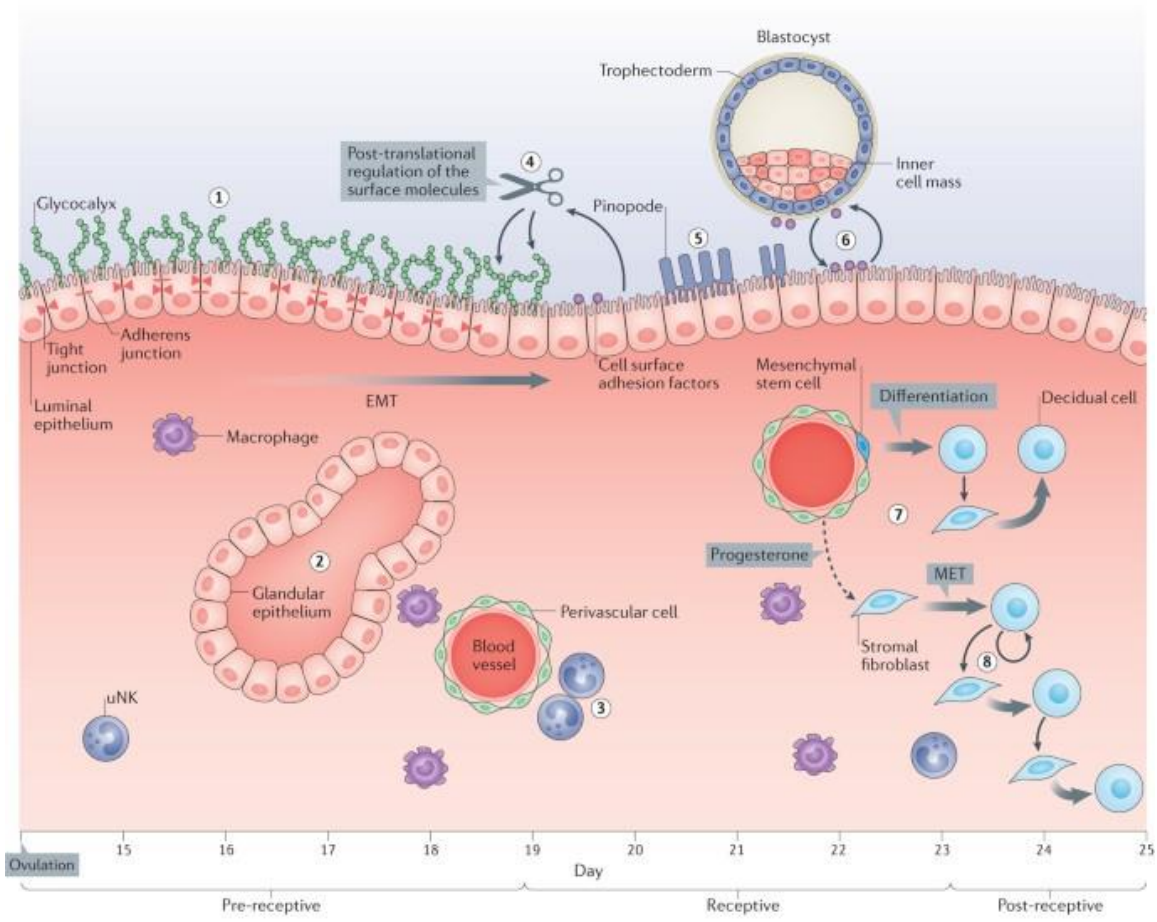

Figure 4: (Evans *et al.*, 2016) The pre-receptive luminal epithelium (1) is nonadhesive due to the existence of antiadhesive elements such as the glycocalyx, polarized epithelium, and lateral junctions that tightly bind cells together. During the pre-receptive phase, the glandular epithelium secretes heavily (2), uterine natural killer (uNK) cells multiply, and macrophages enter the endometrium (3). To become receptive, the luminal epithelium goes through significant changes (4): epithelial and blastocyst-secreted enzymes post-translate the glycocalyx; the epithelium undergoes epithelial-mesenchymal transition (EMT), becoming less polarized with fewer lateral junctions; and the adhesion-factor repertoire on the luminal epithelial surface changes. Pinopodes (5) develop on the surface of the luminal epithelium at the beginning of receptivity, but their involvement in blastocyst-epithelium adhesion is yet unknown.

eEP cells, eMSCs, eSCs/eSFs, eENs, vascular smooth muscle cells, and migrating immune cell populations are among the cell populations that make up the endometrium (Osteen *et al.*, 1989; Gargett and Masuda, 2010; Wang *et al.*, 2020). These cell populations are also visible in global transcriptome data-derived separate clustering. Wang et al.'s (2020) single-cell transcriptome research indicates that the activation of the window of implantation (WOI) results in considerable transcriptional alterations in the epithelium and more consistent changes in the stroma.

1.2 Human Endometrial cycle

The human menstrual cycle is intricately controlled by endocrine, autocrine, and paracrine factors, working in conjunction with ovarian follicular development and corpus luteum formation. The

typical menstrual cycle recurs every 21–35 days, with an average duration of 28 days (**Figure 5**). Over a female's lifespan, approximately 450 menstrual cycles occur, during which endometrial regeneration/degeneration takes place (Mihm, Gangooly and Muttukrishna, 2011; Critchley *et al.*, 2020).

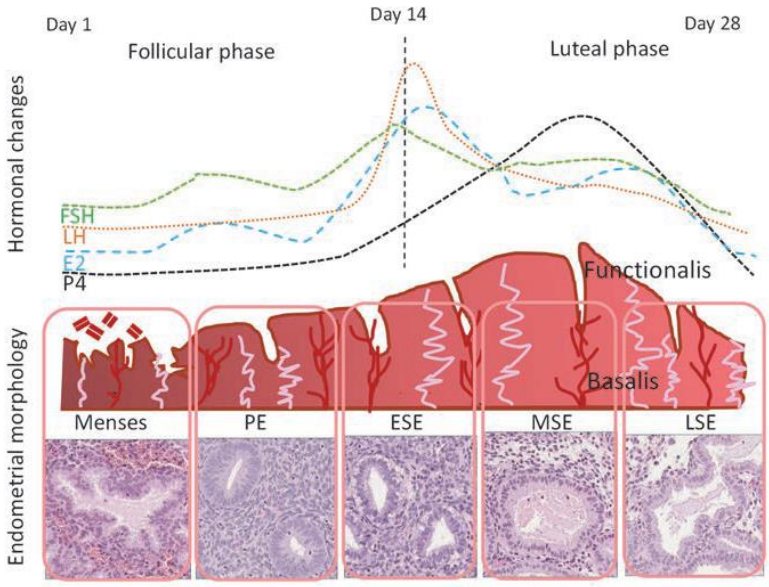

Figure 5: Adapted from (Spencer *et al.*, 2005). Histology of the human endometrium across the menstrual cycle. PE, proliferative phase, narrow glands with pseudo stratification of nuclei; ESE, early secretory phase, subnuclear vacuoles and reduced proliferation; MSE, mid-secretory phase, dilated glands with secretion in the lumen. Stroma is loose, glands tortuous, and only perivascular pseudo decidualization can be observed; LSE, late secretory phase, smaller glands and noticeable decidualization**.**

The proliferative phase (PE), which is the second phase of the uterine cycle after menstruation, often starts within the first 14 days of the cycle. Three stages of the PE can be distinguished: early, mid-, and late (Noyes, Hertig and Rock, 2019). Short, narrow, and thin epithelial glands are produced by the endometrium during the early proliferative phase (EPE), which normally starts around Cycle Day (CD) 4–7 and lasts for a short while following menses. The stroma appears compact and has little mitotic activity during the EPE. After that, on days 8–10 of the cycle, the endometrium enters the mid-proliferative phase (MPE), characterized by the adoption of a columnar shape by the lining epithelium. In this phase, the endometrium has longer, curved glands and stromal oedema. Finally, there is a substantial amount of mitotic activity between CD 11 and CD 14, which causes the surface epithelium to undulate. Known as the late proliferative phase (LPE), this stage results in the formation of the columnar epithelium, characterized by fully elongated, curved, compact glands and dense stroma. In order to provide the endometrium with sufficient blood flow, taking into account its increasing thickness,, the spiral arteries elongate (Rock, 1937; Acosta *et al.*, 2000). The luteal phase of the ovarian cycle is linked to the endometrial SE, which is the last phase of the uterine

cycle. This phase occurs in a 28-day cycle starting on CD 14 and occurs following the LH surge. The secretory phases of the SE can be divided into three groups: the early (ESE; cd 15–21; LH + 1-6), mid- (MSE; cd 22–25; LH + 7–9), and late (LSE; cd 26–28; LH + 10–12). With a few dispersed subnuclear vacuoles in the glandular epithelium, the histological appearance of the ESE is comparable to that of the LPE. By CD 17–21, the glands show regular tortuosity and change from intraluminal secreting subnuclear glycogen vacuoles to luminal vacuoles. the MSE, maximal stromal oedema with prominent spiral arterioles can be seen and the decidualization process is initiated. A high P4 concentration causes the endometrial cells to expand noticeably, and enhances the decidualization process by increasing secretory activity (Dunn, Kelly and Critchley, 2003). In order to guarantee an ideal niche for embryo development and to create an ideal environment for the implanting embryo, more nutrients are being gathered and more vasculature is being formed (Critchley *et al.*, 2020). In the absence of conceptus, during the LSE, the endometrium starts collapsing, which is manifested by prominent stromal granulocytes, focal necrosis, and hemorrhage that leads to gland disruption and stromal breakdown and tissue necrosis (Rock, 1937; Acosta *et al.*, 2000). In addition to traditional endometrial dating by pathologists, during the last decade, global gene expression analysis has given information about endometrial phase-specific transcriptome changes (Kao *et al.*, 2002; Yanaihara *et al.*, 2005; Talbi *et al.*, 2006; Díaz-Gimeno *et al.*, 2011). A recent single-cell transcriptome of the human endometrium also confirmed a distinct cluster of four phases as menstrual/early proliferative, late proliferative, early secretory, and mid/late secretory (Wang *et al.*, 2020).

CHAPTER 2 ENDOMETRIAL RECEPTIVITY AND EMBRYO IMPLANTATION

The implantation window is a brief period in the mid-secretory phase when the endometrium is highly receptive to the implantation of a blastocyst. This window commences 6-10 days following the LH surge (Psychoyos, 1974). During this period, the human endometrium is primed for blastocyst attachment, once it has acquired the accurate morphological and functional state induced by ovarian steroid hormones (Finn and Martin, 1974). The initial adhesion of the blastocyst to the uterine wall, called apposition, is unstable. Microvilli on the apical surface of syncytiotrophoblasts interdigitate with microprotrusions from the apical surface of the uterine epithelium, known as pinopodes (Norwitz, Schust and Fisher, 2001) (**Figure 6**).

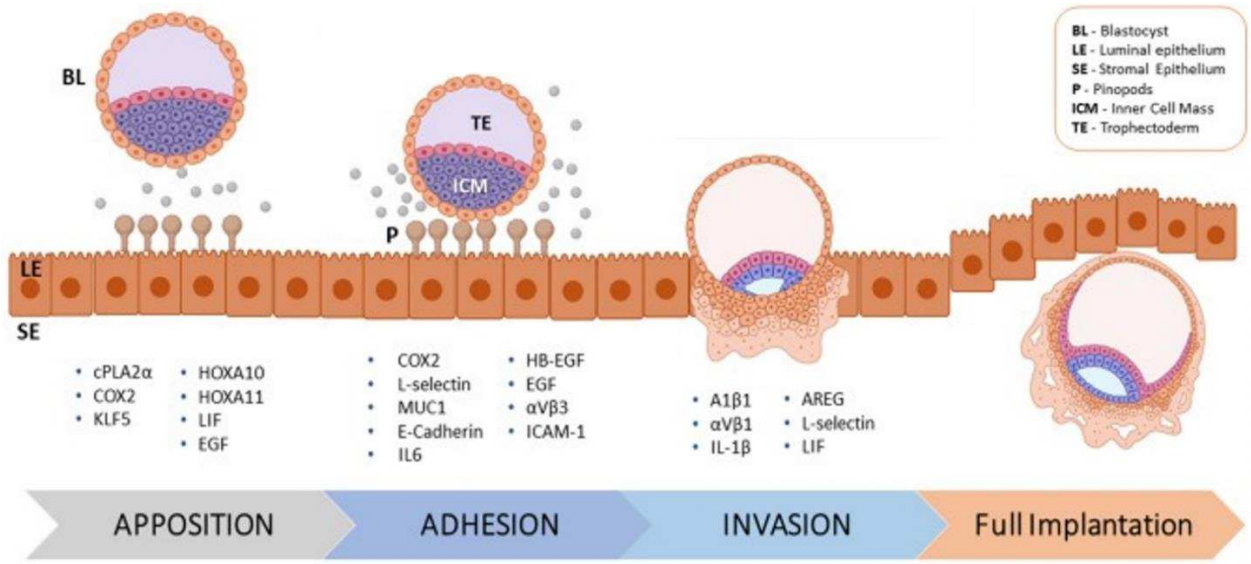

Figure 6: adapted from (Governini *et al.*, 2021) The three phases taking place during embryo implantation.(i) APPOSITION: the blastocyst contacts the implantation site; (ii) ADHESION: the trophoblast cells attach to the receptive epithelium; (iii) INVASION: the trophoblast cells invade the endometrial stroma and migrate into the maternal decidua.

Despite its importance in human fertility and regenerative biology, our understanding of this unique type of tissue homeostasis remains rudimentary. The endometrium is a fascinating and unique tissue that has tremendous plasticity as the biological interface dedicated to the interactions with the embryo and with the feto-placental unit; therefore, the endometrium represents a critical tissue for normal fertility and reproductive success. Reduced endometrial receptivity is thought to be associated with unexplained infertility; hence, a healthy endometrial environment might be regarded as the primary determinant influencing fertility (Strowitzki *et al.*, 2006). The maternal endometrium needs to be selective in addition to receptive for a successful embryo implantation to achieve successful reproductivity. The human endometrium serves as both a sensor of superior

embryo quality and a determinant in determining fertility (Macklon and Brosens, 2014). In fact, even with successful ART, recurrent implantation failure (RIF) may be caused by an inadequate endometrial milieu (Timeva, Shterev and Kyurkchiev, 2014).

2.1 BIOMARKERS OF THE WINDOW OF IMPLANTATION

Numerous molecular mediators, influenced by ovarian hormones, are believed to play a role in the initial feto-maternal interaction. These mediators embrace a large variety of inter-related molecules including adhesion molecules, cytokines, growth factors, lipids and others (Apparao *et al.*, 2002; Luddi, Marrocco, *et al.*, 2020; Luddi, Pavone, *et al.*, 2020; Governini *et al.*, 2021). The acquisition of adhesion ligands together with the loss of inhibitory components that may act as a barrier to an attaching embryo represent key steps in the acquisition of the endometrial receptivity (Aplin, 2000). Implantation failure remains an unsolved problem in reproductive medicine and is considered a major cause of infertility in healthy women. Indeed, the implantation rate in IVF is around 25% (De Los Santos *et al.*, 2003). Inadequate uterine receptivity is responsible for approximately two-thirds of implantation failures, whereas the embryo itself is responsible for only one third of these failures (Ledee-Bataille, 2002). The recent discovery of molecules crucial for successful embryo implantation has offered researchers precious insight into this field. Nevertheless, important questions regarding the molecular mechanisms governing this process remain to be deciphered. A better understanding of the mechanisms regulating embryo implantation may improve the ability of clinicians to treat infertility, prevent early pregnancy loss and develop new contraceptive approaches and discover the causes of recurrent implantation failure (Cakmak and Taylor, 2011). Knowledge of the human implantation process is compromised by both ethical issues, which do not allow the study of this process in vivo, and by the accuracy and reproducibility of in vitro models of human endometrium. Effective and reliable embryo implantation models are necessary to mimic the molecular event cascade that occurs in vivo; many steps have been taken towards a model that is reliable and reproducible. Human in vitro models have been successfully developed by many groups with the goal of obtaining effective tools to explore the complexity of this process(Teklenburg *et al.*, 2010; Weimar *et al.*, 2013; Stern-Tal *et al.*, 2020; Rosner *et al.*, 2021). Despite the enormous importance of in vivo models and the fact that they represent an invaluable asset in many aspects, these are laborious and expensive and do not yet address the human translational medicine issues represented by interspecies variability. It is important an adequate and robust 3D endometrial and placental model able to recapitulate all the cascade of events that surrounds embryo implantation without the use of animal models.

CHAPTER 3 HUMAN ENDOMETRIUM MODELS IN VITRO

3.1 STATIC MODELS

Despite being crucial, the biology of the human endometrium during pregnancy establishment and most of pregnancy is incomplete, given the ethical and practical limitations of obtaining and studying endometrium from pregnant women. As such, in vitro models of the human endometrium are required to fill significant gaps in understanding endometrial biology.

2D MODELS

Two-dimensional (2D) models of endometrium have been used since 1985 to study early feto-maternal interactions. The most used cells type for endometrial models are stromal and epithelial cells, obtained from endometrial tissues digested into single-cell suspension by various methods such as filtration, cell adhesion, density gradient centrifugation, immunomagnetic selection and fluorescence-activated cell sorting (Liszczak *et al.*, 1977; Kirk *et al.*, 1978; Varma *et al.*, 1982). Stromal and epithelial monolayers have been largely employed to study in a 2D environment the early feto-maternal interactions (Lindenberg, Nielsen and Lenz, 1985), and trophoblast spheroids were added to mimic human blastocysts to investigate molecular events beyond the luminal epithelium-embryo attachment and endometrium dysfunction in reproductive failure (Weimar *et al.*, 2013; Lee *et al.*, 2015; Aplin and Ruane, 2017; Huang, Liu and Li, 2017). The main disadvantage of the 2D culture of primary endometrial cells is their reduced biological activities after several passages and diminished responsiveness to sex hormones. This limitation hinders to the comprehensive study of their morphological and functional characteristics (Hannan *et al.*, 2010; Fitzgerald, Schust and Spencer, 2021). Considering the limited availability of primary human endometrial tissues, many researchers started to use endometrial adenocarcinoma and immortalized epithelial cell lines in 2D models to investigate endometrial epithelial functions. However, even though the cell line models are relatively easy to access and maintain, the potential genetic aberration associated with prolonged culture is an obstacle to investigating the physiological properties of the endometrium (Hannan *et al.*, 2010). Another major aspect that needs to be considered in 2D models is that they cannot address questions about the complex environment related to the tridimensional (3D) architecture; indeed, cell-to-matrix interactions cannot take place. The endometrial cell-extracellular matrix (ECM), a tridimensional matrix scaffold surrounding the cells, provides biochemical and biophysical support to the endometrial cells and plays pivotal roles in the menstrual cycle and embryo implantation. A monolayer culture without ECM alters the functional activities of the endometrial epithelial cells;

they lose their polarities and change their secretory functions (Aplin, Charlton and Ayad, 1988). Meanwhile, monolayers of multiple cell types are difficult to co-culture, and thus are unable to reproduce the in vivo crosstalk between the endometrial stromal and epithelial cells. All these critical issues have pushed the scientific community towards the search for alternative approaches. 3D cell culture has been shown to be more effective to model a cell in vivo while being cultured in vitro, also enduring specific methods of cell culture depending on the type of tissue to be mimicked(Jensen and Teng, 2020)(**Figure 7**).

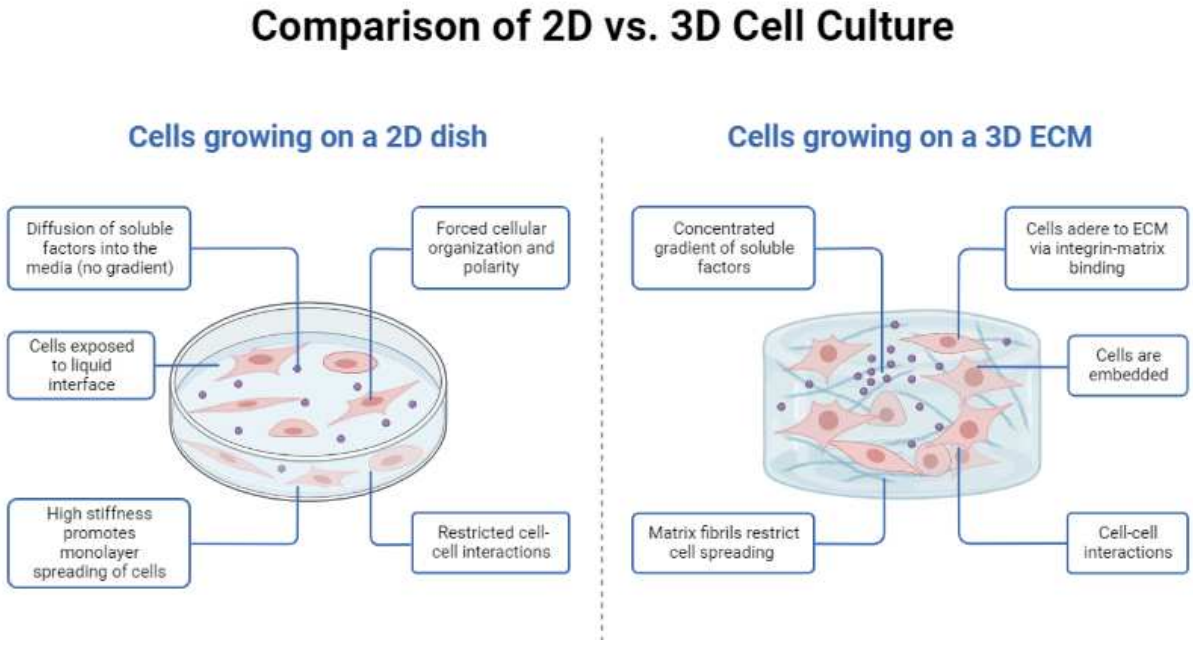

Figure 7: Schematic of the comparison between 2D and the 3D *in vitro* models.

3D MODELS

Three dimensional (3D) in vitro models are recently developed techniques capable of mimicking the three-dimensional structure in vivo, effectively reproducing the physiology and physio-pathological characteristics of the native tissues. A 3D cell culture model can be set up by using either a scaffold, cell supporting matrix, or non-scaffold-based culture method (Li *et al.*, 2022). A variety of 3D culture, 3D model of the human implantation process methods have been used to mimic human endometrium, such as organoids, 3D hydrogels, 3D bioprinting, and organ-on-a-chip (OOAC) platforms. Some of these approaches will be described in depth in the following sections. Organoids are defined as self-organizing, genetically stable 3D culture systems that replicate the tissue of origin

and contain both progenitor and differentiated adult cells of the tissue of interest (Cui *et al.*, 2020; Li *et al.*, 2022). The first mention of the endometrial organoid-like structures (EOs) was 34 years ago (Rinehart, Lyn-Cook and Kaufman, 1988). In this study, the endometrial glands were isolated from the endometrial tissue biopsies and embedded in Matrigel at a ratio of 1:1 with a culture medium. The endometrial gland fragments initially spread in the Matrigel as monolayers of tiny colonies and eventually formed a gland-like structure. Similarly, some other studies also found the development of prominent glandular structures from endometrial epithelial cells when they were cultured on basement membrane extracts (BME) or Matrigel. These cells showed polarization, hormone responsiveness and secretory functions that recapitulate the endometrial glands in vivo (Negami and Tominaga, 1989; Schatz *et al.*, 1990; White, Sant'agnese and Miller, 1990; Classen-Linke *et al.*, 1996b). Even though the gland-like structures were not well characterized, these studies set the basis for the development of the endometrial glandular organoid model. EOs are considered an important tool for the study of female reproductive biology. Compared with conventional 2D and 3D culture models, organoids contain more cell types within the intact 3D structure, along with the presence of ECM that reproduce the physiological microenvironment. Unlike most 3D culture models of the endometrium, which can be cultured for up to 10 days, organoids are more stable and can be cultured for a much longer period, with high genetic stability. Therefore, the organoid culture model has been gradually applied for the study of embryonic development, diseases, and drug testing in regenerative medicine (Rossi, Manfrin and Lutolf, 2018). EOs may derive from endometrial tissue from all stages of the menstrual cycle, as well as from decidua and atrophic endometrium (Nikolakopoulou and Turco, 2021). Only recently has the derivation of epithelial organoids from menstrual blood also been possible (Cindrova-Davies *et al.*, 2021). This new methodology, less invasive, can allow researchers to have a broad spectrum of samples considering the limited amount of "healthy" endometrial biopsies. Currently, many protocols have been established for 3D endometrial epithelial organoids (EEOs) in a chemically defined medium to fully generate and analyze their functions (Boretto *et al.*, 2017; Turco, Gardner, Hughes, Cindrova-Davies, Gomez, Farrell, Hollinshead, Marsh, Brosens, Critchley, Benjamin D. Simons, *et al.*, 2017). In addition, these studies have shown that EEOs also exhibit physiological hormonal activity, demonstrating that they can maintain intrinsic disease properties and resemble the human endometrium, which undergoes extensive remodeling during the menstrual cycle, regulated mainly by ovarian estrogen and progesterone (Boretto *et al.*, 2017; Turco, Gardner, Hughes, Cindrova-Davies, Gomez, Farrell, Hollinshead, Marsh, Brosens, Critchley, Benjamin D. Simons, *et al.*, 2017; Luddi, Marrocco, *et al.*,

2020, p. 2; Luddi, Pavone, *et al.*, 2020). Recent progress has been achieved with the creation of organoids incorporating both epithelial and human stromal cells (also named assembloids) (**Figure 8**) (Rawlings *et al.*, 2021).

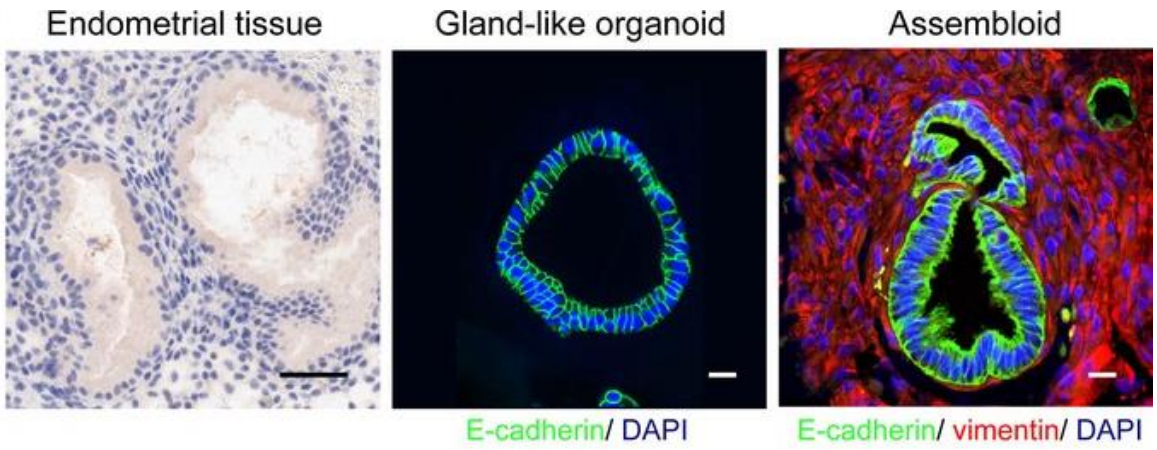

Figure 8: Adapted from (Rawlings *et al.*, 2021) Structural appearance of hematoxylin and eosin stained secretory endometrium, E-cadherin (green) labelled gland-like organoids, and E-cadherin (green) and vimentin (red) stained endometrial assembloids. Scale bar = 50 µm.

Based on transcriptomic analysis, these assembloids contain different subpopulations of stromal and epithelial cells that secrete implantation factors. Therefore, the upgraded EOs represent a powerful tool for precision medicine in static conditions. An improved version of the 3D endometrial model, composed of both epithelial and stromal cells, was established for examination of the impact of two contraceptive drugs, levonorgestrel and mifepristone, on the expression of endometrial receptivity markers (Lalitkumar *et al.*, 2007). This model demonstrated not only that the epithelial and stromal cells expressed estrogen receptor (ER), and progesterone receptor (PR), but also that the treatment with estrogen and progesterone induced the expression of several endometrial receptivity markers including LIF, IL-1β, VEGF and cyclooxygenase-2 (COX2). Interestingly, mifepristone inhibited the expression of these markers like that observed *in vivo*, and inhibited blastocyst attachment, thus confirming EOs as suitable in vitro models to study endometrial receptivity. Most importantly, human embryos can be incorporated to interact with the established 3D endometrial model, enabling the use of the model to study embryo implantation as well (Lalitkumar *et al.*, 2007). A 3D culture model of the human endometrium may also combine the use of both primary and continuous cell lines. Arnold et al., (Arnold *et al.*, 2002) cultured primary endometrial stromal cells in Matrigel and seeded directly on top of Matrigel the Ishikawa cells (a cancer cell line of endometrial

glandular origin) expressing epithelial-like phenotype. This model demonstrated that the interaction between stromal and glandular cells induced the Ishikawa cells to produce glycodelin, a key glycoprotein produced by the endometrial glands in the secretory phase of the menstrual cycle (Seppälä *et al.*, 2002; Lee *et al.*, 2016). This confirms that stromal cells control in a paracrine way the proliferation and differentiation of the cocultured endometrial epithelial cells. This study further showed that the absence of Matrigel reduces the regulatory functions of secretory factors derived by stromal cells on the Ishikawa. This suggests that in the 3D culture model, secretory factors from the Matrigel support the cells' function in a more physiological way. One limitation of the study was the use of Ishikawa cells (adenocarcinoma cell line) as epithelial cell surrogates instead of primary cells. Another aspect of the 3D model culture is that ECM materials such as collagen and Matrigel, are easily degraded in culture, which reduces the length of the coculture. Therefore, different inks, such as agarose and fibrin, have been used as ECM to set up more effective endometrium-like in vitro 3D models. Moreover, the use of several compounds, including calcium chloride, to stabilize the ECM was reported (Wang *et al.*, 2012). In this model, the endometrial stromal cells (primary or immortalized cell lines) were cultured in the supplemented fibrin-agarose, and the epithelial cells (primary or Ishikawa cell line) were seeded on top of the gel. By this approach, the cells maintain an intact structure for at least 10 days, outperforming the previously established 3D endometrial models. These modifications make this model suitable for the integration of trophoblast spheroids, allowing a comprehensive study of the trophoblast invasion into the endometrium (see following sections). 3D tissue-slice culture models are 3D tissue explants that can be cultured ex vivo for an extended period (Majorova *et al.*, 2021). In the beginning, the tissue slice culture model had major limitations, due to the inaccuracy of the razor blades used and the suboptimal incubation conditions; this resulted in a very rapid decrease in cell viability. These problems were solved by the advent of new tissue slicers, and through the improvement of incubation technologies. 3D tissue-slice culture models have the advantage of retaining not only the physiologic architecture of the in vivo tissue, but also maintaining some important tissue-specific functions, such as metabolism and immunologic functions. This makes 3D models an efficient alternative to animal models. Their use as in vitro models of human endometrium is so far very limited and recent. Muruganandan and colleagues (2020) (Muruganandan *et al.*, 2020) reported the setup of a 3D tissue slide model obtained from full thickness biopsy of human endometrium embedded into a 3D matrix scaffold of type I collagen gel, incorporating an air-liquid interface, which allows sustained tissue viability over three weeks. Compared to the conventional cell-based models, which generally show diminished cell viability and

hormone responsiveness in vitro approximately after 5 days, the endometrial tissue slice in this double-dish tissue-based model was viable after 21 days. Noteworthy, these 3D models retain the ability to respond to ovarian hormones, eliciting a correct gene expression profile and the typical changes in endometrial morphology, usually found in the in vivo tissue. This model further confirmed the importance of ECM in preserving the functionality of endometrium in vitro. Although further studies are needed to optimize preparation protocols, these models have the undisputed advantage of including all cellular populations present in the endometrium.

3.2 Dynamic models

While 3D organoid cultures represent a distinct improvement over monolayer cultures, they still fail to exactly mimic the architecture of tissues, which includes vascular and interstitial fluid flow. Organ-on-a-chip (OOC), flexible devices representing the convergence of microfluidics and tissue engineering, are an emerging technology able to address this limitation. In these devices, cells are cultured in micrometer chambers that are continuously perfused, thus creating a sheer force that provides nutrition and waste transport to mimic in vivo vascularized tissues. Micro-physiological systems, or MPSs, are microfluidic devices that can, according to their intended use, simulate the biology of humans or any other animal species *in vitro* at the smallest scale that is still considered acceptable to biology. One important feature of these systems that sets them apart from static cells and tissue cultures is the application of fluid flow for the physiological nourishment of the tissues and the generation of micro-environmental biomolecular gradients in response to mechanical stimuli (Marx *et al.*, 2016).

The term "system" in MPS refers to devices that sustain human-like physiology of tissues and organ equivalents *in vitro*. Maintaining physical parameters, including temperature, appropriate pH, oxygen supply and regulation, and humidity levels, may fall under this category. It also includes the mechanical coupling of organs through the imitation of blood, urine, air, bile, pancreatic juice, or cerebral fluid flow; shear stress on blood and lymphatic vessels; physical pressure on bone and cartilage; strain on the skin, lungs, and stomach wall; muscle contractions; and the reading of electrical activity of neuronal and cardiac tissue(Marx, 2020).

MPS can be classified into three categories. Single organ systems are intended to replicate organ structure and improve early predictability of human single organ toxicity to particulate matter, chemicals, and medication candidates. Multi-organ systems (MOC) simulate the systemic interactions of two or more organ models inside a single system, allowing for the development of adverse outcome route and mode of action data through crosstalk. More complicated systems,

commonly labeled "human/body-on-a-chip" systems, are envisioned to replicate the physiological interplay of a number of organs capable of imitating whole organismal capability (Marx *et al.*, 2016). The first MPS with tissue-tissue interface was the “lung-on-a-chip” a multifunctional micro-device that reproduce key structural, functional and mechanical properties of the human alveolar-capillary interface, the fundamental functional unit of the living lung. This microfluidic system contains two closely apposed micro-channels separated by a thin, porous flexible membrane made of polydimethylsiloxane (PDMS) coated with an ECM. The compartmentalized channel configuration makes possible to manipulate the fluid flow, as well as delivery of cells and nutrients to the epithelium and the endothelium independently. An example of MOC can be seen in the system designed and prototyped by Uwe Marx and collaborators at the Technische Universität Berlin (**Figure 9**). The platform, in a standardize chip format of the area of a microscopic slide, is equipped with a peristaltic on-chip micro-pump, and can integrate biological vasculature into the microfluidic channels (Schimek *et al.*, 2013a; Marx *et al.*, 2016).

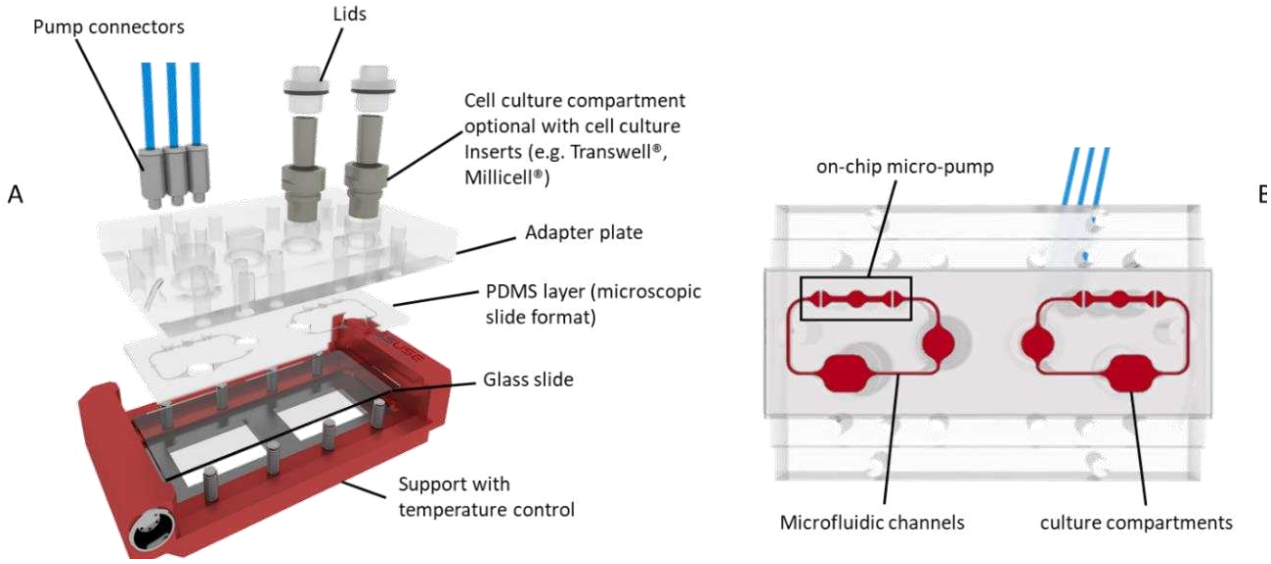

Figure 9: TissUse GmBH Humimic Chips pictures. The multi-organ platform allows the interaction of two or more organ models within one system. It presents an area of a microscopic slide, is equipped with a peristaltic pump and can integrate vasculature into the microfluidics channels. (A) Humimic Chip 2 (B) Humimic Chip 2 view from below. Source: TissUse GmBH https://www.tissuse.com/en/

Another approach concerning the culture of endometrial cells in a MPS consisted in a microfluidic chip contained three layers, in which a polycarbonate membrane was sandwiched between a top and a bottom PDMS layer. The aim was to investigate the crosstalk between the internal layer of the uterus and the oocyte thanks to the perfusion culture and the mass exchange achieved by molecule diffusion through the membrane micropores (Li *et al.*, 2022). Another approach is a dual reproductive organ-on-a chip system that enables bidirectional communication between the ovaries and endometrium. This model reproduces the multicellular complexity of both tissues: the ovarian compartment contains granulosa and theca cells, while the endometrial compartment includes fibroblasts, vascular epithelial cells, immune cells, and endometrial stem cells) (Park *et al.*, 2021). A new microengineered 3D device of vascularized endometrium on a chip was recently conceived. This model faithfully reproduces the endometrial microenvironment, consisting of three distinct cell layers, epithelial cells, stromal fibroblasts, and endothelial cells, in a spatially and temporally 3D extracellular matrix. Two central channels are intended for 3D culture and morphogenesis of stromal fibroblasts and endothelial cells. In addition, the outermost channel is intended for the culture of additional endometrial stromal cells that secrete molecules to induce proangiogenic directional responses of endothelial cells (Ahn *et al.*, 2021). An important breakthrough in generating more sophisticated *in vitro* models has been the application of microfluidic technologies by Xiao and colleagues (Xiao *et al.*, 2017). This Multi-Organ" EVATAR" microfluidic system simulates in vitro the 28-day human menstrual cycle by combining murine ovary, fallopian tube, uterus, cervix, and human liver explants with steroid hormones released from ovarian follicles (**Figure10**).

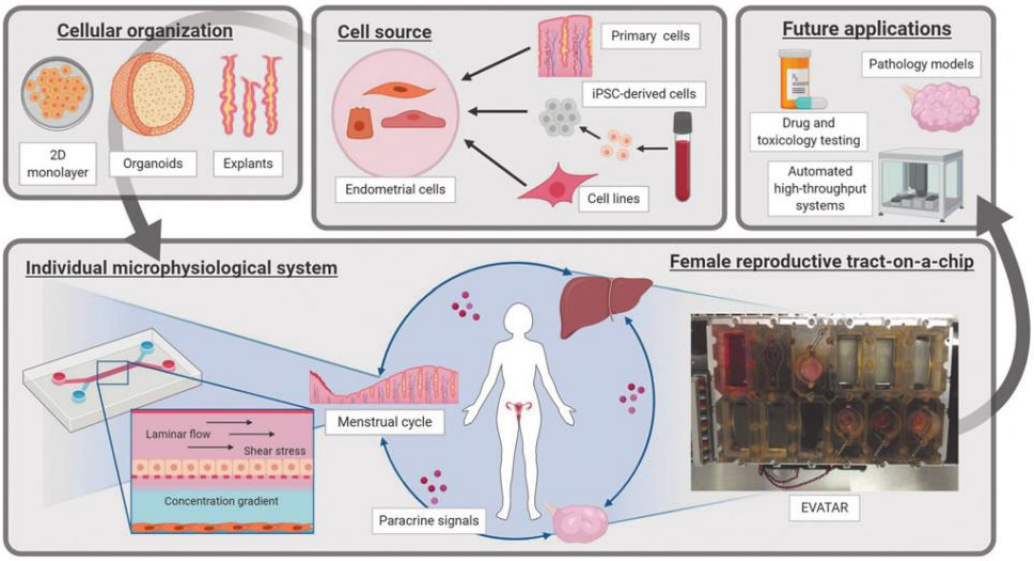

Figure 1. The most complex example of MPS called EVATAR (on the lower right) contains the culture of ovary, fallopian tubes, endometrium, ectocervix and liver tissues. Source:(Campo *et al.*, 2020)

Less complex systems were used to examine physiological changes during the decidualization process, focusing the attention on the crosstalk between two cell types. For example, a dual chamber microfluidic device that integrates a resin based micro-fabricated porous membrane was developed by Gnecco et al. to allow long term co-culture of human umbilical vein endothelial cells and endometrial stroma under sex steroid regulation and better understand the interactive role of perivascular stroma in the human endometrium (Gnecco *et al.*, 2017). Since decidualization is a critical process for embryo implantation, the ability to explore the earliest stages will provide a unique screening tool for fertility studies. Pharmaceutical agents, or environmental toxicants that may alter the reproductive health or promote reproductive dysfunction, as well as structural and hormonal changes could be better investigated in a microfluidic system that offer the opportunity to study the interaction between different type of cells in a vascularized environment (Gnecco *et al.*, 2017).

RESEARCH STUDY PURPOSE

Embryo implantation has been defined as the "black box" of human reproduction. Most of the knowledge on mechanisms underlying this process derives from animal models, which cannot always be translated to humans. Therefore, new technologies such as the 3D cell models are considered a new step to foster the study of human endometrial biology and an advanced tool for studying endometrial-associated diseases and understanding the complex mechanisms surrounding endometrium-embryo crosstalk. The aim of this thesis is to develop from both primary and immortalized cells human endometrium *in vitro* models that can be applied to mimic the decidualization process during the Window of Implantation (WOI).

The first aim of this thesis was to investigate a noninvasive model using human primary cells in static condition. The menstrual flow was used as source to establish a reliable and complete human 3D model. In fact, from human menstrual flow, is possible to isolate both stromal and epithelial cells to generate the 3D model. Subsequently this model was characterized and stimulated to mimic different phases of the menstrual cycle.

The second aim of this thesis is to develop a 3D model of the human endometrium using Microfluidic devices to better recapitulate the physiological changes occurring during menstrual cycle. In particular, the decidualization process has been a focal point and the two main cell populations of the endometrium, epithelial and stromal cells, have been considered. In this model, two different cell lines have been used: the endometrial epithelial cell line EM42, and the immortalized endometrial stromal cell line THESC. The survival and reactivity of the model have been tested in this thesis, aware of the lack of important cellular interactions necessary to fully mimic the endometrial environment *in toto*. The model was also enriched with the addition of endothelial cells, HUtMECs, important contribution for the process of vascularization. In the future other cell types should be included in this model to a micro-physiological-system (MPF), for example the cells of immune system.

MATERIALS AND METHODS

SECTION 1: FOCUSING ON THE ESTABLISHMENT OF A RELIABLE AND NON-INVASIVE HUMAN ENDOMETRIUM 3D MODEL IN STATIC CONDITIONS

1.SAMPLE COLLECTION

For this thesis endometrial tissues samples and Menstrual blood (MB) were collected by the Obstetrics and Gynecology clinic University Hospital of Siena. Endometrial biopsies, collected by hysteroscopy, and Menstrual blood samples from women of proven fertility. The study has been approved by the Ethics Committee of Siena University and signed informed consent was obtained from all patients who participated in the study. All methods were carried out in accordance with the relevant national guidelines and regulation and with the Declaration of Helsinki. The age ranged from 22-37 years. Current infections, endocrine disorders, or the use of hormonal treatment within the past three months were common exclusion criteria. A complete medical history, physical examination and transvaginal ultrasound evaluation have been performed for each patient. All endometrial biopsies have been classified according to the phase of the menstrual cycle based on ultrasonographic features and hormonal profile.

2. EXPERIMENTAL SET UP

The following experiments were performed at Siena University Hospital following the schematic in **Figure 11**. Endometrial specimens were differently treated, according to the several analyses to which they were subjected.

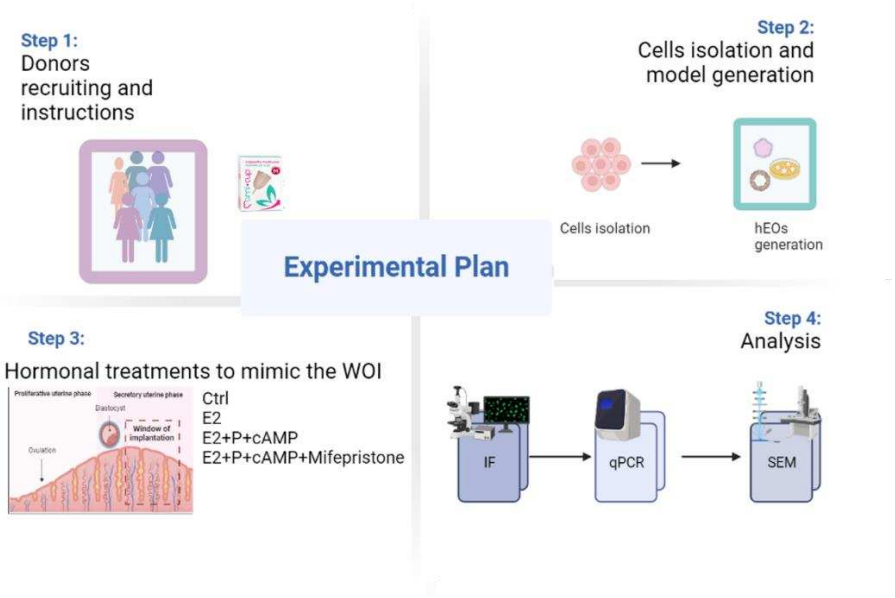

Figure 11: Schematic of the experimental plan. Step 1: recruitment of patients. Step 2: cells isolation and Organoids generation. Step 3: Hormonal treatments to mimic the WOI. Step 4: endpoint analysis, IF=immunofluorescence SEM=Scanning electron microscopy.

2.1 *IN VITRO* EXPERIMENTS

Fragments of endometrial biopsies collected during proliferative phase from healthy endometrium have been immediately treated to obtain endometrial glandular organoids.

2.1.1 ISOLATION AND CULTURE OF ENDOMETRIAL GLANDULAR ORGANOIDS AND STROMAL CELLS FROM BIOPSIES

The protocol for isolation and culture of Organoids from biopsies was adapted from Turco and coworkers (Turco, Gardner, Hughes, Cindrova-Davies, Gomez, Farrell, Hollinshead, Marsh, Brosens, Critchley, Benjamin D. Simons, *et al.*, 2017). Tissues have been washed in Phosphate Buffer Saline (PBS) 1X, plus penicillin 5000IU/ml and streptomycin 5mg/mL and cut into 0.5-1 mm^3pieces. Tissue fragments were enzymatically digested in 20-30 mL 1.25U/mL Dispase II (Sigma, D4693)/ 0.4mg/mL collagenase V (Sigma, C-9263) solution in DMEM (Dulbecco's modified Eagle's medium)/10% FBS with gentle shaking at 37°C for 30-60 min. The supernatant was passed through one or more 100 µm cell sieves (Corning, 431752) and the sieve washed several times with medium. The flow-through was collected for stromal cell culture in Advanced DMEM/F12 (ThermoFisher Scientific)

+10%FBS+1%pen/strep +L-glutamine for several days and subsequent analysis. The sieves were inverted over a petri dish and retained glandular elements were backwashed from the sieve membranes, pelleted by centrifugation and resuspended in ice cold Matrigel (Corning, 536231) at a ratio of 1:20 (vol:vol). 20-25 µL drops of Matrigel-cell suspension were plated into 48-well plate, allowed to set at 37°C and overlaid with 250 µL organoid Expansion Medium (ExM) (**Table1**). The medium was changed every 2-3 days. Cultures were passaged by manual pipetting every 7-10 days. For freezing organoids, Matrigel was removed using Cell Recovery Solution (Corning, 354253) and organoids were resuspended in Recovery cell culture freezing medium (ThermoFisher Scientific, 12648-010).

Table 1. ExM composition

Product	Company	Product Number	Final Concentration
Advanced DMEM/F12	Life Technologies	12634010	1X
N2 supplement	Life Technologies	17502048	1X
B27 supplement minus vitamin A	Life Technologies	12587010	1X
N-Acetyl-L-cysteine	Sigma	A9165-5G	1.25 mM
L-glutamine	Life Technologies	25030-024	2 mM
Recombinant human EGF	Peprotech	AF-100-15	50 ng/ml
Recombinant human Noggin	Peprotech	120-10c	100 ng/ml
Recombinant human Rspondin-1	Peprotech	120-38	500 ng/ml
Recombinant human FGF-10	Peprotech	100-26	100 ng/ml
Recombinant human HGF	Peprotech	100-39	50 ng/ml
ALK-4, -5, -7 inhibitor, A83-01	System Biosciences	ZRD-A8-02	500 nM
Nicotinamide	Sigma	N0636	10 M

2.1.2 ISOLATION AND CULTURE OF ENDOMETRIAL GLANDULAR ORGANOIDS FROM MENSTRUAL BLOOD (MB)

Organoids and stromal cells were isolated adapting the protocol of Cindrova-Davies and colleagues (Cindrova-Davies *et al.*, 2021). Patients were supplied with a reusable menstrual cup (OrganiCup or MamiCup and size was chosen depending on their age and/or obstetric history) and its proper use was explained. Patients were instructed to collect MB in a sterile 50-ml tube as soon as the flow became heavy maximum on day 1–2. The heavy flow sample was obtained having the cup overnight, and the sample was given in the morning Menstrual samples were couriered to the laboratory and processed immediately. To eliminate red blood cells, samples were spun down at 600× g for 5 minutes and washed with PBS numerous times. The bloody supernatant was discarded, and only the cellular material was collected after each wash. The cellular sediment was passed through a 100-µm

sieve (Corning, 431752) and rinsed with additional PBS. The sieve was inverted over a Petri dish, and the remaining cellular debris was backwashed from the sieve membranes to collect the solid endometrial gland-containing material. The rest of the protocol followed until the generation of Organoids (**Figure 12**) the description in Paragraph 2.1.1.

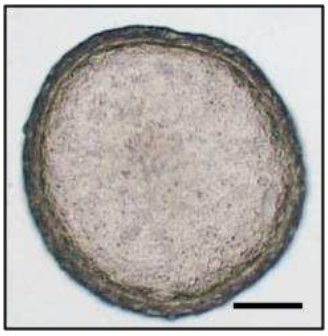

Figure 12: Representative image of single Organoid generated using as source the MB. Scale bar 50 µm.

2.1.3 Hormonal treatments

The organoids culture and stromal cells culture have been exposed to hormonal treatments to induce the typical changes of the proliferative and secretory phase of the menstrual cycle. To mimic the proliferative phase, the ExM or the hESC has been supplemented with 10-8 Estradiol, meanwhile for the secretory phase 10-8 Estradiol, Medroxyprogesterone 17-acetate 10 mM and 500 µM 8-Bromoadenosine 3',5'-cyclic monophosphate (cAMP) and Mifepristone a cell-permeable synthetic steroid that acts as a potent antagonist of progesterone and glucocorticoid receptors to block the decidualization process.

2.1.4 Organoids Preparation

In order to prepare the organoids to further analysis, Matrigel droplets containing the organoids have been washed three times with PBS and detached using a 1ml pipette tip, to scrape the growth surface of each well. The contents of the wells have been centrifuged at 600 g for six minutes to pellet the organoids. Additional centrifuges have been done until the Matrigel was completely removed. Organoids pellet have been treated according to the different analysis.

-Treatment for Immunofluorescence analysis

For Immunofluorescence analysis the organoids have been resuspended and fixed in 10% neutral buffered formalin at room temperature for 24hours. 2-3 organoids have been placed in a drop of 4% agar and it has been left to solidify. Subsequently, Organoids were paraffin embedded and sectioned at 4 µm thickness and mounted on Super frost Plus slides (FisherScientific).

-TREATMENT FOR SCANNING ELECTRON MICROSCOPY

For Scanning Electron Microscopy (SEM) Cultures of human endometrial organoids were fixed for 2 hours at 4 °C in cold Karnovsky's fixative, washed with cacodylate buffer 0.1 M pH 7.2 overnight, post-fixed in 1% buffered osmium tetroxide in veronal acetate buffer for 2 h and washed in cacodylate buffer 0.1 M pH 7.2 and kept until analysis.

3. GENE EXPRESSION

3.1 SAMPLES PREPARATION

In order to perform the RNA isolation, cells from Organoids and stromal cells were collected four days after seeding (Day 1), and three days after treatment (Day 4), were washed with PBS, centrifuged and then resuspended in lysis solution in 300 µl of lysis buffer with β-Mercaptoethanol. The samples were than snap-frozen in liquid nitrogen and stored at -80°C until further processing.

3.2 RNA ISOLATION

RNA was extracted by using the Qiacube (Qiagen) automatic extractor following the manufacturer protocol of RNeasy Microkit (Qiagen). At the end of the protocol, the RNA extracted from each sample was eluted in a final volume of 20µl of water. The purity and the concentration of RNA were evaluated by reading on NanoDrop® ND-100 UV-vis Spectrophotometer (Thermo Fisher Scientific).

3.3 cDNA TRANSCRIPTION

Extracted RNA was reverse transcribed into cDNA, using the iScript gDNA Clear TM cDNA Synthesis Kit (Bio-Rad Laboratories, Hercules, CA, USA). We started with a treatment of samples with a master mix of DNase to remove contaminating genomic DNA. To inactivate the effect of DNase, the samples were incubated in a thermal cycler at 25 °C for 5 min and at 75 °C for another 5 min. 4 µL of the iScript reverse Transcription Supermix was added to each sample; they were then incubated in a thermal cycler (5 min at 25 °C, 20 min at 46 °C, 1 min at 95 °C).

3.4 qPCR

Gene expression was evaluated using a specific assays and primers (**Table 2**). To normalize the expression levels of the gene transcripts of stromal cells and organoids, a simultaneous mRNA expression profiling of the housekeeping genes *HPRT1* and *GADPH* were also performed in all the analyzed samples. All amplification reactions were conducted in triplicate by qRT-PCR on a CFX connect Real-Time PCR Detection System (Bio-Rad Laboratories) using SsoFast EvaGreen Supermix (Bio-Rad Laboratories); gene-specific primer sets used in this study are listed in Table 2. Melting

curve analysis was also performed to confirm the specificity of the products obtained. Changes in gene expression levels were calculated by the $2^{-\Delta\Delta Ct}$ method.

Table 2: Primer list for Gene Expression analysis

Target Genes	Acronym	Sequences
FK506 binding protein 5	FKBP5	FW-TCT CTT TGG GCA GAG CGG AA RV-TCT AGC CTT CTG CAG CGT GG
Insulin-like growth factor-binding protein-1	IGFBP-1	FW-CTG CTG GTG CGT CTA CCC TT RV- AGT TGG GGT CTC CCC TGA TCT
Prolactin	PRL	FW- TTCGAGACCTGTTTGACCGC RV- TCTTTTTGATTCATCATCTGTTGGGC
Zinc Finger and BTB Domain Containing 16	ZBTB16	FW- CAG CCG AGT CCA GCA TCT CA RV- CTG CTC GGC ACT CTC CTC TC
Hypoxanthine-Guanine Phosphoribosyl Transferase 1	HPRT1	dHsaCPE5192871
Glyceraldehyde-3-phosphate dehydrogenase	GAPDH	Hs02706624_g1

4. Immunofluorescence Analysis

Formalin-fixed, paraffin-embedded organoids were sectioned at 4-µm thickness, and then fixed in deparaffinized with xylene and dehydrated with ethanol. Antigen retrieval has been obtained by incubation with buffer 10 mM citrate pH 6.0, at a temperature sub-boiling for 20 minutes. Slides were left to cool for 10 minutes. Subsequently, they were incubated in a blocker solution containing 5% goat normal serum in PBS/BSA (bovine serum albumin) 1% and then incubated for 1 hour at room temperature with the primary antibody used according to the manufacturer's instructions (**Table 3**). The specificity of immunostaining was confirmed by both omissions of primary antibody and staining of sections with unrelated antibodies. The slides have been washed in PBS, and the bound antibodies were revealed by incubation with Alexa Fluor 488-labeled and/or 568 (**Table 3**). After washing in PBS, the slides have been mounted in ProLong antifade with 4',6-diamidino-2-phenylindole (DAPI) (LifeTechnologies) to counterstain the nuclei and then they have been observed with a Leica DMB 6000 microscope (Leica). Images have been captured with a CFTR6500 digital camera (Leica).

Table 3. List of Antibodies

Antibody	*1° or 2°*	*Anti-*	*Concentration*	*Dilution*
Cytokeratin 8/18	1°	Mouse	200µg/ml	1:100
Vimentin	1°	Rabbit	1.04 mg/ml	1:100
Glycodelin A	1°	Rabbit	1.5 mg/ml	1:100
Goat Anti-Mouse IgG (H+L), Alexa Fluor Cf®568	2°	Mouse	2mg/ml	1:350
Goat Anti-Mouse IgG (H+L), Alexa Fluor Cf®488	2°	Rabbit	2mg/ml	1:200
Goat Anti-Rabbit IgG (H+L Alexa Fluor Cf®568	2°	Rabbit	2mg/ml	1:200
Goat Anti-Rabbit IgG (H+L), Alexa Fluor Cf®488	2°	Rabbit	2mg/ml	1:200

5.Morphological analysis

5.1. Scanning Electron Microscopy (SEM)

Organoids were dehydrated in a graded series of ethanol, placed in tert-butanol and frozen at 0 °C before being dried by sublimation of the tert-butanol in a vacuum chamber. The samples were cut to expose the internal surface and coated with 20 nm gold/palladium and observed in a Quanta 400 (FEI) scanning electron microscope. Two independent SEM analyses have been performed; for each experiment, hundreds of organoids were fixed and observed at scanning electron microscopy by two independent operators.

6. Statistical analysis

Statistical analysis was carried out with GraphPad Prism 9.0 (GraphPad Software). Analysis of Variance (ANOVA) allows comparisons to be made between three or more groups of data. One -way ANOVA was used to compare three or more groups of data. Data are reported as mean ± standard deviation (SD). Statistical significance was set at $p < 0.05$.

SECTION 2: PRESENTING THE SET-UP OF A DONOR-INDEPENDENT HUMAN 3D MODEL IN DYNAMIC

1.CELL CULTURE

The following experiments were performed at Bayer AG, Pharmaceutical, Advanced Cellular Models and TISSUSE GmbH Berlin, Germany. Cell culture procedures were conducted under a laminar flow hood using aseptic techniques and sterile equipment. Incubation of cell cultures was performed at 37°C, 97% air humidity and 5% CO2. For the establishment of the endometrial organ-on-a-chip model, TissUses microphysiological system (MPS) was used, specifically the HUMIMIC Chip2 96-well format (Figure 13). The MPS system consists of an external control unit, which enables media flow by vacuum and pressure. The HUMIMIC Chip2 contains two circuits. A microfluidic channel connects two 96 well culture compartments on chip connectors control the fluidic flow. The microfluidic channels were colonized with primary endothelial cells (HUtMEC) and after three days, in the culture compartments, the 3D models (consisting of the epithelial and stromal cells of the endometrium) were added. Subsequently decidualization was initiated by the addition of a hormone cocktail to mimic the window of implantation, the experiment was stopped after 4 days. All the endpoint analysis were carried out.

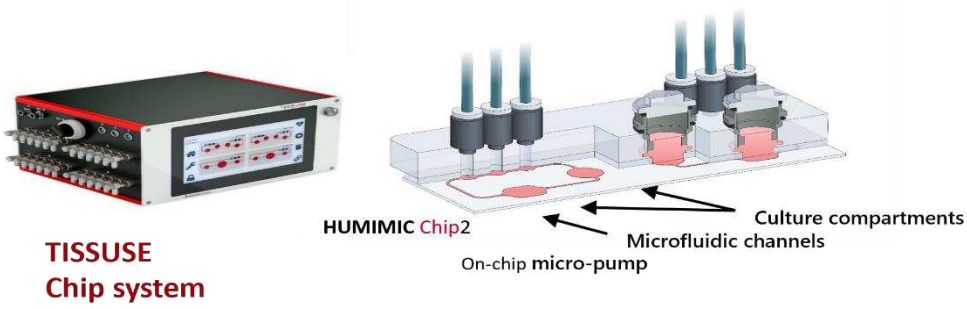

Figure 13: Schematic of the TISSUSE Chip system and HUMIMIC Chip2 composed by 2 separated microfluidic channels and the culture compartments linked to the micropumps connected to the TISSUSE Chip system.

1.1 EM42 CELL LINE

The endometrial epithelial cell line EM42 (**Figure 14**) was provided in a cryopreserved state by the Cleveland Clinic Foundation to De Leo's group from Bayer AG (under signed license). The cells were cultured in EM42 Culture Medium, a Dulbecco's modified Eagle Medium (DMEM) supplemented with 10% foetal bovine serum (FBS) (See **Table 4**).

Table 4. EM42 culture medium.

Substance	***Concentration in Medium***
DMEM	88%
Penicillin/Streptomycin	1%
L-Glutamine	1%
FBS Supreme	10%

This cell line was established in 1989 from benign proliferative endometrium from a patient undergoing a hysterectomy for leiomyoma by Desai and colleagues (Desai *et al.*, 1994).

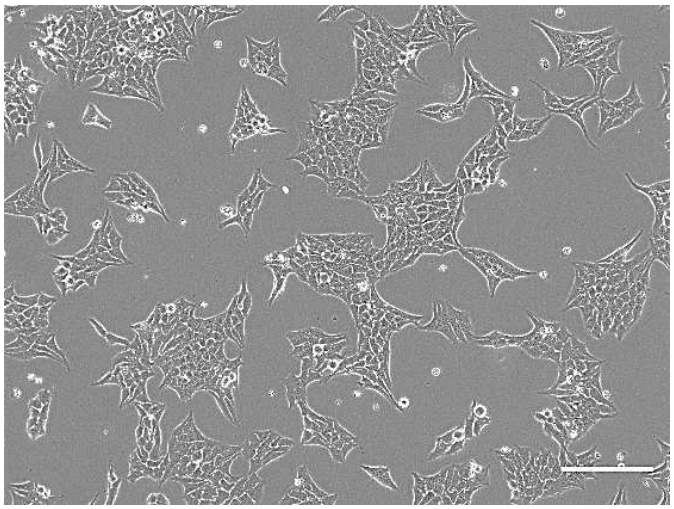

Figure 14: Phase contrast picture of EM42 cells. Passage 2. Scale bar 200 µm.

1.2 THESC CELL LINE

T-HESC (**Figure 15**) immortalized human endometrial stromal cells, were purchased in the cryopreserved state from ATCC® in complete growth medium supplemented with 5% DMSO. The cells were then cultured in the THESC culture medium (**Table 5**).

Table 5. THESC culture medium

Substance	***Concentration in Medium***
DMEM/Nutrient Mixture F-12 Ham (with L-glutamine, 15mM HEPES, and sodium bicarbonate)	88%
Hyclone Charcoal/Dextran Treated Foetal Bovine Serum	10%
ITS+ Premix Universal Culture Supplement	1%
Puromycin	0.005%
10000 U/ml Penicillin + 10 mg/ml Streptomycin	1%

This endometrial cell line was derived from stromal cells obtained from an adult female with myomas. Immortalization of primary HESC derived from secretory phase endometrium was achieved by infection with supernatant from the packaging cell line pA317-hTERT (Geron Corp.; Menlo Park, CA) which expressed the human telomerase reverse transcriptase (hTERT) and the puromycin resistance genes.

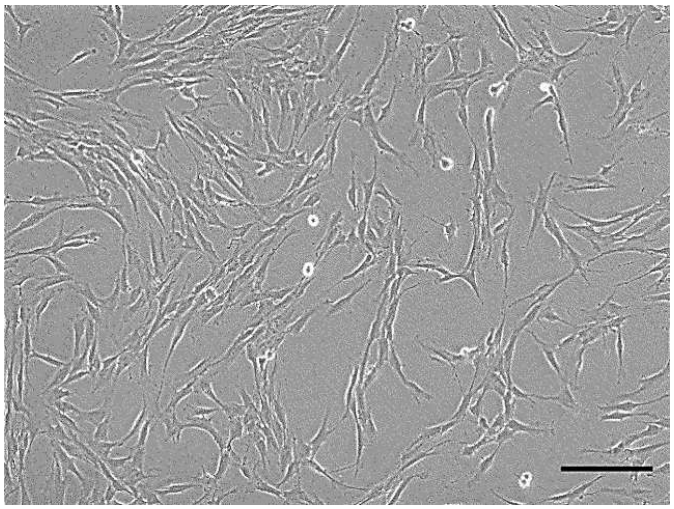

Figure 15: Phase contrast picture of THESCs. Immortalized human endometrial stromal cells were purchased in cryopreserved state. Scale bar 200 µm.

1.3 Primary Human Uterine Endothelial cells (HUtMEC)

Primary Human Uterine Microvascular Endothelial Cells (HUtMEC) (**Figure 16**) were isolated from the myometrium (middle layer of the uterine wall) from a single donor who is not pre-treated with hormones. The cells are routinely analyzed by immunofluorescent staining: they stain positive for CD31 and von Willebrand factor and negative for smooth muscle alpha-actin.

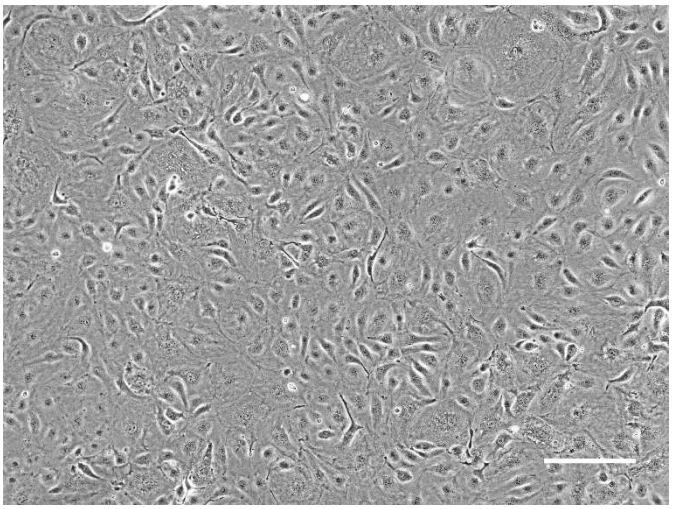

Figure 16: Phase contrast Picture of HuTMEC cells in culture. Scale bar 200 µm.

The cells, purchased from Promocell, were cultured in ECGM-MV2 Culture Medium (Promocell) supplemented with 1 % of Penicillin/Streptomycin (See **Table 6**).

Table 6: HuTMEC culture medium

Substance	***Quantity (mL)***
Endothelial Cell Growth Medium MV2	500
Supplement Mix ECGM-MV2	27.1
10000 U/ml Penicillin + 10 mg/ml Streptomycin	5

HUtMEC cells were used at early passages (P3-P5). HUtMEC are involved in medical conditions like uterine fibroma or adenomyosis. Two different donors of this cell type have been tested (**Table 7**).

Table 7. HUtMEC Donor data

	LOT NUMBER	**AGE**	**RACE**	**VIABILITY**
DONOR 1	475Z006	48	Caucasian	72%
DONOR 2	8100809	53	Caucasian	91%

1.4 Passaging and Harvesting

Prior thawing of cells, T25 culture dishes and T150 culture flasks were prepared by adding 20 ml of THESC culture medium and 25 ml of EM42 and HUtMEC culture medium, respectively (**Table 5-6**). Prefilled flasks were incubated at 37°C 5%CO_2 for 15 minutes to allow the medium to reach its normal pH (7.0-7.6). Frozen cells were thawed rapidly in the water bath (37°C) and then diluted in 5-9 ml of the respective pre-warmed culture medium. Cell number and vitality was determined with the EVE™ Automated Cell Counter. After centrifugation cells were resuspended in fresh pre-warmed medium, and then transferred to the culture vessels at the recommended seeding density (**Table 8**).

Table 8. Seeding density

Cell Type	*Seeding density/culture plate*
EM42	$1.5x10^6$ viable cells
THESC	$9.0x10^3$ viable cells
HUTMEC	$2.0x10^4$ viable cells

After three days, the culture reached a confluence of 80% and were split. Therefore, the medium was completely removed and collected to be used as a stop medium after the trypsin treatment. The cells were washed with phosphate-buffered saline (PBS) without calcium and magnesium and incubated for 5 minutes at 37°C with either 0,25% Trypsin EDTA (5x) or 0,05% Trypsin EDTA (1x) to detach THESC´s or EM42 cells and HUtMECs, respectively. Detachment of the cells was observed under the microscope followed by the addition of stop medium (containing FCS). They were rinsed off with PBS and centrifuged. Medium supernatant was removed, and the cell pellet was resuspended in 1 ml fresh culture medium. Subculture ratios ranged between 1:8-1:10 for THESC cells with 5-$6x10^5$ cells per dish, and around $1,5x10^5$ cells per flask for EM42 cells.

1.5 Counting

The viability and number of cells was assessed at every passaging step. Cells were then washed with 1 ml PBS and treated for 5 minutes at 37°C with the respective amount of trypsin/EDTA. depending on cell type. Subsequent the detachment of the cells, 400 µl of stop medium were added to the well and cell suspension was transferred in a 1.5 ml tube. To make sure that no cells remained attached to the bottom of the well, two washing steps with 400 µl PBS (-) were performed. Cell suspension was centrifuged at 125g for 7 minutes, the supernatant removed, and cell pellet resuspended in 200 µl fresh pre-warmed assay medium. EVE Automated Cell Counter EVE™ is a bench-top size cell counter that is designed to count cells and verify viability (live, dead, and total cells) using trypan blue staining.

2. EXPERIMENTAL SET UP

The following experiments were performed at Bayer AG, Advanced Cellular Models Lab and TISSUSE GmbH Berlin, Germany, according to the Scheme reported in Figure 17. Under static conditions culture 24 well plates were tested and for the dynamic in addition to the standard HUMIMIC Chip2 96-well Polydimethylsiloxane (PDMS) version was also used a PDMS-free Prototype of the HUMIMIC Chip2 96- well made with cyclic olefin copolymer (COC version).

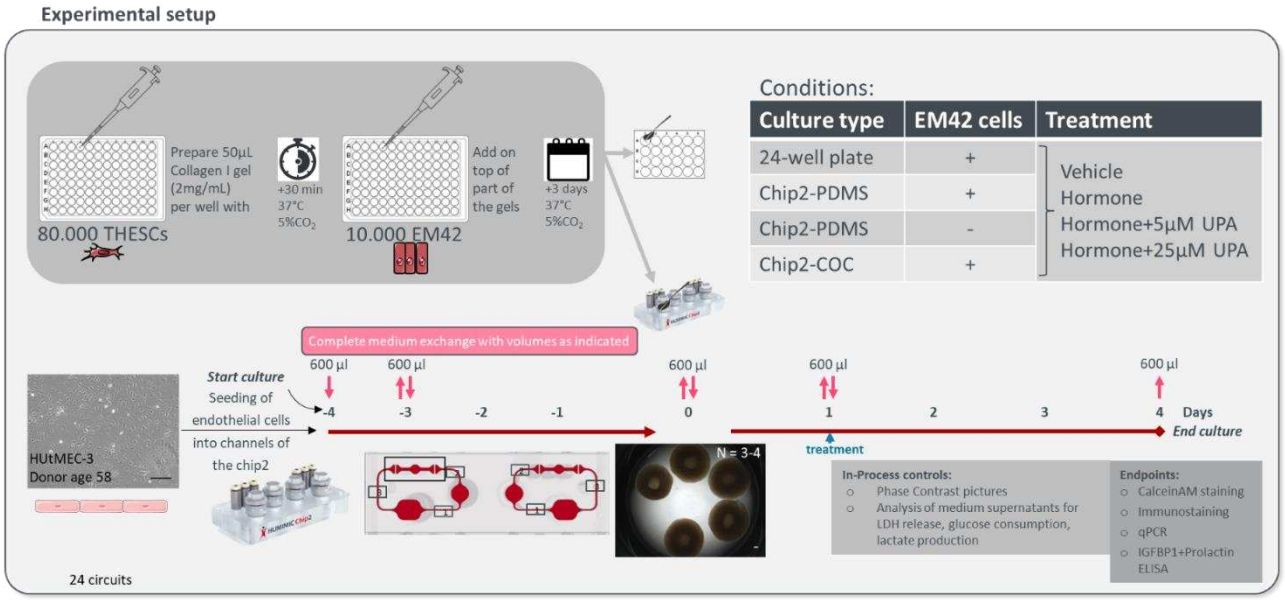

Figure 17: Schematic of Experimental Set Up.

2.1 COLONIZATION OF THE HUMIMIC CHIP2 96-WELL CHANNELS WITH HUTMECS

The Chip2 was coated with collagen IV and fibronectin one day prior to colonization of the channels with HUtMECs (endothelialization) to ensure adherence of the endothelial cells to the surface areas of the Chip2. An injection kit (HUMIMIC injectfit C2-96) provided bei Tissuse was used to endothelialize the Chip. Stock solutions of 1mg/mL collagen IV and 0.5mg/mL fibronectin in cell culture-grade water were prepared. For each circuit, 150 µL coating solution containing 40% cell culture grade water, 40% of the 1mg/mL collagen IV and 20% of the 0.5mg/mL fibronectin solution. Thereafter, the channels of each chip were then washed twice with PBS. and with the help of syringes, the coating solution was injected homogeneously.

The coating solution was injected with syringes homogeneously. The chips were incubated with the coating solution overnight in the incubator (37°C, 5%CO_2) without pumping. Prior to seeding, each

Multi Organ Chip (MOC) was washed twice with PBS and afterwards flushed with HUtMEC culture medium.

HUtMECs of passages 4 or 5 were harvested from expansion cultures. The cell suspension was concentrated by centrifugation and cell counts were performed. Centrifuged cells were resuspended with HUtMEC culture medium to a final concentration of 25x106 cells/mL. Afterward, 100 µL of the cell suspension was transferred to a 1 ml syringe. The cells were injected through one of the two compartments of each circuit. A syringe containing approximately 30 µL of cell culture medium was connected to the second compartment. After even cell infusion into both circuits, the device was incubated in 5% CO2 at 37 °C under static conditions for 3 h to allow the cells to attach to the channel walls. The chip was cultured upside down for the first 0.5 - 1 h. The HUMIMIC inject kit was then exchanged to standard culture compartments and an amount of 300 µL fresh HUtMEC culture medium was added to each compartment. Using the on-chip micro-pump, the medium was then flushed through the PDMS channels of each circuit. A pressure and vacuum of +/- 300 mbar, respectively, and a frequency of 0.5 Hz (30 beats per minute) was applied to every microvascular circuit of the chips for continuous dynamic operation.

Every 1-3 days the medium in the culture compartments was completely replaced by fresh culture medium. Cell growth and viability were monitored by light microscopy. The endothelialized chips were run for 3-4 days prior to the co-culture. At the end of each experiment, cell viability was determined with by calcein AM staining and subsequent fluorescence microscopy analysis. Cultures were fixed and stained with endothelial specific markers at the end of the culture.

2.2 3D DROPLETS GENERATION

In order to determine the number of cells which were used in monolayer and 3D culture, De Leo's group of Bayer AG laboratories calculated epithelial/stromal cell ratios from endometrial tissue samples after performing a DAB immunohistochemistry staining for CD10 (method not included). Individual pixels were classified into three categories; Stroma, Epithelial and Other; using the software Ilastik (https://www.ilastik.org/) based on the 5x images. The 'Other' category mainly included empty areas without cells. The number of pixels, that represent the reporting area for each group, was used as an estimation of the number of cells for that class (**Figure 18** and **Figure 19**).

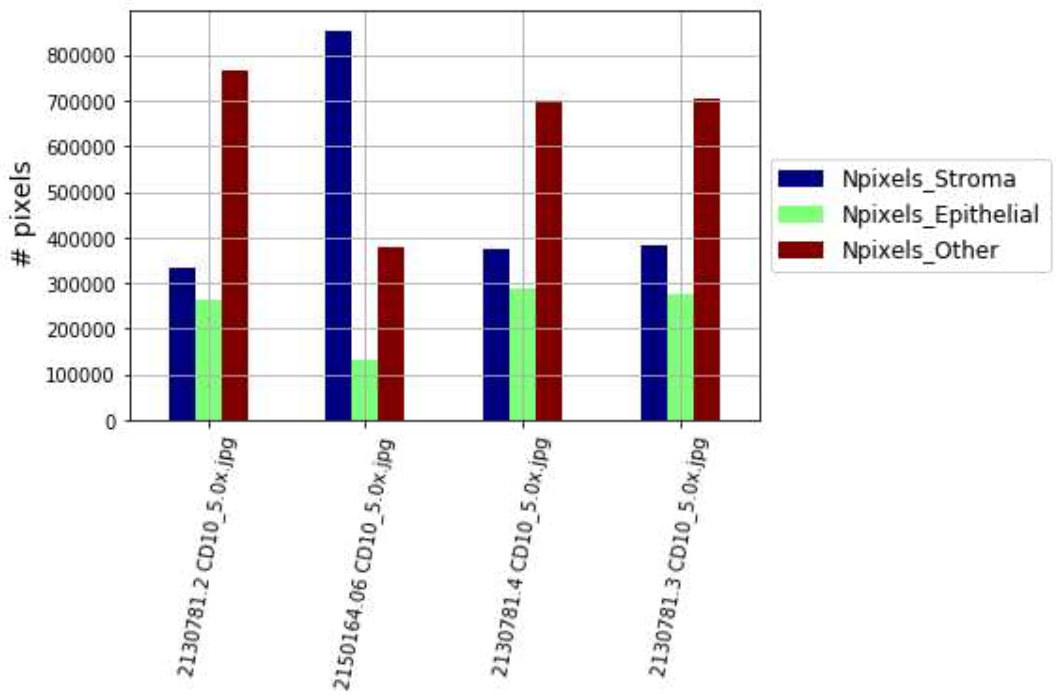

Figure 18*:* Number of pixels for each category from tissue sample pictures. The number of pixels that represent the reporting area for each category was used as an estimation of the number of cells in that class. Stroma (blue), Epithelial (green), Other (red). The Other category included empty areas without cells.

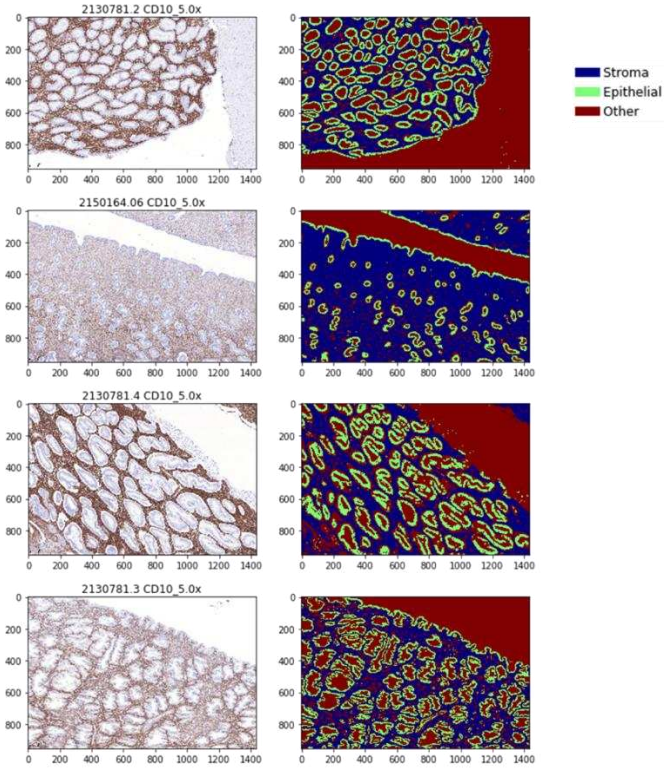

Figure 19: Endometrial tissue sample images analysed with Ilastik software to determine epithelial:stromal cell ratio. Individual pixels were classified into three categories (see right column): Stroma (blue), Epithelial (green) and Other (empty areas in red). Pictures´ magnification: 5x

3D constructs contained $8 \cdot 10^4$ THESCs (if not stated otherwise) embedded in 2 mg/ml collagen I. A master mix of 10x PBS with Ca/Mg, 2 M NaOH and distilled H2O was prepared according to manufacturer's instruction, aliquoted at 420 µl and stored on ice. 1.5mL reaction tubes containing the required cell number of $8 \cdot 10^4$ cells per 5 µL, sufficient for 13 gels, and stored on ice. Subsequently, 280 µl 5 mg/ml collagen I stock solution was added to one aliquot of the master mixes and mixed thoroughly. 50 µl of the prepared cell-collagen mix were added to each well of a 96-well flat bottom ULA plate. Subsequently, the plate was stored for 30 min at 37 °C. Polymerization of the collagen I gel was stopped by the addition of 50 µl collagen gel medium. The process was repeated until the required amount of collagen I constructs was prepared. The collagen constructs with 8-10·103 EM42 cells in 100 µL were added carefully on top of the polymerized THESC´ domes.

2D STATIC

THESCs, EM42 cells, HUtMECs were harvested and seeded into 24-well plates with $8 \cdot 10^4$ cells per well for THESCs, $8 \cdot 10^3$ - $15 \cdot 10^4$ cells for EM42 cells, $5 \cdot 10^4$ cells for HUtMECs and $8 \cdot 10^4$ THESCs plus $8 \cdot 10^3$ EM42 cells for MIXED cultures. The plates were then cultured (30 min - 4 days, depending on the experimental setup) under standard cell culture conditions until the start of the treatment described. The 400 µL of medium was exchanged completely every 2-3 days and at the beginning of the treatment. The cells were cultured, and the assay was performed in their corresponding culture medium or spheroid culture medium depending on the experiment.

3D STATIC

Three days after 3D model formation, they were pooled in a 24-well ULA plate. 2-5 collagen constructs were transferred with the help of a sterile spoon from the 96-well plate into each well of the 24-well ULA plates already prepared with 400 or 600 µL of fresh pre-warmed culture medium depending on the experimental setup.

2.3 IN VITRO DECIDUALIZATION ASSAY

One to three days after starting the culture (either seeding in static conditions or starting the 3D/chip culture), cultures were treated in a formulation media made for the multi-cellular model (**Table 9**) with a decidualization cocktail, containing 500µM 8-BR-cAMP, 1µM MPA, 10nM E2 (**Table 10**), to mimic the *in vivo* process of decidualization.

Table 9: Multicellular model culture media

Substance	*Quantity*
ECGM - MV2 (BASAL MEDIUM W/O SUPPLEMENTS)	94%
HYCLONE CHARCOAL/DEXTRAN TREATED FETAL BOVINE SERUM	5%
10000 U/ml Penicillin + 10 mg/ml Streptomycin	1%
ASCORBIC ACID PHOSPHATE	1 µg/ml

Table 10: Compounds for the decidualization experiment

Name	Item	Vendor	Concentration [g/l]	Storage Conditions
Hormone cocktail	Medroxyprogesterone 17-acetate	Sigma (M1629-1G)	10 mM	-20°C in DMSO
	β-Estradiol	Sigma (E2758-250MG)	10 mM	-20°C in DMSO
	8-Bromoadenosine 3',5'-cyclic monophosphate	Sigma (B5386-100MG)	100 mM	-20°C in PBS
UPA	Ulipristal acetate	Sigma (SML1469-10MG)	5, 25 µM	-20°C in DMSO

Ulipristal acetate (UPA), a selective progesterone receptor modulator was added 30min or 1h prior to adding the decidualization cocktail at concentrations of 5 or 25µM, to test an inhibitory effect on the induced decidualization process. A vehicle control treated with 0.1% DMSO in the respective culture medium was run in parallel (**Table 8**). The treated cultures were incubated for 72h under standard cell culture conditions. After 72h, medium supernatants and endometrial models were collected and used for further endpoint analysis.

Table 11. Treatments summary

Condition	*Cocktail*	*Medium volume (µl) x well*	*Cocktail volume (µl) x well*
VEHICLE	DMSO + Medium	300 µl	100 µl
HORMONES	MPA+E2+Br-CAMP + Medium	300 µl	100 µl
SUBSTANCE+HORMONES	Ulipristal in DMSO + Medium and MPA+E2+Br-CAMP + Medium	200 µl	100 µl and 100 µl

3.ENDPOINT ANALYSIS

3.1. METABOLIC PROFILE

In order to monitor cell death and/or cell proliferation in the chip cultures, LDH, Glucose and lactate concentrations were measured by the BAYER Advanced Cellular Models Lab and TissUse central laboratory in parallel with other measurements (as IGFBP1 and PRL release in the media).

3.1.1 GLUCOSE

Media collected during the medium exchange were measured by the TissUse and or BAYER AG laboratory in parallel with other measurements using the Glucose Hexokinase kit (Thermo Fisher Scientific) according to the manufacturer's instructions on an Indiko Plus chemical analyzer (Thermo Fisher Scientific). The quantification of glucose is based on a photometric analysis. The assay principle is as follows: using ATP, glucose is phosphorylated to glucose-6-phosphate, in a reaction catalyzed by hexokinase (HK):

$$glucose + ATP \xrightarrow{HK} glucose\ 6 - phosphate + ADP$$

The formed glucose-6-phosphate is further oxidized to 6-phosphogluconate while NAD+ is reduced to NADH/H+, in a reaction catalyzed by Glucose-6-phosphate dehydrogenase (G-6-P-DH):

$$glucose\text{-}6\text{-}phosphate + NAD^+ \xrightarrow{G\text{-}6\text{-}P\text{-}DH} 6\text{-}phosphogluconate + NADH/H^+$$

The reduction of NAD^+ to $NADH/H^+$ leads to a shift in the ultraviolet absorption spectrum of the molecule. Therefore, an increased absorption of ultraviolet light at a wavelength of 340 nm can be directly correlated with the glucose concentration in the sample. The results of the photometric analysis are calculated automatically by the Indiko Plus based on a two-point calibration with substrate calibrator serum (sCal) and 0.9% NaCl performed every 30 days or in case of reagent batch change. A quality control is measured before starting the measurements using abnormal (Abtrol) and normal (Nortrol) human control serum (Thermo Fisher Scientific).

3.1.2 LACTOSE

Lactate concentrations of conditioned medium were measured using the Fluitest® Lactate kit (Analyticon® Biotechnologies) on an Indiko Plus chemical analyzer (Thermo Fisher Scientific). The quantification of lactate is based on a photometric analysis. The assay principle is as follows: Lactate is cleaved to pyruvate and H2O2 in a reaction catalyzed by lactate-oxidase (LOX):

$$L\text{–}\,lactate + O_2 \xrightarrow{LOX} pyruvate + H_2O_2$$

The produced H2O2 is used to generate a colored dye, by the conversion of 2,4,6-tribromo-3-hydroxybenzoic acid (THB) and 4-aminoantipyrine (4-AAP) to a red quinoneimin dye in a reaction catalyzed by peroxidase (POD):

$$2\ H_2O + THB + 4AAP \xrightarrow{POD} quinoneimin + 4\ H_2O$$

The color reaction is proportional to the lactate concentration in the medium and leads to a linear decrease in absorbance at a wavelength of 510 nm. The results of the photometric analysis are calculated automatically by the Indiko Plus based on a two-point calibration with lactate calibrator (R4 provided in the kit) and 0.9% NaCl performed every 3 days or in case of reagent batch change. A quality control is measured before starting the measurements using abnormal (Abtrol) and normal (Nortrol) human control serum (Thermo Fisher Scientific).

3.1.3 Lactate dehydrogenase

Lactate dehydrogenase (LDH) is a cytoplasmic enzyme which is ubiquitously present in nearly all living cells. In case of cell damage, LDH is released into the extracellular space. Based on this, LDH can be used as a biomarker for cellular cytotoxicity and cytolysis.

In order to monitor cell death and/or cell proliferation in the chip cultures, LDH concentrations were measured by the TissUse central laboratory in parallel with other measurements using the LDH IFCC kit (Thermo Fisher Diagnostics) on an Indiko Plus chemical analyzer (Thermo Fisher Scientific). The quantification of LDH is based on a photometric analysis. The assay principle is as follows: LDH catalyzes the oxidation of lactate to pyruvate with a concomitant reduction of NAD+ to NADH:

$$L\text{–}\,lactate + NAD^+ \xrightarrow{LDH} pyruvate + NADH/H^+$$

The reduction of NAD+ to NADH leads to a shift in the ultraviolet absorption spectrum of the molecule. Therefore, an increased absorption of ultraviolet light at a wavelength of 340 nm can be directly correlated with the LDH concentration in the sample. The results of the photometric analysis are calculated automatically by the Indiko Plus based on a two-point calibration with enzyme calibrator serum (eCal) and 0.9% NaCl performed every 10 days or in case of reagent batch change. A quality control is measured before starting the measurements using abnormal (Abtrol) and normal (Nortrol) human control serum (Thermo Fisher Scientific). LDH release per day (mU/day) was then

calculated by dividing the LDH concentrations by the total medium amount changed inside the chip (full medium exchange) per exchange and the number of days between the media exchanges.

3.2 Imaging

Cells and Chips were checked with the Confocal DMI8 LEICA microscope using LAS X Sofware. Brightfield, phase contrast and fluorescent images (4x, 10x, 20x magnification) were taken every day during the experiment and after immunohistochemistry procedures.

3.2.1 Calcein AM

The CellTrace™ Calcein-AM dye (Thermo Fisher) stains live cells in culture. After permeating the cell membrane, cellular esterases are converting the nonfluorescent dye into green fluorescent calcein by an acetoxymethylester hydrolysis (User Guide Calcein AM). First, a staining solution containing HUtMEC culture medium supplemented with 1 µg/mL Calcein-AM was prepared. The medium on top of the cells was removed from the cell culture compartments of the chip and the staining solution was added to both compartments of each circuit at a volume of 300 µl for staining of HUtMECs in the microfluidic channels. The chip was pumped for 5min with the integrated micropump and then incubated under static conditions at 37°C, 5% CO_2 for further 30 min. Thereafter, the micro-channels were washed twice with medium by replacing the medium in the compartment inserts with fresh medium. Live and dead cells were visualized immediately after finishing the staining using an inverted fluorescence microscope.

3.2.2 Cryosectioning

One 3D model construct from each replicate was collected at the endpoints of the experiment and embedded in a cryomold by covering with Tissue-Tek®. Collagen constructs were fixed with 150 µL 4% paraformaldehyde for 1h followed by a dehydration step prior to embedding. Dehydration was achieved by incubation the samples in 15 % sucrose at 4 °C overnight followed by an overnight incubation in 30 % sucrose at 4°C. Subsequent embedding, the samples were snap-frozen and stored at -80 °C until further processing. The sectioning was carried out using a cryostat (Leica CM1950). The tissue slices prepared were 8-µm thin and four slices were always combined on one glass slide. The glass slides were stored at RT for drying and, subsequently, stored at -20 °C until staining.

Tissue slides were fixed in acetone at -20 °C for 10 min, shortly dried at RT and encircled with Pap pen liquid blocker. Thereafter, slides were washed two times in PBS for 5 min each and staining was performed with 30 µL staining solution per section as described above for 2D cultures.

3.2.3 Histology/IF Staining

Immunofluorescence (IF) was performed to analyze cells cultured in monolayer after fixation in 4% PFA as well as sections of the 3D models after cryo-sectioning or on Chip2 channel to visualize Endothelial cells. The staining followed a two-time PBS wash. After shortly drying the slides, stained tissue sections were embedded by coverslips using mounting medium. Mounting solution was dried for 1h at RT and thereafter either directly analyzed or stored at -20°C. Images were taken using an inverted fluorescence microscope (Keyence) and staining normalized to respective negative control.
To allow the identification of stromal and epithelial cells, cryosections and cells from monolayer culture were stained with the epithelial marker Cytokeratin8/18 (Santa Cruz biotechnology Inc., sc-70939) and the stromal marker Vimentin (Thermo Fisher Scientific, PA5-27231). Endothelial cells were stained for VE-Cadherin (Abcam, Ab33168).

2D cultures

In monolayer cell culture, the corresponding wells were fixed in 4% paraformaldehyde (PFA). The medium was removed, the cells washed with 1 ml PBS for 5 min and 200 µl of PFA was added into the wells. After 10 min incubation at room temperature, the wells were washed twice with 1 ml PBS (-). Fixed cells were stored at 4°C with 2 ml PBS (-).
Following fixation, the wells were filled with 150 µl of 0.2% Triton X100 in PBS (-) for the membrane permeabilization. Antibodies were diluted in PBS with Ca/Mg containing 10 % goat serum and 150 µL added to each well. Negative control was covered by PBS with Ca/Mg containing 10 % goat serum only. First antibody was incubated overnight at 4 °C in a wet chamber or 2h at room temperature. The wells were then washed two times by PBS with Ca/Mg for 5min each. Secondary antibodies (**Table 12**) were diluted in PBS containing 1 µg/ml DAPI. Cells, covered with 150 µl antibody/DAPI mix, were incubated for 45 min at RT in the dark. The staining followed a two-time PBS wash. The wells were filled with 2 ml PBS and observed under fluorescence microscope.

HUMIMIC CHIP2 96-WELL

After finishing the chip culture, the HUtMECs were fixed inside the microvascular circuit with 200 µL of 4% PFA for 5 min, rinsed twice with 300 µL PBS for 3 min (all with pumping and volumes given per compartment) and stored filled up with PBS at 4°C. Prior to starting the staining procedure, the chips had to be permeabilized with 0.2% TritonX-100 in PBS (-/-). 400 µL of the solution was added to each circuit (200 µL per compartment) and incubated 5 min with pumping and 5min statically at room temperature.

Staining for primary and secondary antibodies was performed (**Table 12**), as described above with the difference that at the beginning of each incubation step the chip was pumped for 5 minutes to ensure even distribution inside the chip. All microvascular channels were imaged through their microscope slide wall. Images were taken directly after the staining using a confocal fluorescence microscope LEICA.

Table 12. List of Antibodies

Antibody	***1° or 2°***	***Anti-***	***Concentration***	***Dilution***
Goat Anti-Rabbit IgG (H+L) Alexa Cf®488	2°	Rabbit	2 mg/ml	1:200
Goat Anti-Mouse IgG (H+L) Alexa Cf®594	2°	Mouse	2 mg/ml	1:200
Cytokeratin 8/18	1°	Mouse	200µg/ml	1:100
Vimentin	1°	Mouse	1.04 mg/ml	1:100
Vimentin	1°	Rabbit	200µg/ml	1:200
VE-CADHERIN	1°	Mouse	1.5 mg/ml	1:200
Goat Anti-Rabbit IgG (H+L), Highly Cross-Adsorbed CF488	2°	Rabbit	2 mg/ml	1:200

3.3 HORMONE SECRETION

Decidualized endometrium synthesizes and secretes a 32-kDa insulin-like growth factor-binding protein (termed hIGFBP-1) at high levels during the first trimester of pregnancy. IGFBP-1 is the major soluble protein product of this tissue and is principally localized to the differentiated endometrial stromal cell, the decidual cell (Bell *et al.*, 1991). Moreover, also the secretion of the Prolactin in this decidualized models was investigated. Prolactin is secreted by the decidualized endometrium at the time of predicted conception and, in the event of pregnancy, local expression and secretion of prolactin persists until term. Prolactin mediates its effect on target cells through interaction with single-pass transmembrane receptors (Jabbour and Critchley, 2001).

3.3.1 IGFBP1 ELISA

The procedure was performed using Human IGFBP1 ELISA Kit (AB233618) from Abcam according to the manufacturer's instructions.

Media samples of different conditions collected 72 hours after treatment were stored at -20°C. After thawing, treated samples were diluted 1:2, 1:5, 1:10 or 1:20, depending on the experiment by mixing the sample with Calibrator Diluent RD5P, while untreated samples were used without dilution. For each condition three to four biological replicates were analyzed.

A dilution series of the Human IGFBP-1 Standard was prepared before starting the assay. Absorbance was measured at 450 nm using a microplate reader (CLARIOstar). In order to determine sample concentrations, all measured values were blank-corrected, the average over replicates calculated and the standards plotted against their concentrations. A 4-parameter fit of standard concentrations was modeled. The resulting regression equation was applied to determine IGFPB1 sample concentrations. The whole calculation was carried out by MARS data analysis software. Lastly, the dilution factor was calculated out and the total amount of IGFBP1 (pg/ml) determined.

3.3.2 Prolactin ELISA

The procedure was performed using Human Prolactin/PRL ELISA Kit is a single-wash 90-min SimpleStep ELISA® from Abcam ab226901 according to the manufacturer's instructions. Media samples of different conditions collected 72 hours after treatment were stored at -20°C. All samples were used without dilution. For each condition three to four biological replicates were analyzed.

A dilution series of the Human Prolactin Standard was prepared before starting the assay. The readout relied on absorbance at 450 nm using a microplate reader (CLARIOstar). In order to determine sample concentrations, all measured values were blank-corrected, the average over replicates calculated and the standards plotted against their concentrations on a log/log graph. A 4-parameter fit of the standard concentrations was modeled. The resulting regression equation was applied to determine Prolactin sample concentrations. The whole calculation was carried out by MARS data analysis software. Lastly, the dilution factor was calculated out and the total amount of Prolactin [ng] per mL determined.

3.4 Gene expression

The transcription of genes known to be involved in the endometrial decidualization process was analysed by a qPCR and ddPCR proceeding with the following steps.

3.4.1 Samples preparation

In order to perform the RNA isolation, cells from 2D culture and spheroids from 3D culture of different conditions, collected four days after seeding (Day 1), and three days after treatment (Day 4), were washed with PBS, centrifuged and then resuspended in respective lysis solution: 100 µl of Lysis buffer 1 (LB1), for samples with less than 1.5*105cells, or 300 µl of RA1 with β-Mercaptoethanol (>1.5*105 cells). Subsequently samples were snap-frozen in liquid nitrogen and stored at -80°C until further processing.

3.4.2 RNA isolation

After thawing, RNA isolation was performed using the RNeasy® Micro kit from QIAGEN according to the manufacturer's instructions. The cell lysate was then transferred into a silica membrane and processed. Genomic DNA was digested by DNase and several washing steps ensured further purification. The final elution step of RNA was conducted in 15 µl of RNase-free water for LB1 samples and 50 µl RNase-free water for RA1 samples. The RNA concentration and purity were measured at 260 and 280 nm with the CLARIOstar® Platereader® in the LVis plate. The absorbance at 280 nm provides information regarding RNA concentration while the purity of the RNA is determined by the absorbance ratio at 260 nm and 280 nm: a concentration higher than 5 ng/µl and a purity ratio of 1.8-2.0 indicated that the RNA could be used for reverse transcription into cDNA. Isolated RNA was then stored at -80 °C until further processing.

3.4.3 cDNA transcription

For the reverse transcription of RNA into cDNA the TaqMan® Reverse Transcription Kit from Thermo Fisher was used. For comparability, 100 ng of cDNA was transcribed for each sample.
First the required volume of RNA was determined:

$$\text{Volume of RNA [µl]} = \frac{150\ \text{ng}}{\text{RNA Concentration } [\frac{\text{ng}}{\text{µl}}]}$$

The right amount of RNA was then mixed with RNA-free water to reach the volume of 10.1 µl. After the preparation of the RNA, 10.1 µl of RNA/H_2O mixture was mixed with 9.9 µl master mix (**Table 13**).

Table 13. Master mix for RNA transcription. Volumes given refer to one sample.

Solution	*Volume [µL]*
TaqMan Buffer (10x)	2.0
$MgCl_2$	1.4
dNTPs	4.0
Random hexamer	0.5
Oligo dTs	0.5
RNase Inhibitor	1.0
Reverse Transcriptase	0.5
Total volume	**9.9**

The samples were then centrifuged, and the reverse transcription was started using the QuantStudio™ 5 Real-Time PCR System. The five minutes annealing step at 65 °C is followed by an elongation step of 30 minutes at 37 °C. The last step, the inactivation of the reverse transcriptase, was performed for five minutes at 95 °C (**Table 14**). The resulting cDNAs were stored at -20 °C to be then processed for the qPCR.

Table 14. Thermal profile of the cDNA synthesis

Process	*Temperature*	*Time*
Annealing	65°C	5 min
	4°C	2 min
Elongation	37°C	30 min
Inactivation	95°C	5 min

3.4.4 qPCR

Real-time PCR technique can be classified by the chemistry used to detect the PCR product, specific or non-specific fluorochromes. In these experiments the non-specific detection method, using double-stranded DNA-binding dyes (SYBR® Green) as reporters, was performed. The SYBR® Green binds to all double-stranded DNA which was synthesized in the qPCR reaction, causing a fluorescent signal that can be detected. An increase in DNA product during the qPCR therefore leads to an increase in fluorescence intensity measured at each cycle. In order to check for specific qPCR products, the analysis of the melting curve (64°C-95°C) was included in the procedure. qPCR experiments were conducted using SensiFAST™ SYBR® Lo-ROX kit and a QuantStudio™ 5 Real-Time PCR 384-well block. The final 10 µl qPCR mixture for each sample consisted of 2.5 µl of primer mix and 7.5 µl of cDNA mix. Once both mixtures had been prepared (**Table 15**), first the primer mix was

pipetted to the bottom of the PCR microplate and then the cDNA mix was dispensed at the side of the well.

Table 15. Volumes for the cDNA Mix each primer

Solution	***Volume [µL]***
SensiFAST SYBR Lo-ROX kit	5
cDNA	0,5
H_2O	2

The plate was centrifuged at 2000 rpm for 1 min before inserting it into the thermal cycler. An appropriate plate layout was prepared beforehand including housekeeping genes (**Table 16**) on each qPCR plate, technical replicates (duplicates) of each sample, a negative control using water instead of cDNA in order to check for the purity of the reaction mixture, a positive control using cDNA of the universal RNA and a tissue positive for the genes of interest. The housekeeping (HK) are genes that are not influenced by any of the experimental parameters (e.g., the application of a substance). This means that they retain a stable level of expression throughout the entire experiment. To select the more appropriate calibrator gene, the expression levels obtained from each sample of six housekeeping genes (HKGs) were analyzed with the use of two different Visual Basic (VBA) applets, geNorm (integrated in the qbase+ software at: https://www.qbaseplus.com) and Normfinder (https://moma.dk/normfinder-software). The geNorm analysis ranks selected HKGs according to the determined control gene-stability measure (M, average pair-wise variation of a particular gene with all other control genes), from the most stable (lowest M values) to the least stable (highest M values). Normfinder ranks the set of candidate genes according to their expression stability value in a given sample set and a given experimental design.

Table 16: PrimePCR Gene Expression Probe Assays

Target Genes	**Acronym**	**ID assay**
Estrogen Receptor1	ESR1	Hs00174860_m1
FK506 binding protein 5	FKBP5	Hs1561006_m1
Insulin-like growth factor-binding protein-1	IGFBP-1	Hs00236877_m1
Prolactin	PRL	Hs00168730_m1

Progesterone	PGR	Hs00172183_m1
Prostaglandin E Synthase 2	PTGES2	Hs00228159_m1
Zinc Finger and BTB Domain Containing 16	ZBTB16	Hs00121213_m1
Reference Genes	**Acronym**	**ID assay Probe**
Hypoxanthine-Guanine Phosphoribosyl Transferase 1	HPRT1	dHsaCPE5192871
Glyceraldehyde-3-phosphate dehydrogenase	GAPDH	Hs02706624_g1

3.4.5 ARRAY

TaqMan™ Array Human Extracellular Matrix & Adhesion Molecules (Thermo Fisher, 4414133) panel targets genes involved in ECM structure & remodeling, defining connective tissue, cell adhesion, transmembrane inhibitors, basement membrane construction and collagen proteins. Gene Signature Plates are 96-well plates that are pre-configured with the most appropriate TaqMan™ Gene Expression Assays for a specific biological process, pathway, or disease state. Each plate contains predefined assays and endogenous controls dried-down in the wells, ready for accurate assessment of an entire gene signature in one simple experiment. Set up the thermal protocol for your instrument. TaqMan® Fast Advanced Master Mix (StepOnePlus™, ViiA™ 7, and QuantStudio™ systems with fast cycling mode) **Table 17**.

Table 17. TaqMan® Fast Advanced Master Mix with fast cycling mode)

Cycling Step	**Temperature**	**Time**
Enzyme activation	95°C	20 seconds
Denature	95°C	3 seconds
Anneal/ Extend	60°C	30 seconds

3.4.6 QPCR DATA ANALYSIS

For all qPCRs the passive reference dye ROX was applied to normalize signals and thus to reduce the variance between technical replicates. QPCRs using SYBR Green assay additionally executed a melting curve analysis in order to distinguish products from e.g., primer-dimers. Threshold cycle (Ct)

values were automatically determined by QuantStudio Software. From these data, relative fold gene expression levels were calculated with the help of the comparative Ct method (ΔΔCt):

(1) ΔCt was calculated for each sample using the mean values of technical replicates.

$$\Delta Ct = CtTarget - CtHousekeeper$$

(2) ΔΔCt values were determined from ΔCt of the treated sample (test condition) subtracted by the mean ΔCt values of all control samples.

$$\Delta\Delta Ct = \Delta CtTest\ condition - mean\ \Delta CtControl$$

(3) Relative fold gene expression levels were calculated as follows:

$$Fold\ change = 2^{-\Delta\Delta Ct}$$

Average fold changes were calculated from geometric means as gene expression data were shown to be log-normally rather than normally disturbed. For this reason, the statistical analysis of differences between test groups was based on delta Ct values since normal distributed values were required for subsequent analysis. In addition, homogeneity of variance was confirmed by graphical evaluation. Differences between groups were evaluated for each gene by Multiple t-test using Holm-Sidak post hoc test and delta Ct values for $n > 2$. Differences were considered significant for $p < 0.05$.

3.4.7 ddPCR

The ddPCR is a method that uses an emulsion PCR technology, and it provides a series of steps that lead to the generate tens of thousands, even millions, of single water-in-oil droplets. The droplets serve as sample dispersion carriers for digital PCR and the fluorescence signal within each droplet is detected at the end of the PCR reaction. The droplets in which the amplification reaction of the target gene took place were defined as positive and are fluorescent, a characteristic that their reading through a fluorescence detector; droplets that do not contain the target gene were defined as negative and they were not fluorescent. The primer assays used in this study are shown in **Table 18**. The ddPCR method was applied using the QX200™ Droplet Digital™ PCR System (Bio-Rad Laboratories, Hercules, CA, USA). The samples were prepared, in a 96-well PCR plate, using a reaction mix shown in the following tables.

Table 18. ddPCR Supermix for Probes (No dUTP*)*

2x ddPCR Supermix for Probes (No dUTP)	11µl
20x target probe (FAM)	1.1µl
RNase-free sterile water	6.3µl
cDNA	2.5µl
Total	22µl

Each 20 µl ddPCR reaction was loaded into an 8-channel droplet generation cartridge (Bio-Rad Laboratories, Hercules, CA, USA); 70 µL of QX200 Droplet generation oil (Bio-Rad Laboratories, Hercules, CA, USA) were added into the appropriate wells and the cartridge was loaded in the QX200™ Droplet Generator (Bio-Rad Laboratories, Hercules, CA, USA) to generate the emulsion. The system generates until 20000 droplets in the superior row of the strip, that are transferred in a 96-well plate (Bio-Rad Laboratories, Hercules, CA, USA) plate that is sealed with a PX1 PCR plate sealer at 175°C and amplified by standard PCR using T100™ Thermal cycler (Bio-Rad Laboratories, Hercules, CA, USA).

Table 19. ddPCR Supermix for Probes (No dUTP)

Cycling step	**Temperature**	**Time**	**Ramp rate**	**Number of cycles**
Enzyme activation	95°C	5 min	2°C/sec	1
Denaturation	95°C	30 sec		40
Annealing	58°C	1 min		40
Signal Stabilization	4°C	5 min		1
	90°C	5 min		1
Stabilization	4°C	30 min		1
Hold	4°C	Infinite		1

After PCR reaction (**Table 19**), the plate is stored at 4°C for 24h to stabilize the droplets. After other 30 min at room temperature, the plates were loaded into QX200™ Droplet Reader (Bio-Rad Laboratories, Hercules, CA, USA) for detection, whereby the instrument aspirates the droplets with a needle, separates and aligns each droplet, that is analyzes by two lasers to detect fluorescence. In the final step, the analysis of the data is represented in graphs as EvaGreen® fluorescence relative to each droplet (Event Number). The software is used for data acquisition to calculate the absolute

concentration of target DNA in copies/µl of reaction using Poisson distribution analyses. Primers used in this thesis are Bio-Rad validated primers.

3.4.8 ddPCR DATA ANALYSIS

The software QuantaSoft (Bio-Rad Laboratories, Hercules, CA, USA), provided with the ddPCR system, is used for data analysis; according to international guidelines, only reactions having more than 10,000 droplet events may be analysed. Discrimination between droplets that did not contain target (negatives) and those that did (positives), is achieved by applying a global fluorescence amplitude threshold in QuantaSoft. The data from the ddPCR are given in target copies/µl reaction. Template copies/µl present in the initial sample are then calculated using Poisson statistics.

$$\lambda = -\ln(1-p)$$

In this equation, λ represents the average number of target DNA molecules per replicate reaction and p represents the fraction of positive end-point reactions. From λ, together with the volume of each replicate PCR and the total number of replicates analyzed, an estimate of the absolute target cDNA concentration is calculated. QuantaSoft uses a proprietary signal processing algorithm to automatically perform droplet gating within each run. The threshold was set as the midpoint between the average fluorescence amplitude of positives and negative droplet clusters. In digital PCR an increase of number of replicates produces approximately an increase of dynamic range. Increasing the number of partitions also improves the precision and for this reason it enables resolution of small concentration differences between nucleic acid sequences in a sample.

3.4.9 ddPCR STATISTICAL ANALYSIS

All the data have been normalized using the geometric means of reference genes, and the relative gene expression has been shown as Normalized Sample Amount (NSA). As evaluation of ddPCR gene expression data has been applied to a t-test and have been considerate statistically significant differences with p-value ≤ 0.05.

3.5 Statistical analysis

Statistical analyses and data plotting were performed with Prism 9.0 software (GraphPad). Individual statistical analyses are mentioned in respective method sections.

Significance of data was only calculated if at least data from three independent replicates were present. P values are given at a 95 % confidence interval and were considered significant for $p < 0.05$ (* < 0.05, ** < 0.01, *** < 0.001).

RESULTS & DISCUSSION

The results of this thesis will be organized into two main sections:

SECTION 1: FOCUSING ON THE ESTABLISHMENT OF A RELIABLE AND NON-INVASIVE HUMAN ENDOMETRIUM 3D MODEL IN STATIC CONDITIONS

SECTION 2: PRESENTING THE SET-UP OF A DONOR-INDEPENDENT HUMAN 3D MODEL IN DYNAMIC CONDITION

SECTION 1

1.ORGANOIDS FORMATION

After receiving the samples from the donors, cells have been immediately processed according to the different source (Biopsy -MB). Cells were plated in Matrigel, and pictures were taken in different moments (Day 1- Day 3- Day 5- Day 7) to compare the development and the evolution of the Organoids (**Figure 20**). The Organoids from both sources did not show phenotypical differences in the development. In most cases, the initial yield of tissue fragments from MB was lower and the processing time longer than that obtained from Biopsies. However, the speed of organoids establishment was comparable to that from endometrial biopsies confirming previous published data (Cindrova-Davies *et al.*, 2021).

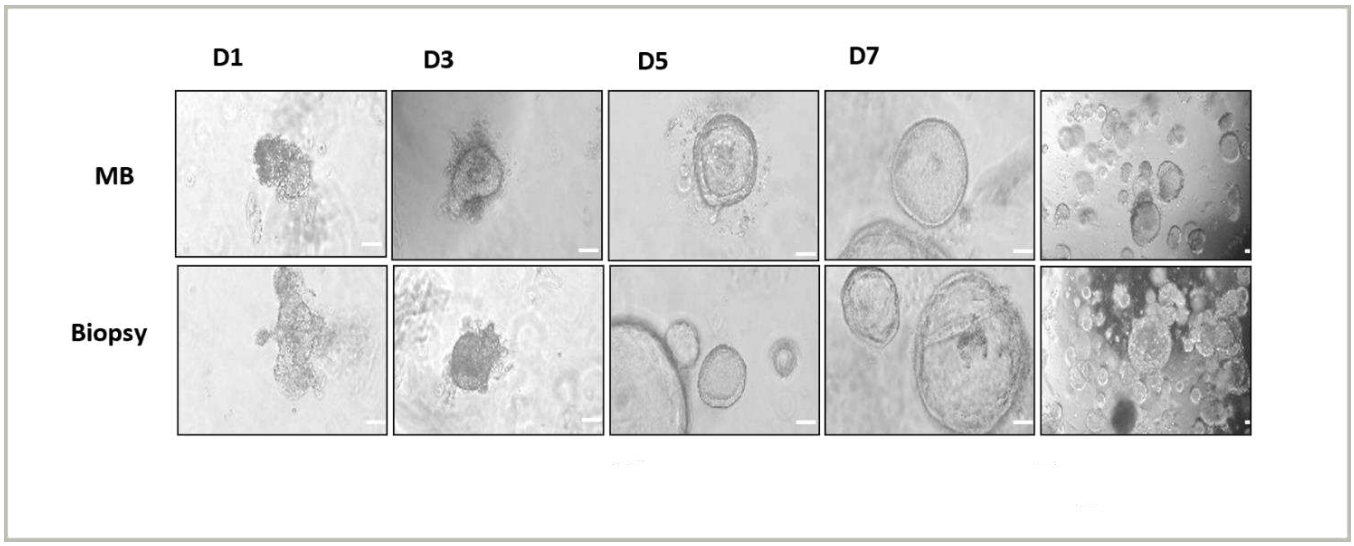

Figure 20: Brightfield micrographs of Organoids culture from MB=Menstrual Blood and Biopsy in different days after plating (D=Day) D1-D3-D5-D7. Scale bars 20 µm.

2.IMMUNOFLUORESCENCE CHARACTERIZATION OF CELLS COMPOSING ORGANOIDS FROM MB AND BIOPSY

In order to characterize cell composition, immunofluorescence techniques have been used to localize and visualize Vimentin, a marker for stromal cells, and cytokeratin 8-18, a marker for epithelial cells, in Organoids at first passages (P2-P3) obtained from both sources MB (**Figure 21** A-B-C) and Biopsies(D-E) without hormonal stimulation. The organoids resulted composed by an external layer of epithelial cells in green (**Figure 21** A-B-D-E) whereas the internal compartment was manly composed by stromal cells (in red). This is in contrast with literature about organoids from endometrium. Other groups consider these 3D structures mainly are composed by epithelial cells (Boretto *et al.*, 2017; Turco, Gardner, Hughes, Cindrova-Davies, Gomez, Farrell, Hollinshead, Marsh, Brosens, Critchley, Benjamin D. Simons, *et al.*, 2017). In a recent preprint paper was found the marker vimentin in the organoid structure confirming a possible mixed population at least in Biopsies sample (Zhang *et al.*, 2023). These discrepancies may be due to the use of first passages employed for the experiments, as is known that stromal cells are not suitable for high passages in Matrigel (Arnold *et al.*, 2001)

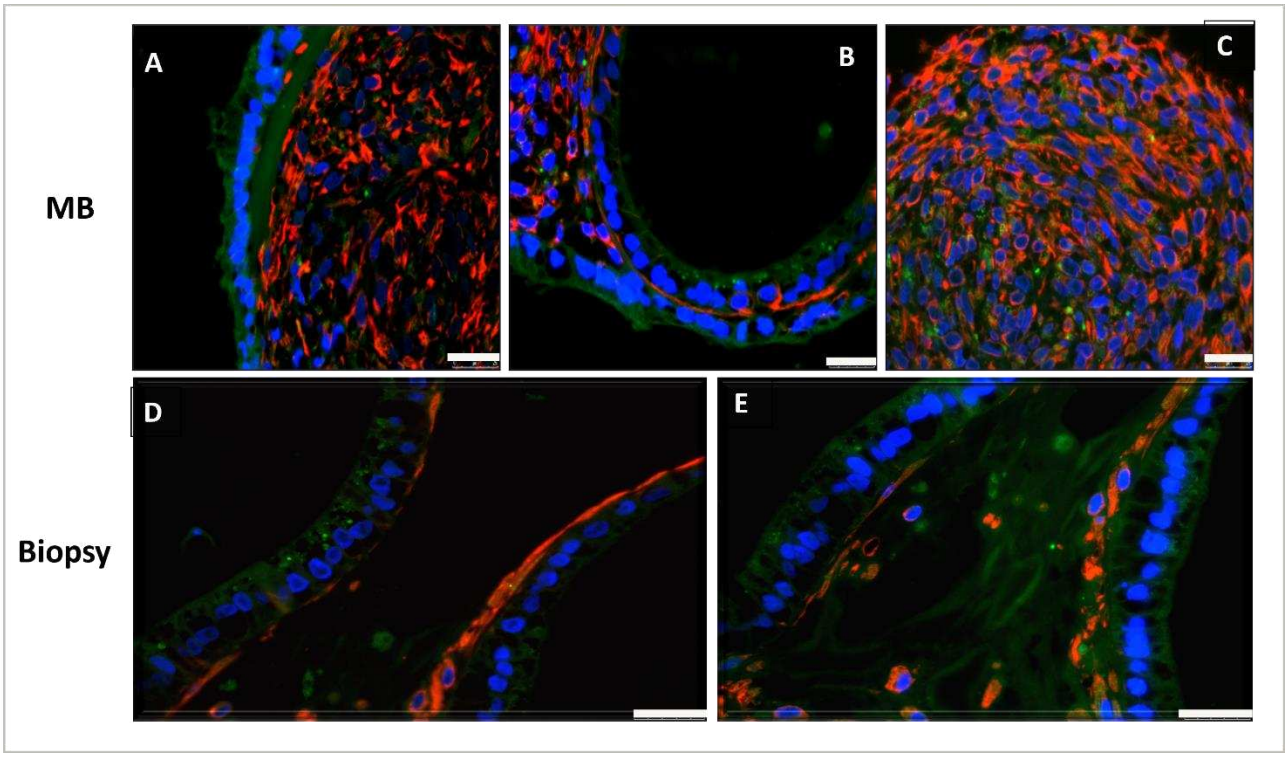

Figure 21: Immunofluorescence staining of Vimentin (in red) and cytokeratin 8-18 (green). Scale bar 25 µm.

3.GdA localization in organoids isolated from MB and Biopsy after hormonal treatment mimicking the phases of menstrual cycle

The cellular localization of GdA, also called progesterone-associated endometrial protein (PAEP), in Organoids isolated from MB and Biopsies has been evaluated by Immunofluorescence. As showed in **Figure 22**, positive staining revealed that GdA is present in all the analyzed sections. In both type of sources is possible to observe a clear and diffuse signal consistent with a cytoplasmic protein distribution. *In vivo* GdA is secreted by endometrium and pregnancy decidua in response to progesterone, human chorionic gonadotropin (hCG) and relaxin (Seppälä *et al.*, 2002). Another group demonstrated that specific isoforms of GdA were differentially expressed during the different phases of the menstrual cycle (Focarelli *et al.*, 2018). In Figure 22 its expression appeared to be modulated by the two hormonal stimulations. In fact, in Images A-C (E2 MPA and cAMP) the intensity of the signal is brighter compared to the intensity in Images B-D (only treated with E2). This was congruent with previously published data on organoids deriving from biopsies (Luddi, Pavone, *et al.*, 2020).

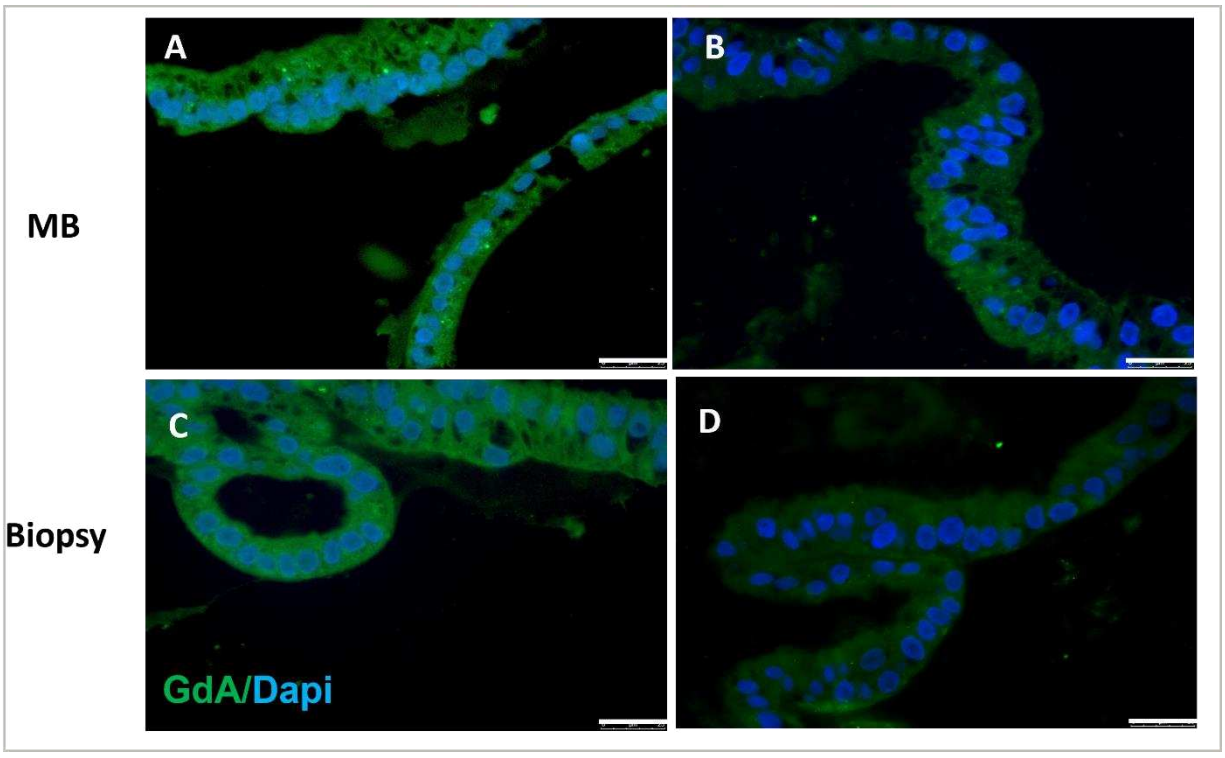

Figure 22: Immunofluorescence staining of the GdA in organoids isolated from MB and Biopsies. Representative micrographs of GdA staining in organoids after hormonal treatment with with E2 MPA and cAMP (A-C) and E2 (B-D). GdA (Green); DAPI, blue. Scale bar 25 µm.

4. GENE EXPRESSION OF *IGFBP-1* REGULATED BY DIFFERENT CONCENTRATION OF MIFEPRISTONE IN HESCS

With the purpose of establish the correct and effective concentration of Mifepristone, a Progesterone modulator, after conducting a literature review to establish which was the effective non-toxic dose (Lalitkumar *et al.*, 2007; Helmestam *et al.*, 2014; Ponandai-Srinivasan *et al.*, 2019), three different concentration of Mifepristone were tested to stop the decidualization process (5, 10, 25 µM). Mifepristone's most important mechanism of action is to compete with progesterone at the level of their respective binding site in the ligand binding domain of the progesterone receptors (Papp *et al.*, 2000). The hESCs were primed for two days with E2 and then stimulated with E2- MPA and cAMP (H), Mifepristone was added 1 hour before stimulating with hormones. In the graph in **Figure 23** was analyzed for the aim, the mRNA level of *IGFBP-1,* regulated during the decidualization process. The *IGFBP-1* expression was upregulated compared to the control in E2 treated group, and significantly increased in H group (*p<0.0001*) compared to the control (26,18 vs 7,33). Inhibitory effect of Mifepristone was visible in all three different concentrations but especially 10 µM (*p<0.001*). For the subsequent experiments 10 µM was chosen.

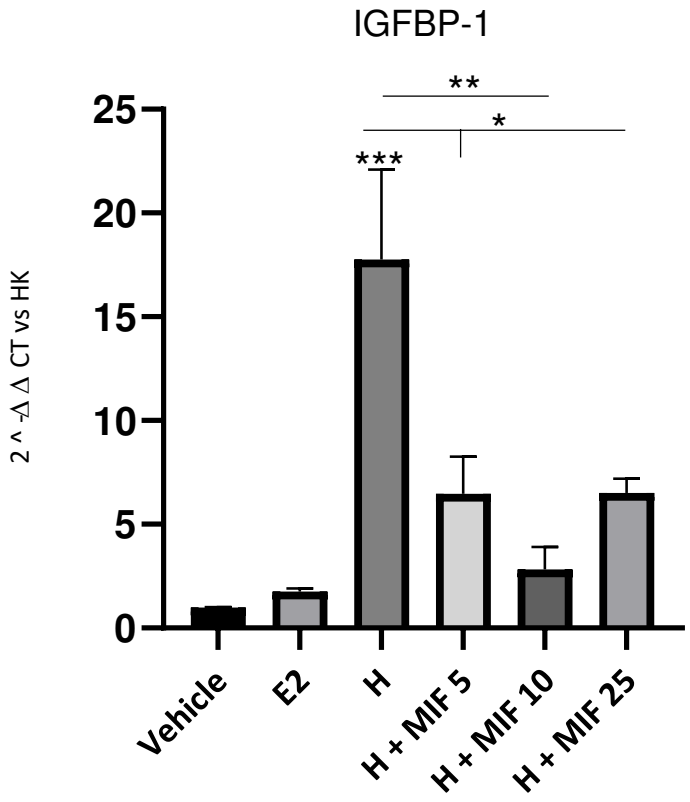

Figure 23: Relative mRNA expression levels of *IGFBP-1* in hESCs calculated using the 2^-ΔΔ Ct method. The means ± SEM mRNA levels are expressed as a relative fold change compared. Vehicle, E2=estradiol, H= E2- MPA-cAMP, MIF=Mifepristone

5. GENE EXPRESSION ANALYSIS OF *IGFBP1*, *FKBP5, PRL* AND *ZBTB16* IN ORGANOIDS FROM MB AND BIOPSY

Gene expression analysis of *IGFBP-1, FKBP5, PRL* and *ZBTB16* was analyzed in Organoids from both sources, MB and Biopsies, with E2 treatment (proliferative phase), E2- MPA and cAMP(H) (secretive phase), and 10 μM Mifepristone with E2- MPA and cAMP, were analyzed (**Figure 24**). Gene expression of *IGFBP-1* resulted significantly upregulated upon Hormone cocktail treatments *p<0.001* when compared to the vehicle and E2 treatment, also significantly negatively modulated (*p<0.01)* when Mifepristone was added. *ZBTB16* showed a significant increase (*p<0.05*) when the organoids were stimulated with the Hormones and E2 and a significant decrease when treated with Mifepristone. In *FKBP5*, *PRL* expression is visible an upregulation upon Hormonal treatment although this effect was not inhibited with Mifepristone treatment in MB samples, maybe due for the high variability of the samples. In another study the Mifepristone inhibitory effect on FKBP5 mRNA levels was demonstrated in blood samples acquired from a phase I study for the Cushing's syndrome (Bali *et al.*, 2016).

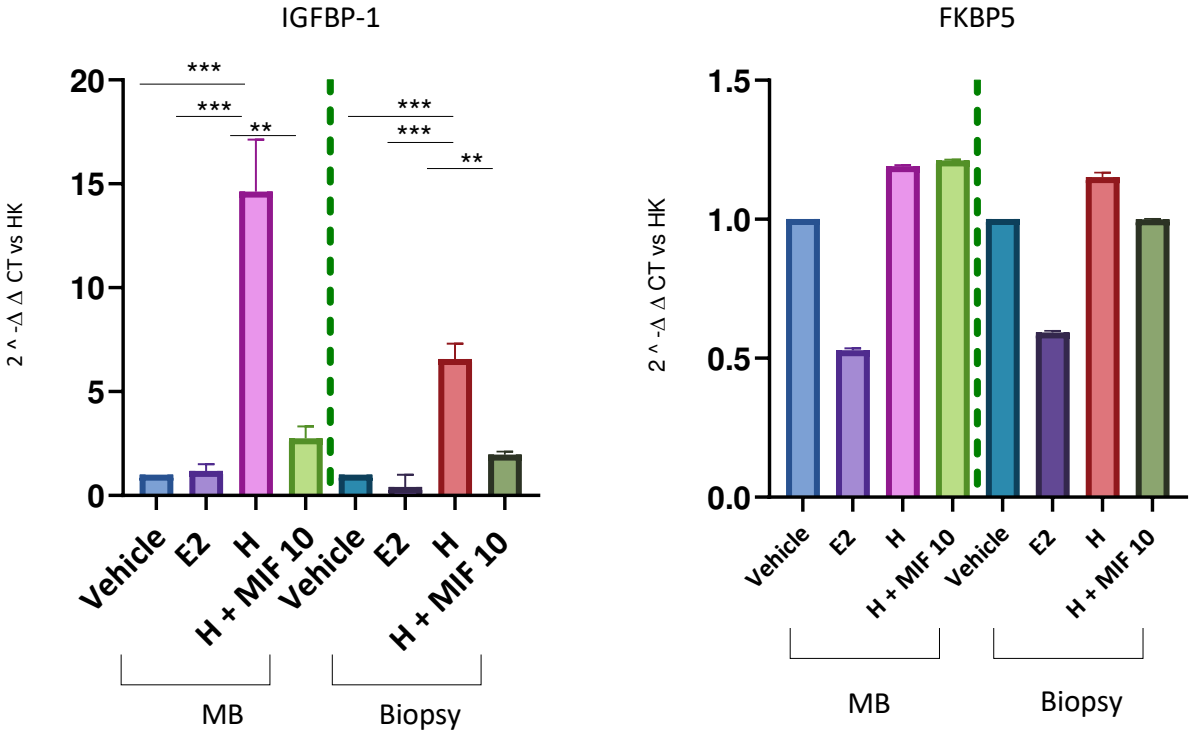

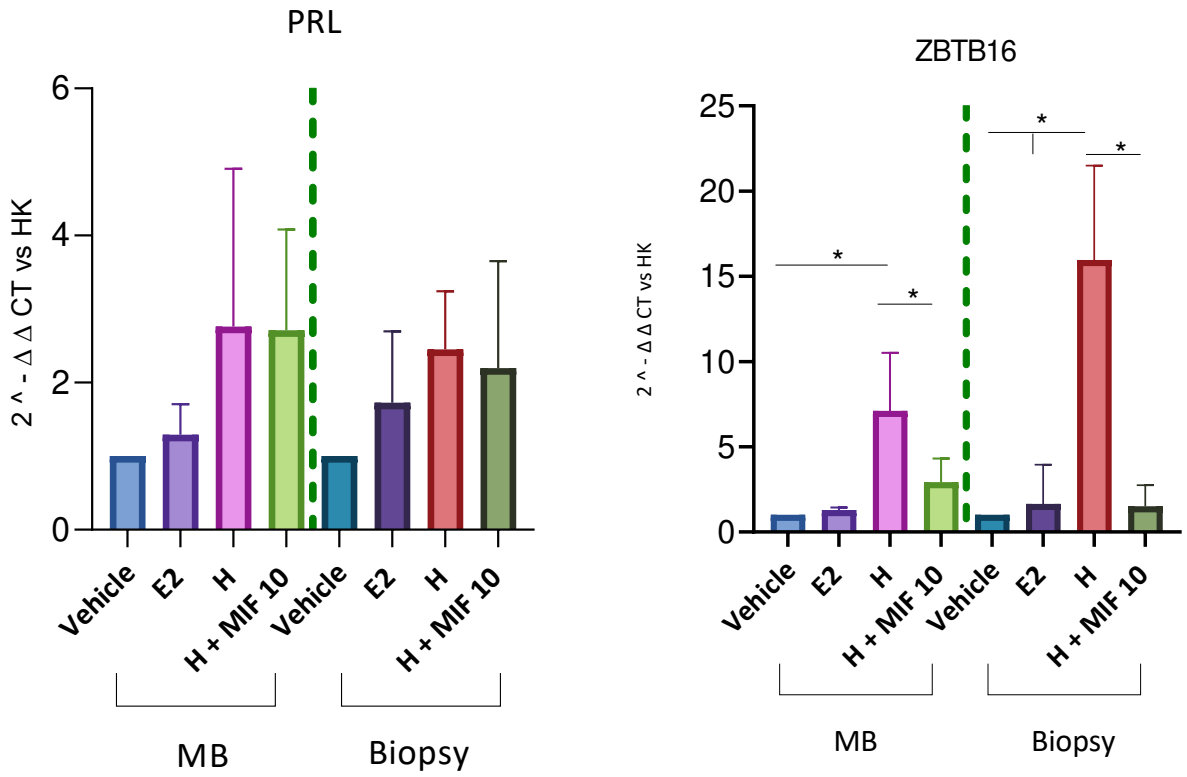

Figure 24: Relative mRNA expression levels of *IGFBP1- FKBP5, PRL* and *ZBTB16* in organoids from MB and Biopsy calculated using the 2^-ΔΔ Ct method. The means ± SEM mRNA levels are expressed as a relative fold change compared. Vehicle, E2=estradiol, H= E2- MPA-cAMP, MIF=Mifepristone

6. Ultrastructural characterization of organoids from MB upon stimulation

A scanning electron microscopic (SEM) inspection of endometrial organoids from MB, definitively demonstrating the dramatic changes occurring at the luminal surface following different hormonal treatments was performed. Hence, in organoids vehicle (**Figure 25** A), the luminal surface is relatively smooth, or it exhibits irregular cytoplasmic micro-extensions; indeed, it appears overlaid with a rich net of microvilli and cilia of different lengths (**Figure 25** A). The luminal surface of endometrial organoids (**Figure 25** C) stimulated by the decidualization cocktail is characterized by the presence of large apical cytoplasmic protrusions traditionally called “pinopodes”. Their presence is reported to be a specific marker of the implantation window (Melkozerova *et al.*, 2019) and is therefore an important and novel feature of the hereby described ex vivo endometrial model. This data definitely demonstrated the ultrastructural capability of the organoids model, whether from MB or Biopsy, to respond to different stimuli to mimic the menstrual cycle.

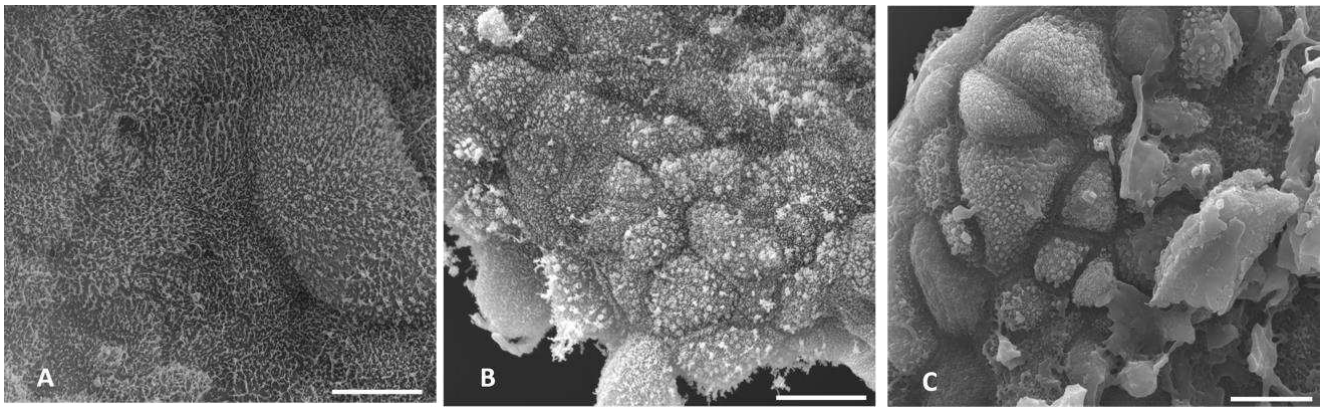

Figure 25: Ultrastructure of the organoid luminal surface showing remarkable changes, the feature of the in vivo endometrium architecture. Representative scanning electron micrographs of Organoids from MB treated with E2 to mimic the proliferative phase(B), showing numerous microvilli and cilia expansion from the apical surface of epithelial cells. Representative scanning (**C**) electron micrographs Organoids treated with E2, P4, cAMP to mimic the mid-secretory phase, showing numerous pinopodes that bulge from the entire luminal cell surface. These large apical cytoplasmic protrusions are characterized by a significant loss of free surface micro-extensions, including cilia and microvilli.

SECTION 2

1.CHARACTERIZATION OF 2D CULTURE OF THESCS, EM42 AND HUTMECS

The following experiment was performed at TISSUSE lab (Berlin, Germany). In order to evaluate the reaction of the three cell types EM42 cells, THESCs and HUtMECs used within this project to the sex hormone treatment, the cells were seeded to 24 well cell culture plates and the decidualization assay described in (**Table 10**) was performed. In this experiment, seeding numbers were the following: $8 \cdot 10^4$ cells, 15×10^4 cells and $5 \cdot 10^4$ cells per well (400 µl) for THESCs, EM42 cells, and HUtMECs respectively. The hormone cocktail was added 24 hours after seeding the cells. The hormone cocktail was added 24 hours after seeding the cells. Immunofluorescence staining for cytokeratin 8/18 and vimentin as well as estrogen and progesterone receptor were performed 72 hours after treatment of the culture (**Figure 26**).

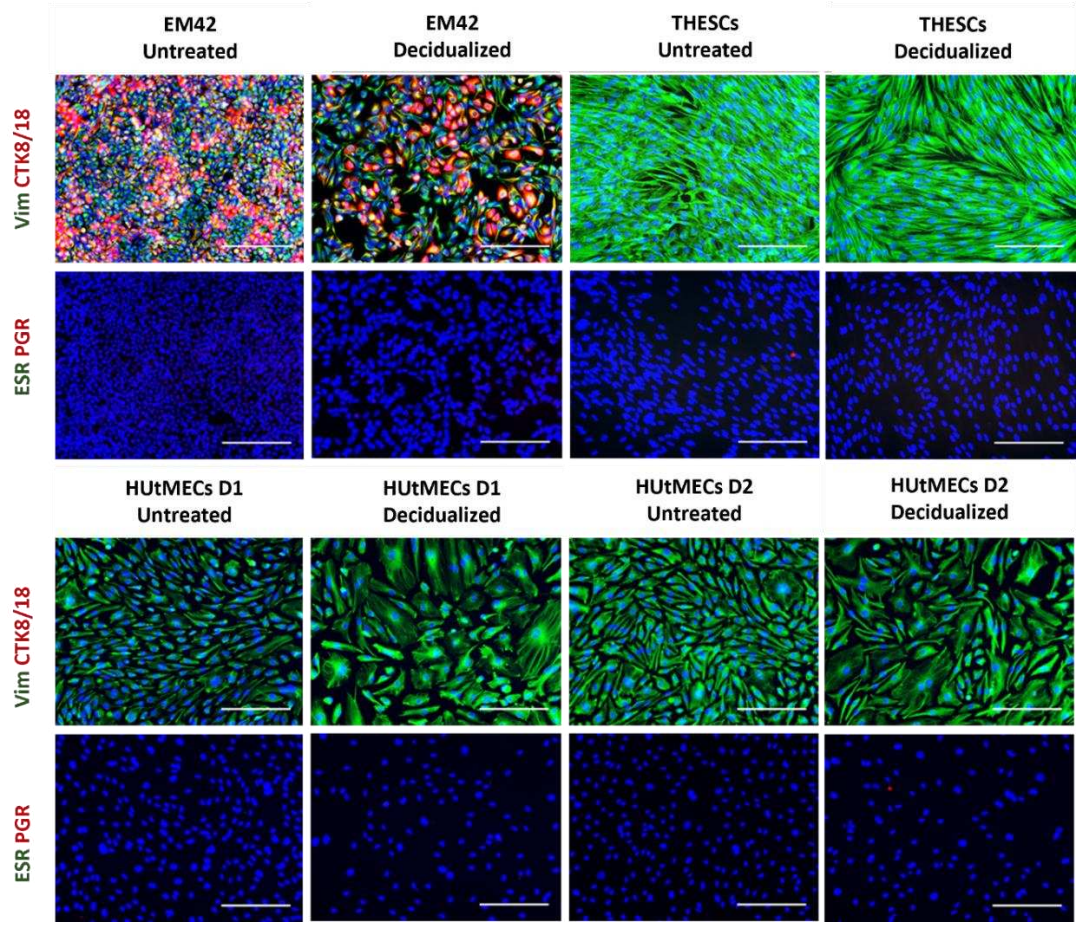

Figure 26: IF staining of EM42, THESC and HUtMECs cultured 2D in static conditions. Cells were fixed 72h after adding the hormone cocktail and compared with untreated cells fixed at the same culture time point. Stromal marker vimentin (Vim, green) co-stained with epithelial marker cytokeratin8/18 (Ctk8/18, red) in upper row and estrogen receptor (ESR, green) and progesterone receptor (PGR, red) in lower row. (Upper panel) Morphology changes and cell growth inhibited after treatment of EM42 cells. EM42 show cells positive for Ck8/18 and vimentin. THESCs are exclusively positive for vimentin but show no morphological changes upon hormone treatment. (Lower panel), both donors show morphological changes upon hormone treatment and are exclusively positive for vimentin. No ESR/PGR signal could be found for all cell types. Counterstaining of nuclei with Dapi (blue). Scale bars: 200µm.

For EM42 cells (**Figure 26**) and both HUtMEC donors (**Figure 26-**bottom panel), the morphology changed, and cell growth was inhibited after treatment with the hormone cocktail, whereas no difference could be observed between untreated and treated THESCs (**Figure 26**). EM42 cells were intended to be used as a cell line showing primarily epithelial characteristics. Therefore, it was expected that these cells express the epithelial marker cytokeratin 8/18 but not the stromal marker vimentin. However, EM42 cells were found positive for both markers, indicating the presence of a stromal fraction within this cell line. THESCs and HUtMECs were exclusively positive for vimentin as expected. No signal for estrogen (ESR) or progesterone (PGR) receptor could be found for all cell types. Although the overall control of endometrial growth and regression is regulated primarily by circulating concentrations of estrogen and progesterone, the role of sex steroids in endometrial angiogenesis is less clear. Most studies have failed to demonstrate estrogen or progesterone receptors in human endometrial endothelium(Gargett and Rogers, 2001), although was successfully demonstrated by (Iruela-Arispe, Rodriguez-Manzaneque and Abu-Jawdeh, 1999).

2.Characterization of the 3D model (EM42-THESCs)

The whole- mount samples were stained and analyzed using a confocal microscope kindly provided by Reschke's group at Bayer Laboratories (**Figure 27**). Confocal imaging enables visualization of whole-mount samples. The 3D models were analyzed both in dynamic culture conditions in HUMIMIC Chip2 and static conditions. The models consisted of 80,000 THESCs (**Figure 27** A-F) or without (**Figure 27** G-L) 10,000 EM42 cells (constructs formed in a 96-well ULA plate).

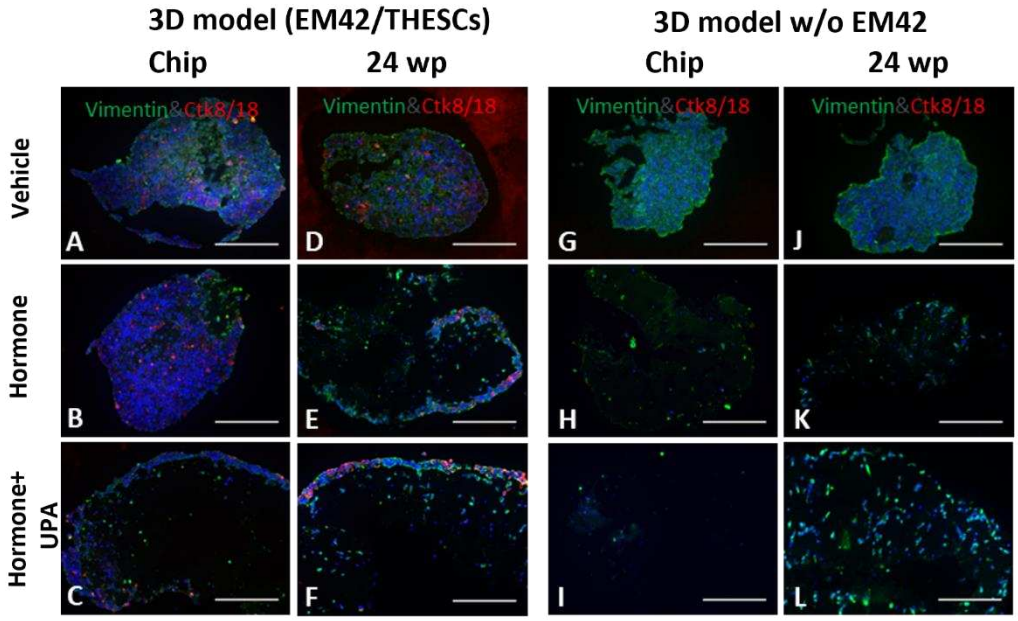

Figure 27: IF staining of EM collagen I construct co-cultured in the HUMIMIC Chip2 with HUtMECs and statically single-cultured EM collagen I constructs. Samples were taken 72h after treatment. Vehicle control (A, D,G,J) , hormone cocktail treated (B,E,H,K). Pre-treatment with ulipristal acetate (UPA) followed by adding hormone cocktail for 30 minutes (C,F,I,L). Constructs with 80,000 THESCs and 10,000 EM42 cells (A-F) were compared with those exclusively containing 80;000 THESCs (G-L). (A-L) The 8µm slices of the different conditions were stained with the stromal cell marker vimentin (green) and the epithelial marker cytokeratin 8/18 (red). Counterstaining of nuclei with Dapi (blue). Collagen constructs in vehicle treated conditions are all densely packed with cells, however, exclusively vimentin positive THESCs (green) are only found in the samples without EM42 cells. Moreover, the cells seem to disappear from Hormone and Hormone+UPA treated samples for all conditions. Scale bars: 200µm.

It was found that the cells in the spheroids were mainly cytokeratin8/18 positive, while the cells that spread out of the spheroids were mainly positive for vimentin. However, again, no difference was detectable between the conditions (Hormone and Hormone + UPA). Collagen constructs in vehicle treated conditions are all densely packed with cells, however, exclusively vimentin positive THESCs (green) are only found in the samples without EM42 cells. Moreover, the cells seem to disappear from Hormone and Hormone+UPA treated samples for all conditions.

3. 3D MODELS CONSTRUCT MORPHOLOGY IN HUMIMIC CHIPS (COC AND PDMS) AND IN STATIC CONDITION

Based on the experiences gained in the previous experiments, THESCs (80,000 cells) were cast in a 96-well ULA plate. EM42 cells (10,000) were seeded on top of the polymerized gels. After 3 days of culture inside the 96-well ULA plate, 5 constructs (per circuit) were collected for further dynamic and static culture. Chip channels were seeded with endothelial cells (HUtMEC donor 2) four days prior to adding the 3D model (THESC, EM42).

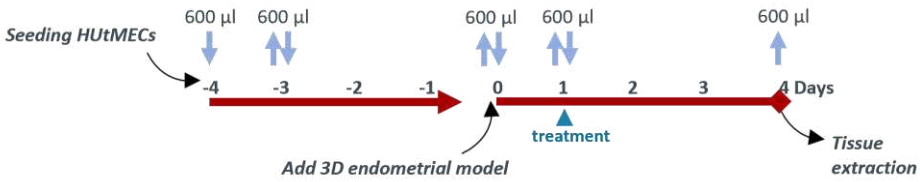

The day when the collagen constructs were added either to the chip or cultured in static condition was defined as Day 0. One day after starting the co-culture (Day 1), the hormone cocktail and 5 or 25µM UPA (1 hour before the hormone cocktail) were added to the cultures. After an additional incubation of 72h, endpoint analyses were performed (Day 4), see the timeline above.

The static cultures were run in parallel to observe the influence of the chip cultures on the established endometrium model. Moreover, in addition, both the standard HUMIMIC chip2 96-well PDMS version and the prototype HUMIMIC Chip2 96-well COC version were used as previous experiments indicated absorption of components of the hormone cocktail and/or UPA into the PDMS.

Brightfield images were taken at culture day 4. At the end of the culture images indicated that vehicle constructs were smaller and attached more compared to the hormone treated conditions (**Figure 28**)**.** PDMS, COC and static culture in 24 well plates showed comparable morphology of the constructs for the same treatment condition. The morphology of all UPA pre-treated conditions appeared similar to the conditions treated exclusively with the hormone cocktail, so no antagonistic effect by the UPA pre-treatment could be observed in the brightfield images.

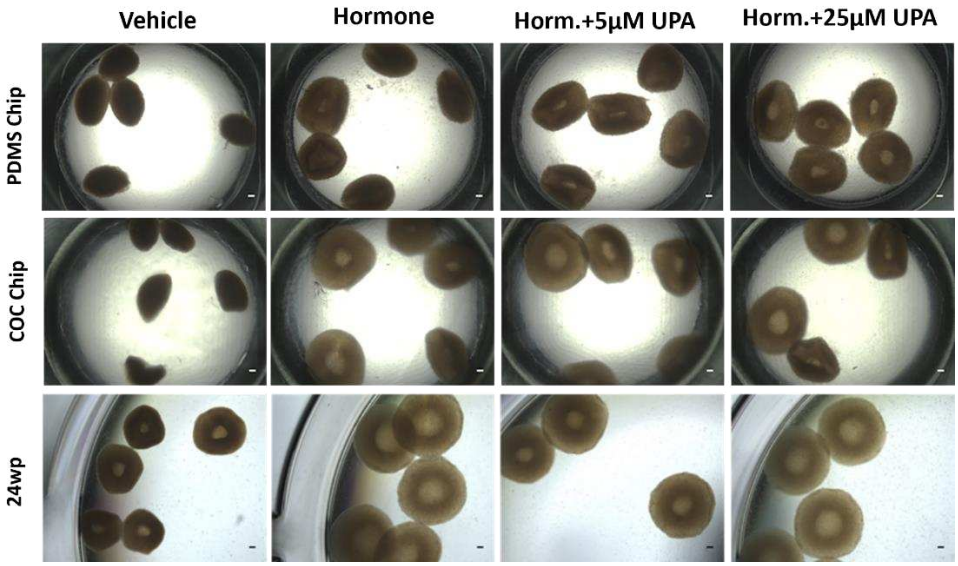

Figure 28: Brightfield images of 3D constructs cultured in dynamic conditions and static conditions. The cultures were treated for 72h with either the vehicle control, the hormone cocktail, or pretreated with UPA (5µM or 25µM UPA). Images were taken at culture day 4 at the end of the culture. The 3D models (THESCs and EM42) appeared smaller and attached more to the glass surface when treated with the vehicle control compared to the hormone treated conditions. No antagonistic effect by the UPA pre-treatment could be observed. Scale bars: 200µm.

4. Metabolism analysis of Chip Experiment

In order to further investigate whether a stable culture under dynamic flow conditions had been achieved, glucose, lactate and LDH concentration was determined. LDH release is indicative of porous cell membranes and cytotoxicity. Medium samples were collected at day 1 and day 4 of the culture **Figure 29**. The glucose and lactate concentration [mg/L] as well as the LDH concentration in the medium in [mU/L] were determined as described in **Paragraphs 3.1**. Cultures in static conditions (black) showed a higher glucose (**Figure 29** A) and lower lactate (**Figure 29** B) concentration compared to the dynamic cultures (red colors and blue) which might indicate a higher metabolic activity due to the presence of endothelial cells in the dynamic conditions.

When cells in culture are actively metabolizing, they produce lactate and take up glucose from the culture medium. Chip Cultures (blue and red) released more LDH into the medium compared, HUMIMIC Chip2 COC from day 1 84 U/L to 160 U/L at day 4, HUMIMIC Chips2 PDMS from 81 U/L day 1 to 145 U/L at day 4 to static culture that started from 48U/L at day 1 reaching 72 U/L at day 4 (black). This increase in LDH concentration for further experiments can be mitigated refreshing the media during the cell culture. However, no difference in glucose and lactate concentration between dynamic culture in HUMIMIC Chip2 PDMS and COC cultures could be observed. After 72h of treatment (day 4), the vehicle control was more metabolic active than most other conditions, however, static and dynamic culture in HUMIMIC Chip2 COC pre-treated with 25µM UPA showed a similar glucose and lactate level to the vehicle control.

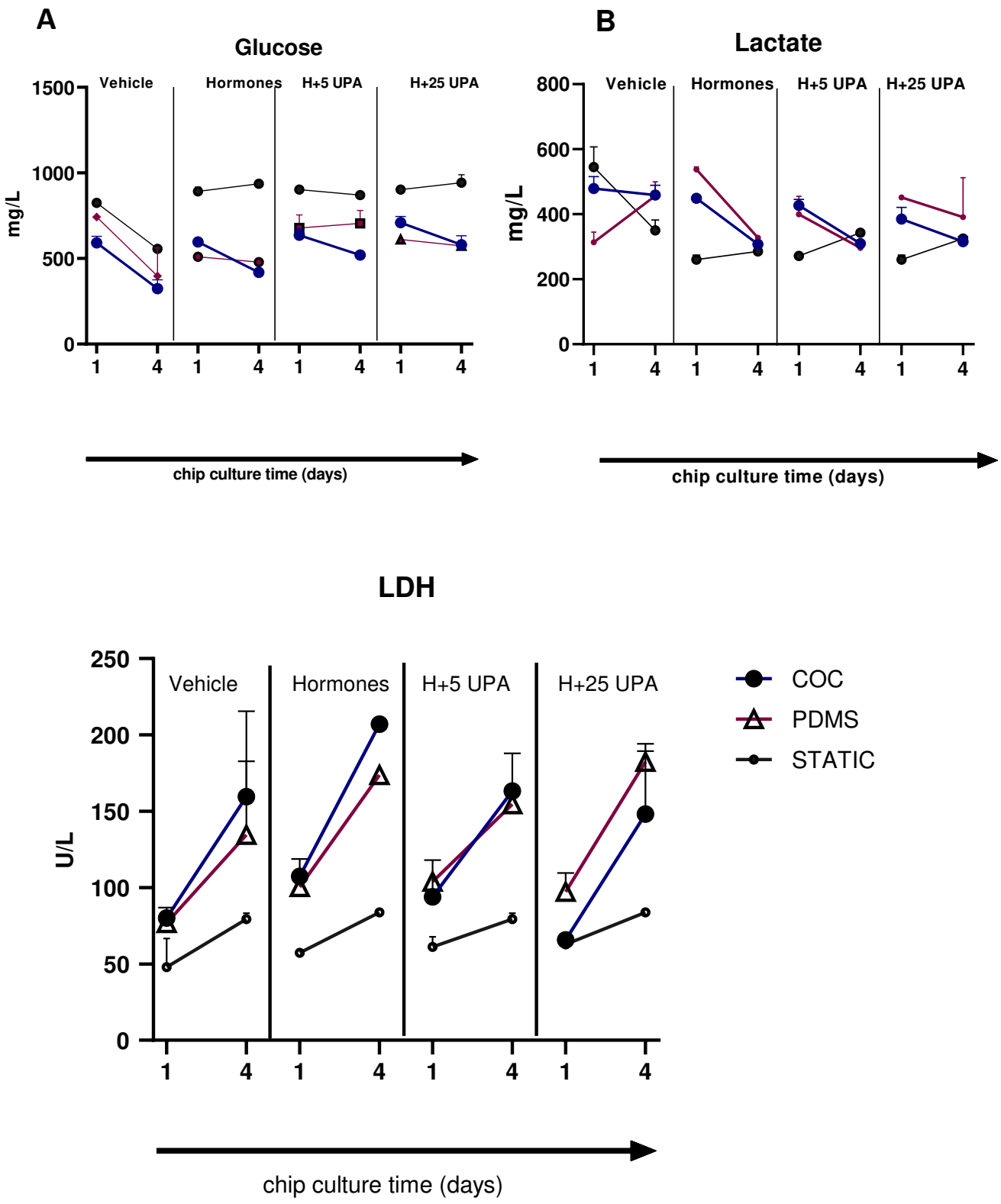

Figure 29: Metabolism analysis and LDH release of HUMIMIC Chip2 96-well co-culture of 3D models constructs (THESC-EM42) and HUtMECs. (A) Glucose concentration in mg/L, (B) Lactate concentration in mg/L, and (C) LDH release in mU/L. Medium was harvested at day 1 at the start of the treatment and at day 4 at the end of the culture. Cultures in the 24 well plate (black) showed a lower metabolic activity compared to Chip cultures (red colors and blue) which might be due to the presence of endothelial cells in the chip culture. Cells in conditions with EM42 (blue, red, grey) were slightly more metabolically active and had more LDH release compared to those without. After 72h of treatment (day 4), the vehicle control was more metabolic active than most other conditions, however static and and dynamic culture in HUMIMIC Chip2 COC pre-treated with 25µM UPA were similar to the vehicle.

5. Metabolic analysis of HUtMECs in Chip without the 3D model

Medium samples of HUtMEC's cultured under static condition (24 well plate) and dynamic condition in HUMIMIC Chips2 (both PDMS and COC) from two different donors were collected at day 1 before starting the decidualization experiment, day 2 and day 5 after 72h of treatments. The glucose and lactate concentration [mg/L] as well as the LDH concentration in the medium in [mU/L] were determined. Cultures in static condition (black) showed similar Glucose levels compared to the HUtMEC cultivated in dynamic conditions.

The hormones treatments showed a higher concentration of glucose for all conditions. HUMIMIC Chip2 in PDMS (blue)and in COC (red) and static (black) (**Figure 30** A). An increase in lactate levels (**Figure 30** B) in HUtMEC cells cultured in dynamic or in static condition can be observed an increase of the level of Lactate in the vehicle group and a decreased concentration in the hormone treated cells in all conditions.

In **Figure 30** C, LDH release into the medium in the static condition (black) resulted slightly higher compared to dynamic condition (blue and red). However, no difference in concentration between the two donors' cultures could be observed. After 72h of treatment (day 5).

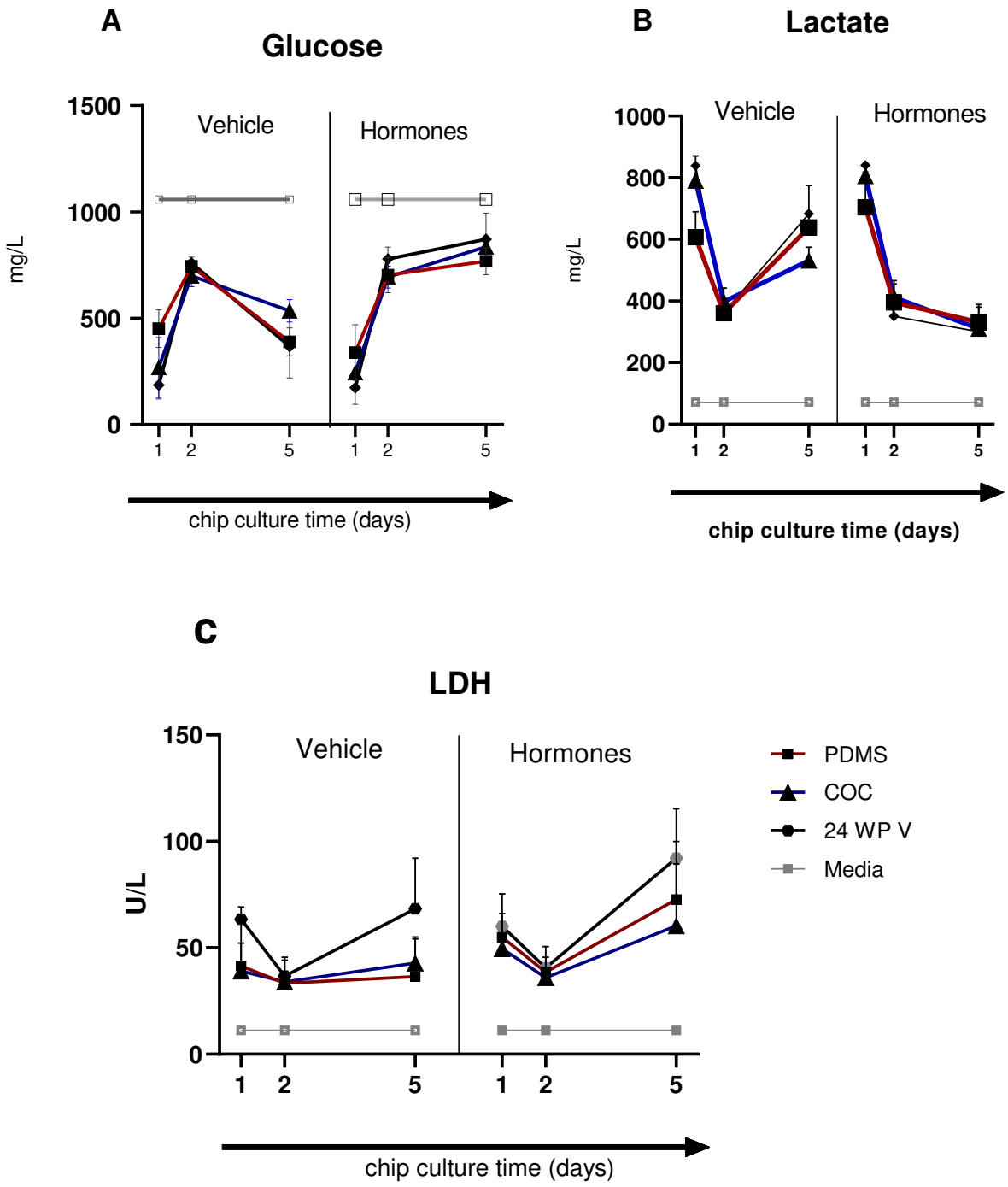

Figure 30: Metabolism analysis and LDH release of HUtMECs cultures in the HUMIMIC COC and PDMS Chip2 96-well - culture and under static conditions (24 well plates). (A) Glucose concentration in mg/L, (B) Lactate concentration in mg/L, and (C) LDH release in mU/L. Medium was harvested at day 1, day2 at the start of the treatment and at day 5 at the end of the culture. Cultures in the 24 well plate (black) had more LDH release compared to those in dynamic conditions (blue and red). After 72h of treatment (day 5), the vehicle control was more metabolic active than most other conditions.

6.Gene expression analysis 3D models vs 2D models

3D models and 2D models were analyzed for the relative mRNA expression levels of genes important during the decidualization process. Following models were treated 72h with the decidualization cocktail and 5 and 25 μM UPA:

a) 3D models composed by 80,000 THESCs embedded in collagen I and after 30 minutes 10,000 of EM42 cells
b) All in one (AIO) 80,000 THESCs and 10,000 EM42 embedded in Collagen I
c) Or 2D cells, THESCs and EM42 plated in 96 well plate without using any matrix

Hormone receptors: Estrogen and Progesterone, (**Figure 31** A) were downregulated in the 3D models upon treatments, although an upregulation after hormone treatments by MPA, Estradiol and cAMP in 2D models was shown. This upregulation was particularly high especially for PGR and after the treatments the inhibitory effect of UPA. The decidualization protein FKBP5 and the transcription factor ZBTB16 (**Figure 31** B) were significantly upregulated in all the models (3D, 3D AIO, 2D) and the inhibitory effect of UPA was visible in all the conditions with a significant downregulation. The decidualization factor IGFBP1, was significantly upregulated in the 3D models and the 2D model, instead Prolactin transcripts were more abundant upon treatments with the decidualization cocktail in all the models, especially in the 2D models (**Figure 31** C).

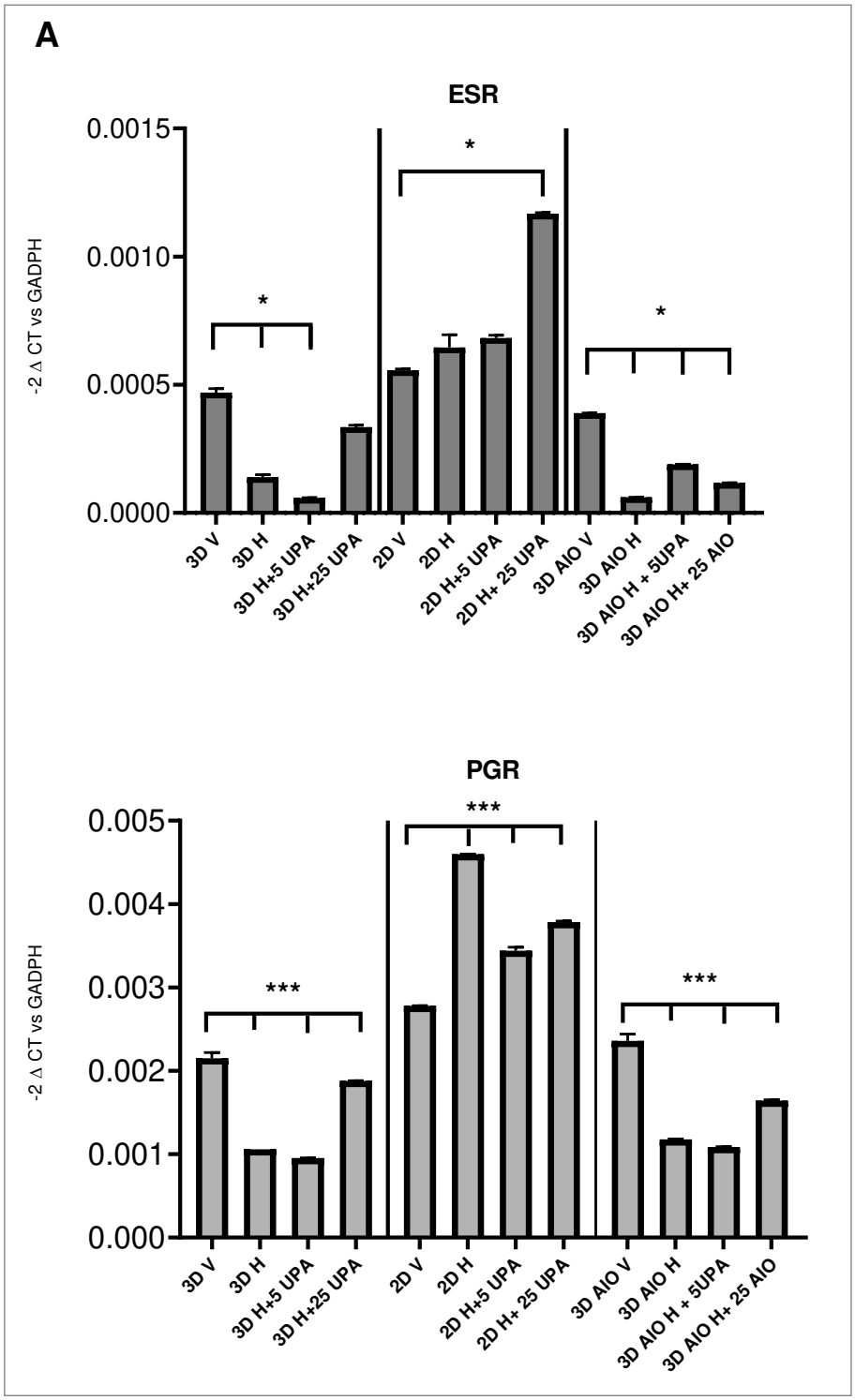
A
ESR
-2 Δ CT vs GADPH
0.0015
0.0010
0.0005
0.0000
*
*
*
3D V
3D H
3D H+5 UPA
3D H+25 UPA
2D V
2D H
2D H+5 UPA
2D H+ 25 UPA
3D AIO V
3D AIO H
3D AIO H + 5UPA
3D AIO H+ 25 AIO
PGR
-2 Δ CT vs GADPH
0.005
0.004
0.003
0.002
0.001
0.000
***
***
***
3D V
3D H
3D H+5 UPA
3D H+25 UPA
2D V
2D H
2D H+5 UPA
2D H+ 25 UPA
3D AIO V
3D AIO H
3D AIO H + 5UPA
3D AIO H+ 25 AIO

B

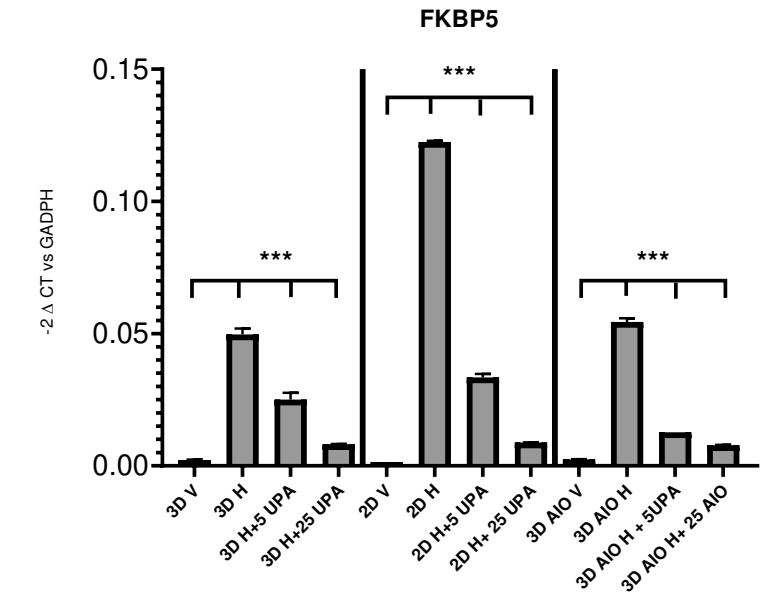
FKBP5
-2 Δ CT vs GADPH
0.15
0.10
0.05
0.00
***
***
***
3D V
3D H
3D H+5 UPA
3D H+25 UPA
2D V
2D H
2D H+5 UPA
2D H+ 25 UPA
3D AIO V
3D AIO H
3D AIO H + 5UPA
3D AIO H+ 25 AIO

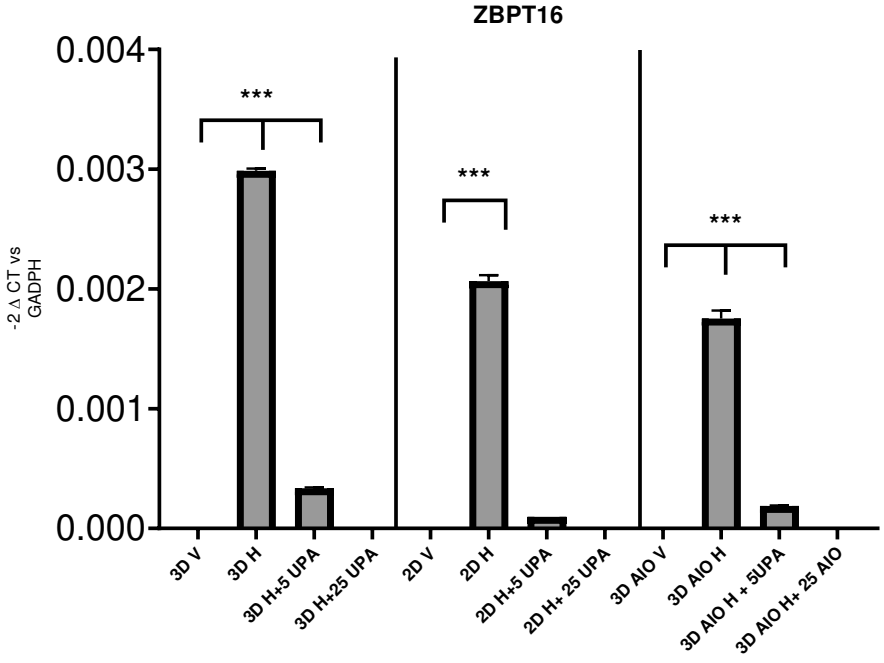
ZBPT16
-2 Δ CT vs GADPH
0.004
0.003
0.002
0.001
0.000
***
***
***
3D V
3D H
3D H+5 UPA
3D H+25 UPA
2D V
2D H
2D H+5 UPA
2D H+ 25 UPA
3D AIO V
3D AIO H
3D AIO H + 5UPA
3D AIO H+ 25 AIO

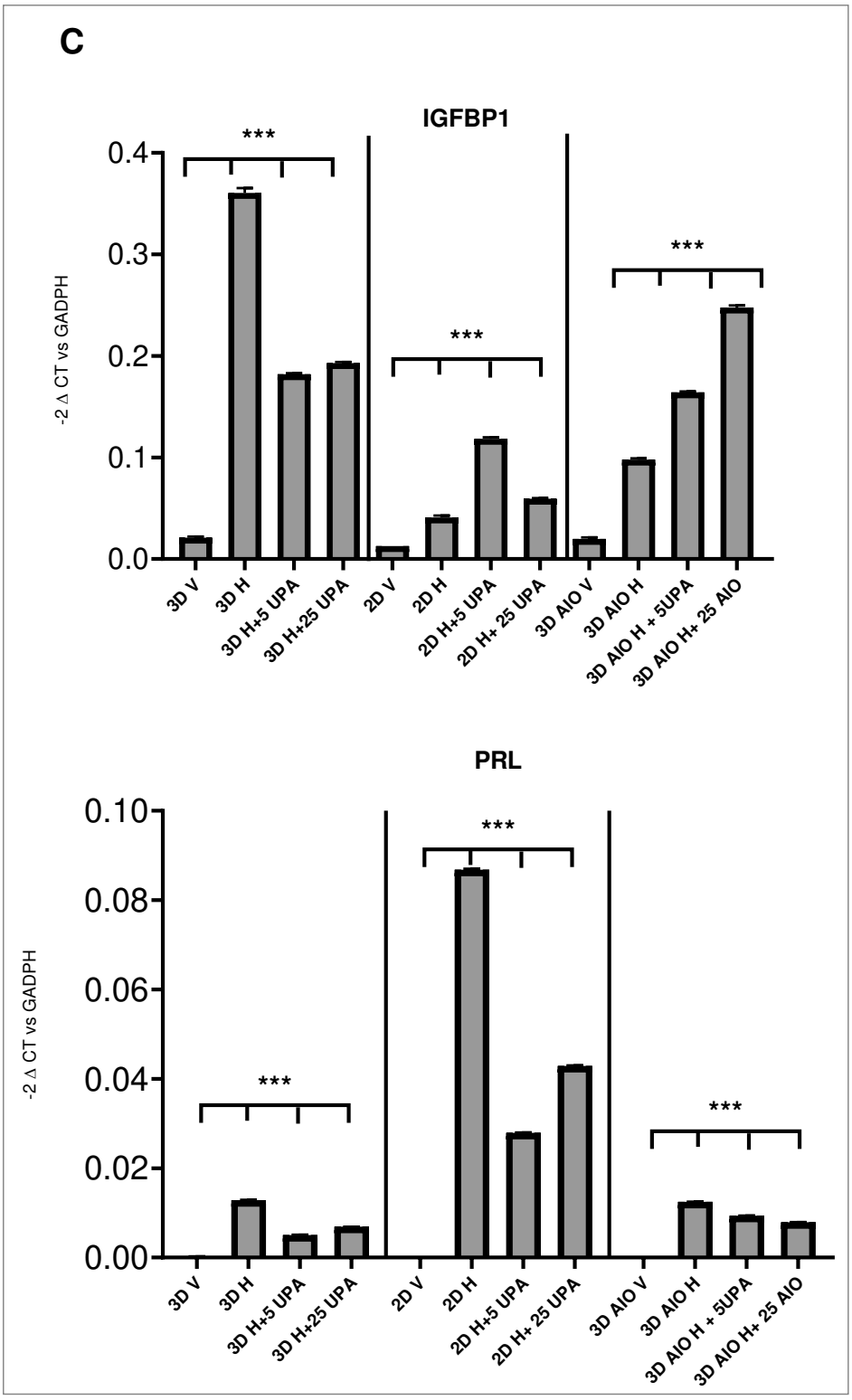

Figure 31: Relative mRNA expression levels of Hormone receptors ESR and PGR, Decidualization proteins IGFBP1, FKBP5, PRL and the transcription factor ZBTB16 in 3D model, 3D model AIO and 2D under different conditions and calculated using the -2Delta Ct Method. The means ± SEM mRNA levels are expressed as a relative fold change compared to vehicle control. The constructs were cultured in static conditions. V = vehicle control treated, H = hormone cocktail treated, 5U or 25U = hormone cocktail treated after pre-treatment with 5 or 25µM ulipristal acetate, respectively. Significance: *p < 0.05, ***p < 0.001

7.IGFBP1 AND PROLACTIN SECRETION 3D MODELS VS 2D MODELS

Secreted protein levels of IGFBP1 and Prolactin (PRL) were investigated using a sandwich ELISA method **Paragraph 3.3.** They are recognized as specific decidualization markers, hence presence of the proteins indicates hormone cocktail dependent decidualization (Kane *et al.*, 2010). Difference in secretion of IGFBP1 was very low in the different conditions (**Figure 32**). When treated with the hormone cocktail, a statistically significant induction of IGFBP1 was observed in the 2D models. No significant decrease of this induction occurred when the cultures were pre-treated with UPA before the hormone treatment to inhibit the decidualization process. Prolactin levels increased in the media of all hormones treated, although not significant downregulation was present after UPA treatments.

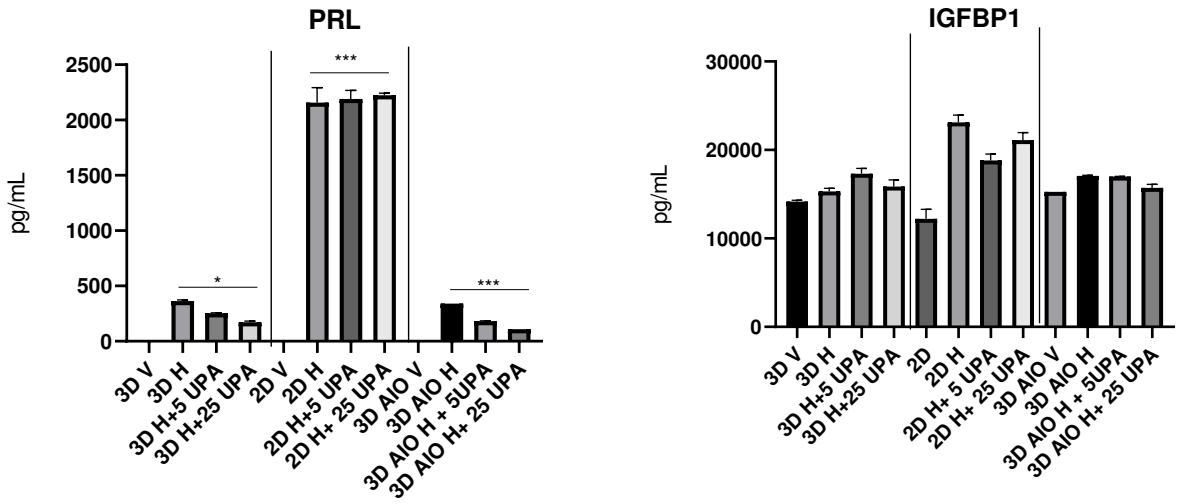

Figure 32: IGFBP1 and PRL protein secretion calculated in pg/mL in 3D model, 3D model AIO and 2D under different conditions. Medium was sampled 72h after treatment with either the vehicle control (V), the hormone cocktail (H), pre-treatment with two different UPA concentrations (5µM, 25µM) and then the addition of the hormone cocktail.

8.GENE EXPRESSION ANALYSIS OF 3D MODELS IN DYNAMIC AND STATIC CONDITIONS

Figure 33 shows the relative expression levels (normalized to GADPH). Gene expression of the endometrial hormone receptor progesterone (PGR) resulted stable and independent from the Hormone condition. ESR transcripts showed high variability upon replicates. Genes coding for the decidualization proteins PRL and IGFBP1 were significantly upregulated by the hormone cocktail, however in IGFBP1 no significant downregulation by the UPA 5µM treatment was visible. *FKBP5* and *ZBTB16* were significantly upregulated by hormone cocktail and was visible a significant downregulation when UPA applied prior to hormone cocktail both in static and dynamic conditions (HUMIMIC Chips2 PDMS), although in HUMIMIC Chip2 COC was not visible a significant upregulation but only a positive trend.

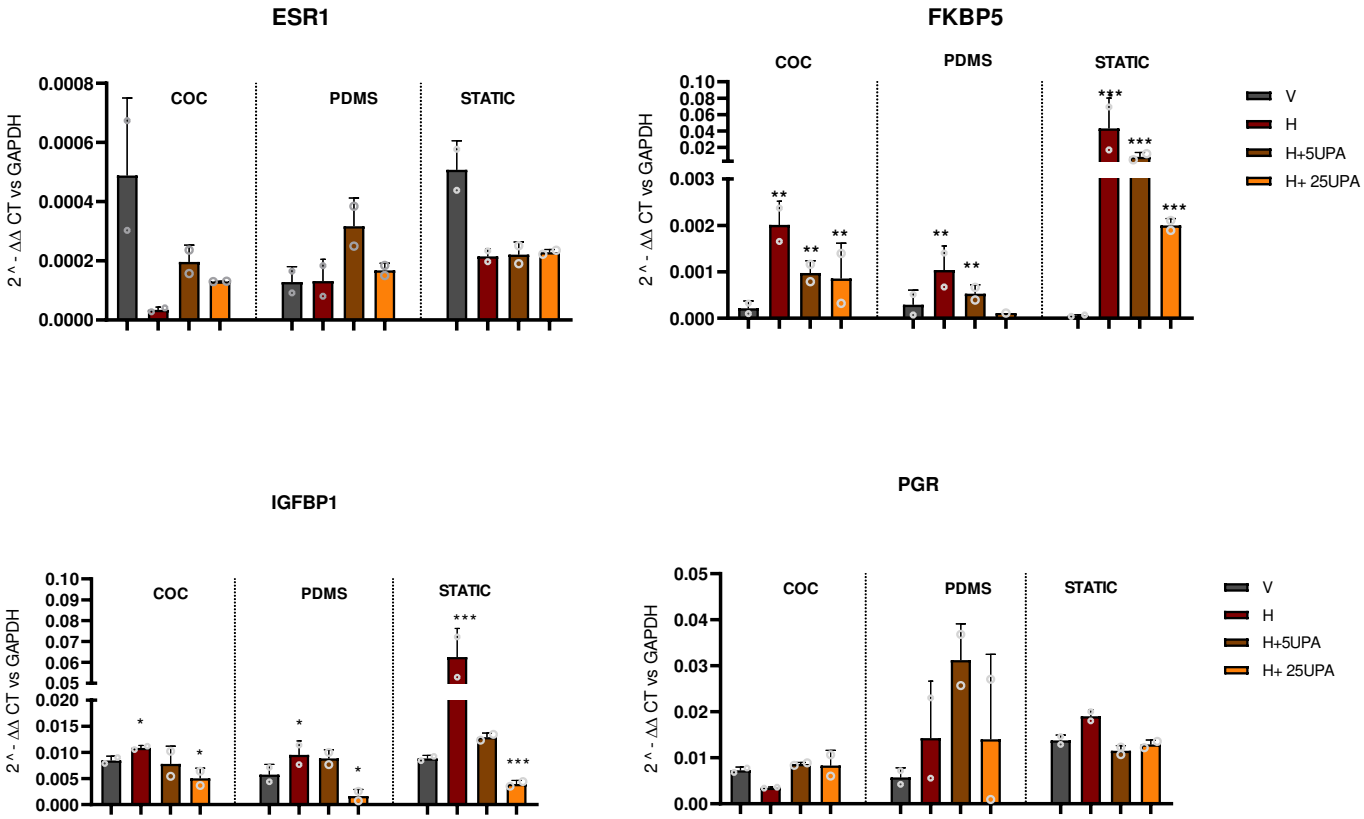

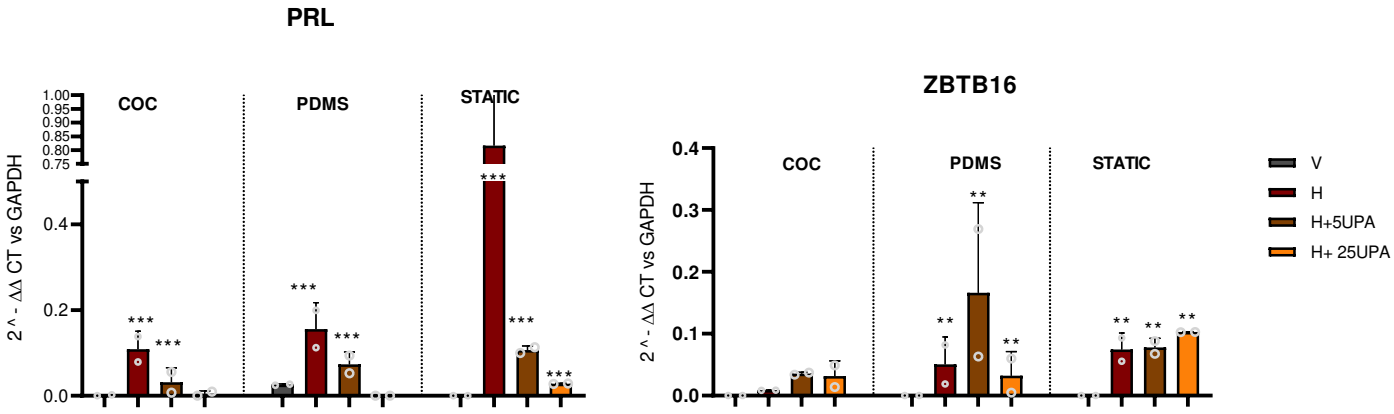

Figure 33: Relative mRNA expression levels of six genes in 3D models co-cultured with HUtMECs inside the HUMIMIC Chip2 96-well. The means ± SEM mRNA levels are expressed as a relative fold change compared to vehicle control. V = vehicle control treated, H = hormone cocktail treated, H+S = hormone cocktail treated after pre-treatment with UPA. Tukey's Multiple comparison test. *p < 0.05, **p < 0.01, ***p < 0.001.

9.IGFBP1 AND PROLACTIN SECRETED PROTEIN LEVEL IN MEDIA FROM 3D MODELS IN CHIP EXPERIMENTS

To evaluate decidualization, secreted protein levels of IGFBP1 and PRL in cells' supernatant recovered from cell culture compartments of HUMIMIC COC and PDMS Chip2 and from 3D models in static culture, were investigated using a sandwich ELISA method (**Figure 34**). Presence of PRL protein suggest the occurred decidualization after 72h of incubation with the hormone cocktail groups (COC and PDMS). Secretion of PRL was undetectable in the vehicle treated condition in both Chips. When treated with the hormone cocktail, a significant induction of PRL was observed ($p<0,0001$). Significant decrease of this induction occurred only in PDMS chips when the cultures were pre-treated with UPA 5 and 25 µM before the hormone treatment to inhibit the decidualization process. IGFBP1 secreted protein was possible only in HUMIMIC COC Chip2 and static condition for technical limitations. IGFBP1 level were increased in Hormone group ($p<0.05$), especially in static condition ($p<0.0001$), with inhibitory action of UPA 5 µM only in static condition, maybe due to absorbance of the substance from the material.

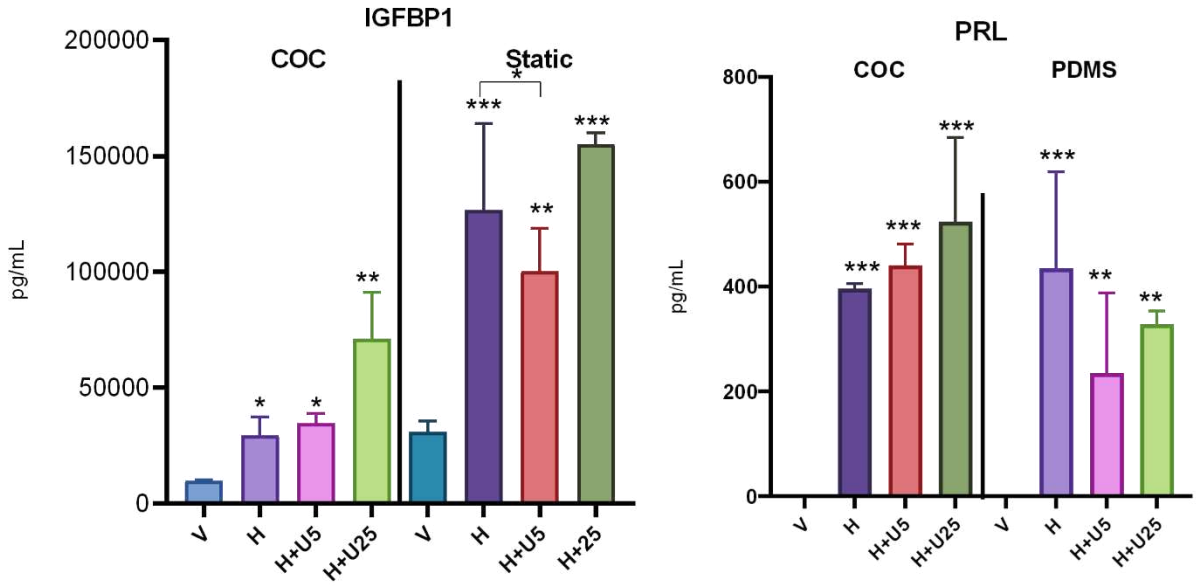

Figure 34: IGFBP1 and PRL protein secretion of HUMIMIC Chip2 96-well co-cultures of 3D models with HUtMECs 72 hours after treatment. V = vehicle control treated, H = hormone cocktail treated, H+S = hormone cocktail treated after pre-treatment with UPA. A 10.000-fold induction of IGFBP1 could be observed when cultures were treated with the hormone cocktail. No significant decrease of induction occurred when cultures were pre-treated with UPA before the hormone treatment.

10. METALLOPROTEINASES EXPRESSION IN 3D MODELS DURING DECIDUALIZATION

MMPs are a family of zinc-dependent endopeptidases that possess proteolytic properties and play crucial roles in various pathological (Gill and Parks, 2011)and such as tissue remodeling and regulation of inflammatory processes, and cancer progression (Cabral-Pacheco *et al.*, 2020). Some of these MMPs and inhibitor were analyzed in the 3D model in dynamic and static conditions, to elaborate their role in the extracellular matrix turnover and degradation. Matrix degradation per se is neither the sole nor the predominant function of these proteinases (Gill and Parks, 2011). Recent findings indicate that MMPs act on a variety of extracellular proteins, such as cytokines, chemokines, antimicrobial peptides, and other proteins, that regulate varied aspects of inflammation and immunity (Parks, 2006). The results show (**Figure 35**) that *MMP1, MMP3, MMP10 MMP11, TIMP2*, were upregulated especially in dynamic culture conditions in HUMIMIC Chip2 whereas COL1A1 was most regulated in static condition. In this study, we surprisingly found significant downregulation of many MMPs and significant upregulation of *MMP1, MMP3* and *MMP14* during 3D models decidualization. Moreover, only *TIMP2* expression was significantly increased among TIMP family members. Such observations collectively led us to conclude that the downregulation of many MMPs and up-regulation of *MMP1, MMP3* and *MMP14* and *TIMP2* must be necessary for decidualization.

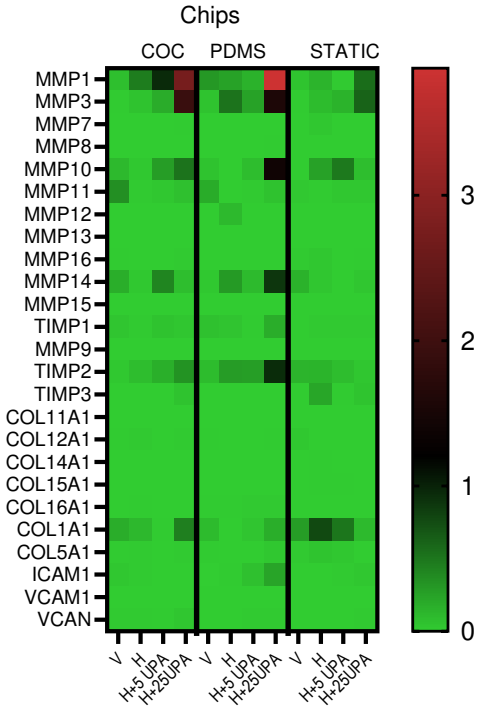

Figure35: Heat maps based on the gene array analysis summarizing the quantitative expression patterns of genes involved in basement membrane remodeling. The mean gene expression value for each patient group was computed and used to calculate the heat map, which thus reflects the cDNA concentration of genes involved in basement membrane remodeling. Expression profiles are color coded (red = high expression level; green = low expression level).

11. LIVE STAINING OF THE ENDOTHELIALIZED CHANNELS

The CellTrace™ Calcein-AM dye (Thermo Fisher) stains live cells in culture. Gnecco et al. (Gnecco *et al.*, 2017) showed an enhanced decidualization capability of the endometrial stromal cells in vitro due to haemodynamic forces applied on uterine endothelial cells. For this reason, HUtMECs were tested for their ability to colonize the channels of the PDMS and COC HUMIMIC Chip2 96-well and following culture over 10 days. The 600µL (300µL in each compartment) of medium inside the chip was renewed every 24h. The HUtMECs were injected into the micro-channels and adhered to the channel walls within 3h of static cultivation before the perfused culture was started. A density of 25x 10^6 cells/ml was sufficient to reach homogeneous cell distribution all over the micro-channels. The endothelialized HUMIMIC Chip2 96-well circuits were then further cultivated and induced by the flow the HUtMECs were elongated and oriented into the direction of flow. Successful endothelialization was achieved in different TISSUSE Chips and using different cells. (Schimek *et al.*, 2013b). Live-cell analysis of the tight Endothelial cells layer was performed by confocal microscopy at day 10 of the culture and revealed striking viability in the entire circuit for all donors, as seen by Celltrace™ Calcein AM staining. A slight difference in cell density could be observed in one spot for PDMS circuits following the hormone treatments, which was less dense and oriented into direction of flow compared to the COC Chips (**Figure 36**).

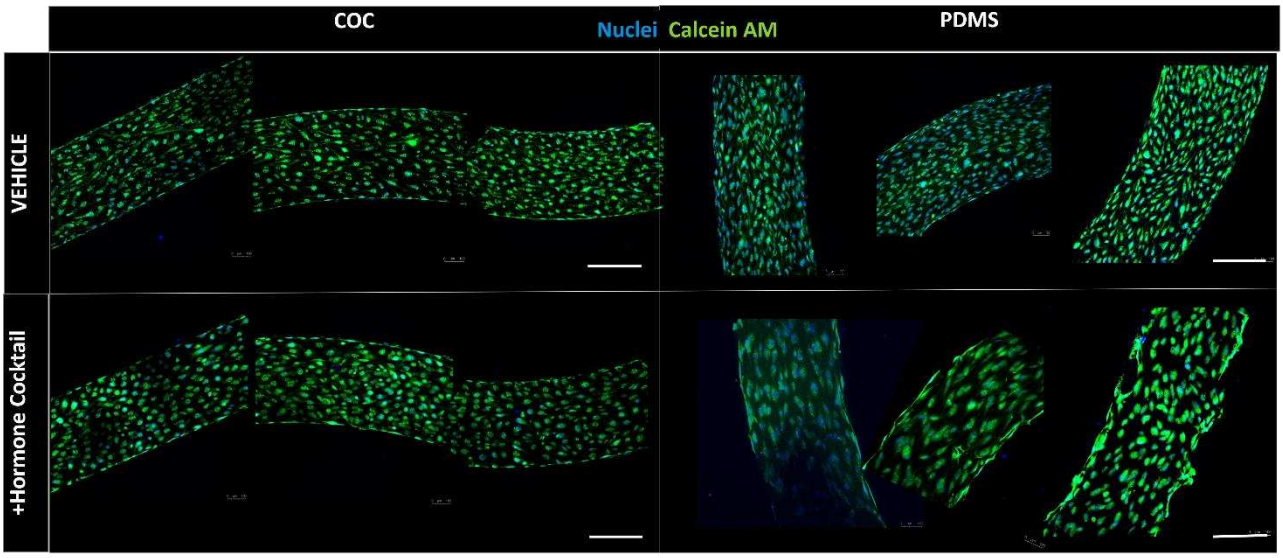

Figure 36: Representative images of HUtMECs in different positions of the HUMIMIC Chip2channels (PDMS and COC) in the vehicle and after 72 h of decidualization cocktail. Live cells were visualized immediately after finishing the staining using an inverted Confocal fluorescence microscope (LEICA). Scale bar: 100µm

12. IMMUNOFLUORESCENCE LOCALIZATION OF VE-CADHERINE IN ENDOTHELIAZED CHANNELS

Immunofluorescence staining of HUtMECs covering the circuit demonstrated the expression of VE-Cadherine, an endothelial specific adhesion molecule located at junctions between endothelial cells (**Figure 37**). HUtMECs cultured in both HUMIMIC Chips (COC-PDMS) expressed VE-Cadherine, although for the nature of COC material, the quality of the images taken by confocal microscopy decreased. Actin filaments form a network providing mechanical support, determining cell shape, and allowing movement of the cell surface, thereby enabling cells to migrate, engulf particles, and divide. Actin filaments in red were visible in all culture conditions, showing the stable structure of the cells in both type of HUMIMIC Chips.

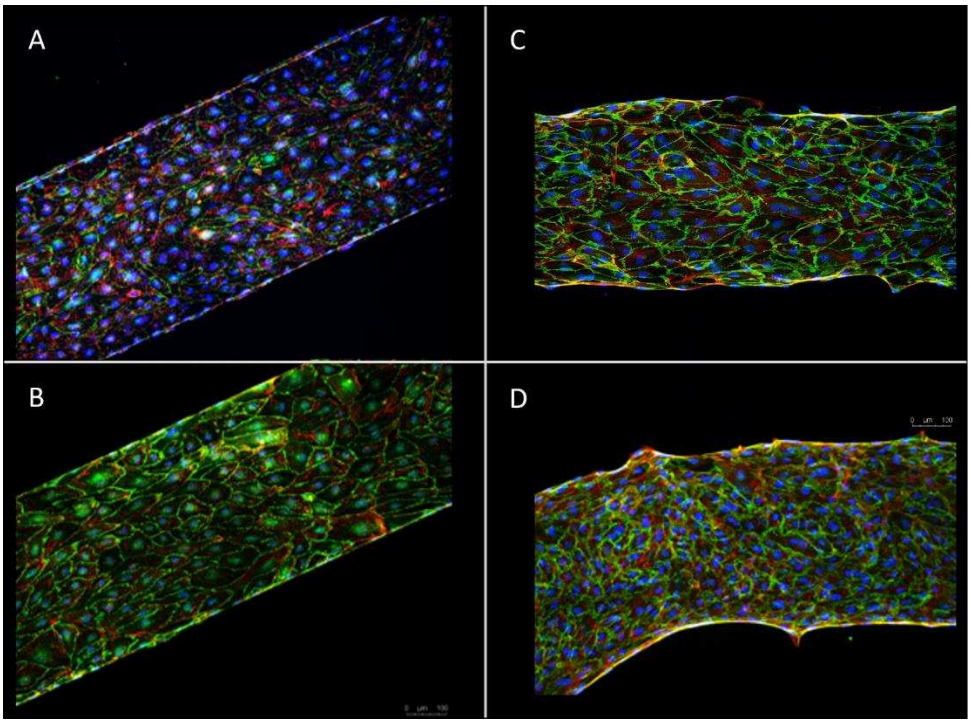

Figure 37: Representative immunofluorescence (IF) staining of HUtMECs inside the COC (A-B) and PDMS (C-D) HUMIMIC Chip2 96-well channels after 10 days of dynamic cultivation. Images B and D show the staining after decidualization. Endothelial specific adhesion molecule located at junctions between endothelial cells VE-Cadherine. (green) and ACTIN (red) stained for all HUtMECs donors. Counterstaining of nuclei with Dapi (blue). Scale bars: 100µm.

13. GENE EXPRESSION OF HUTMECS TREATED WITH DECIDUALIZATION COCKTAIL STATIC

Gene expression of HUtMEC cells from both donors treated for 72 h in 24 well plate with the decidualization cocktail and 5 and 25 µM UPA were analyzed. Transcripts of *ESR* and *PGR*, *Prolactin* were undetectable, suggesting the possible absence. *FKBP5, IGFBP1, ZBTB16, PTGES2* were all significantly upregulated upon Hormone cocktail treatments and this effect could be partially

inhibited with UPA treatments, both 5 and 25μM (**Figure 38**). These data suggest the contribution of Endothelial part in the model and their regulation during the decidualization process.

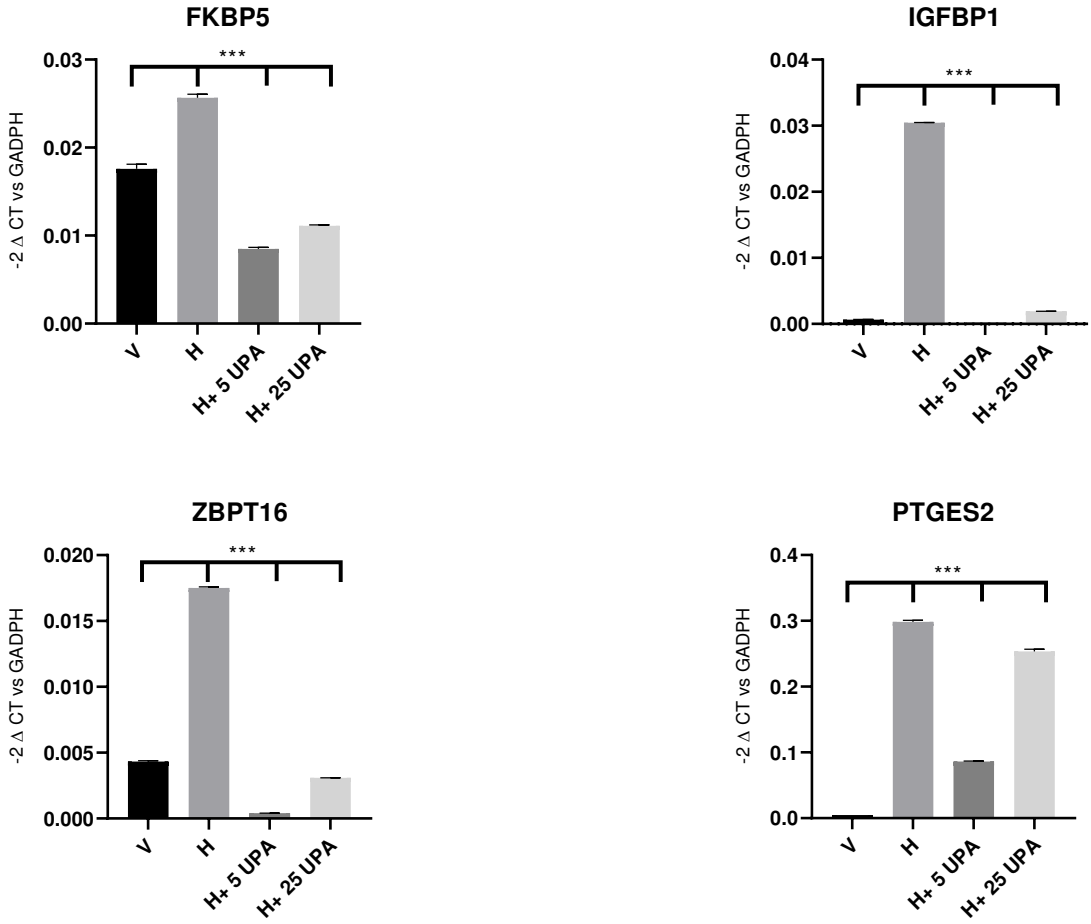

Figure 38: Relative mRNA expression levels of Decidualization proteins IGFBP1, FKBP5, the transcription factor ZBTB16 and PTGES2 in HUtMECs cultured in static condition. V = vehicle control treated, H = hormone cocktail treated, 5U or 25U = hormone cocktail treated after pre-treatment with 5 or 25μM UPA, respectively. Significance: ***p < 0.001

14. DIGITAL DROPLET ANALYSIS OF HUTMEC IN HUMIMIC CHIP AND STATIC CONDITIONS

Absolute concentration of investigated genes of HUtMEC cultivated under static and dynamic conditions was calculated by QuantaSoft® software (Bio-Rad Laboratories). The normalized sample amount (NSA) was obtained by normalizing the absolute concentration as respect to the concentration of selected reference genes (*GADPH, HPRT1*) (for more details, see (Luddi *et al.*, 2018)). **Figure 39** shows the distribution of NSA values of analyzed genes in HUtMECs cultured in dynamic condition (HUMIMIC Chip2 PDMS) and in static condition. Cells were stimulated with the decidualization cocktail for 72h and with 5 and 25 μM UPA only in the static condition. Out of six genes analyzed (*ESR, PGR, IGFBP1, FKBP5, PRL* and *ZBTB16*) only 4 resulted expressed (*IGFBP1,*

FKBP5, PRL and *ZBTB16*). *FKBP5* resulted the most abundant transcript of the analyzed genes in the HUtMECs isolated from dynamic condition (0,261), while for the same cells, in static condition resulted *IGFBP1*.

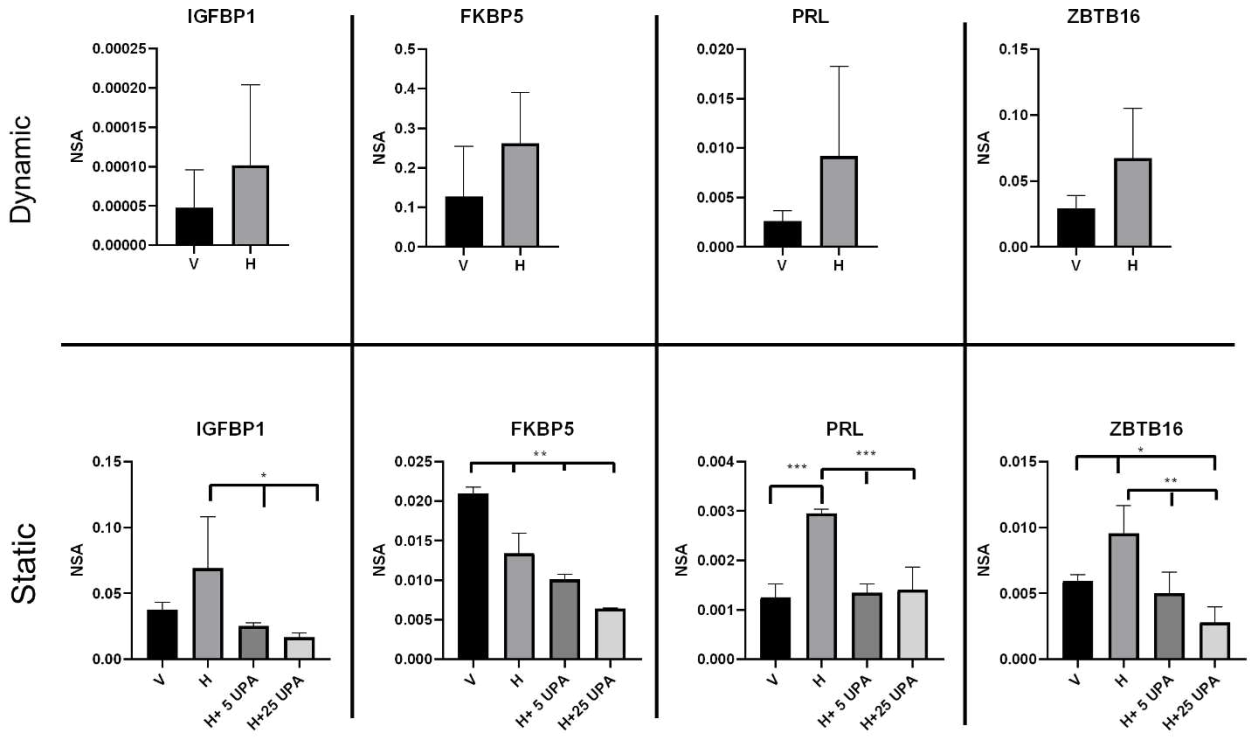

Figure 39: Quantitative expression of *IGFBP1, FKBP5, PRL* and *ZBTB16* in HUtMECs (upper panel) in dynamic condition HUMIMIC Chip2 PDMS and bottom panel in static condition. V = vehicle control treated, H = hormone cocktail treated, 5U or 25U = hormone cocktail treated after pre-treatment with 5 or 25 µM ulipristal acetate, respectively. Statistically significant differences in NSA levels were tested by t test. *p<0.05; **p<0.01; ***p<0.001

As shown in **Figure 39**, in static condition the expression of *IGFBP1* was significantly higher in Hormone treated samples and Ulipristal both 5 and 25 ($p<0.05$). Also, *FKBP5* resulted significantly downregulated in Hormone and UPA treated compared to the vehicle ($p<0.01$) which was not expected. Finally, we found a significant difference in *PRL* hormone treated cells compared to the Vehicle and a significant difference for the treatments with UPA 5 and 25 µM compared to the decidualized (Hormone) group ($p<0.001$), and *ZBTB16* expression level were significant upregulated in Hormone group and significantly downregulated in UPA 25 µM groups. compared to the vehicle ($p\leq0.05$). Furthermore, and a significative downregulation of UPA 5 and 25 µM compared to the Hormone group, pointing a regulatory effect of the substance on HUtMEC cells.

These data were also analyzed in ddPCR to understand the possible contribution of these cells when in dynamic culture environment toward the expression profile.

15.IGFBP1 SECRETED PROTEIN LEVEL IN HUTMEC IN DINAMYC AND STATIC CONDITIONS

In order to evaluate the decidualization process *in vitro*, secreted protein levels of IGFBP1 in HUtMEC supernatant, were investigated using a sandwich ELISA method (**Figure 40**). Presence of the protein suggest the occurred decidualization after 72h of incubation with the hormone cocktail groups (static and dynamic, COC and PDMS). Secretion of IGFBP1 was very low in the vehicle treated condition. The increase of IGFBP1 protein in the supernatant was significant in HUMIMIC Chip2 COC ($p<0.0070$) and in HUMIMIC Chipc2 PDMS ($p<0.0001$). When treated with the decidualization cocktail, a significant induction of IGFBP1 was observed. Significant decrease of this induction occurred when the cultures were pre-treated with UPA 5 and 25 µM before the hormone treatment to inhibit the decidualization process.

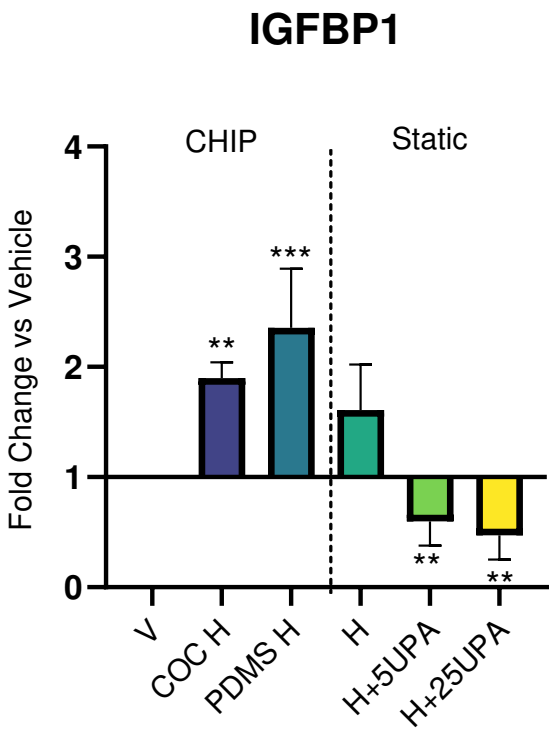

Figure 40: IGFBP1 protein secretion calculated in fold change versus the vehicle group. HUtMECs cultivated in COC and PDMS HUMIMIC chips and in static condition. Medium was sampled 72h after treatment with the vehicle control (V), the hormone cocktail (H), pre-treatment with two different UPA concentrations (5µM, 25µM) following the addition of the hormone cocktail. 3D models construct with THESCs and EM42 cells, a dose dependent effect of the UPA could be observed. Significativity was calculated using Tukey's multiple comparison test.

CONCLUSION & FUTURE PERSPECTIVES

The concept of the Three Rs (*replacement*, *reduction* and *refinement*) in animal experimentation was first introduced many years ago (Russell, WMS; Burch, RL, 1959) and, since then, many technologies have been developed and introduced in order to replace animal models. In the last few decades, considerable advances have been made in human-derived and human-relevant models that mimic human physiology and drug disposition mechanisms (Vangala, Saxena and Satish Chandran, 2022) for example, 3D disease models that can improve the translation of preclinical data from *in vitro* studies to *in vivo* clinical trials. As summarized by Vangala et al., since the 1980s, there have been significant improvements in the application of the Three Rs principles, in the clinical relevance of the alternative models used and in ethical compliance. In addition, there is a global movement toward the adoption of the Three Rs principles in national and international policy and regulations for different stages of drug discovery (Lilley *et al.*, 2021). In the USA, the *FDA Modernization Act* of 2021 ('US Congress. H.R.2565: FDA Modernization Act of 2021', 2021), which allows and encourages the use of "alternative testing methods to animal testing" was also introduced, in order to refine and reduce the use of animals for testing purposes. Finally, on 29 September 2022, the US Senate unanimously passed the updated *FDA Modernization Act 2.0*, this bill permits drug developers to use non-animal methods alongside animal models to test toxicity when feasible.

Successful embryo implantation is an essential requirement for reproduction of mammalian species. In humans, implantation involves complex interactions between the embryo and the maternal endometrium, all of which must be performed within an optimal time frame. Three factors are critical for successful implantation: the embryo's development into an implantation-competent blastocyst, the synchronized transformation of the uterus into a receptive stage and bidirectional cross talk among them. The current study describes the development of a long-term non-invasive and stable organoids culture method using menstrual blood and compares it to biopsy-derived organoids. Endometrial organoids are considered an important tool for the study of female reproductive biology. Their deep characterization is important to address hypothesis and produce meaningful data. Organoids have been found to resemble the tissue epithelium, including glandular-type architecture, as well as functional behavior such as responsiveness to main regulatory hormones (Boretto *et al.*, 2017; Turco, Gardner, Hughes, Cindrova-Davies, Gomez, Farrell, Hollinshead, Marsh, Brosens, Critchley, Benjamin D. Simons, *et al.*, 2017). Furthermore, the establishment of such 3D culture models provides us with a useful tool for investigating glycodelin

A expression in organoids following hormone cocktail activation(Focarelli *et al.*, 2018; Luddi, Pavone, *et al.*, 2020). This is a critical aspect that could be explained by glycodelin A's immunomodulatory and immunosuppressive properties, which are elevated throughout the implantation process. In conclusion, we describe a method for reliable and non -invasive culture of endometrial organoids that closely recapitulates the molecular and functional characteristics of their cells of origin, as well as ultrastructure characteristics like pinopods. Organoids provide powerful tools for mimicking and examining endometrial tissue development, regulation, and disease, with the presence of the mesenchymal compartment of the tissue. Organoids can contribute to a deeper understanding of endometrial diseases, offering insights into their molecular and cellular mechanisms. This knowledge may pave the way for the development of targeted therapies and personalized medicine approaches for conditions affecting the endometrium.

The second part of this thesis was focused on the set-up of a donor-independent human endometrium 3D model in dynamic conditions using a HUMIMIC-Chip2 based technology to mimic the endometrium´s secretory phase. The use of immortalized cells eliminates the bias of donor dependent features (although less useful for regenerative and precision medicine) and can be a promising tool for pharmacological and toxicology application studies. The endometrial stromal cell line THESC, was used as a basis for the model. To improve the functionality and physiology of the model, it further contained the endometrial epithelial cell line EM42, and both cell types were cultured together in the established 3D endometrial model. Best results for the 3D model were achieved embedding THESCs into a collagen I matrix was found to be the best condition and EM42 cells were seeded onto those drop-like constructs forming an in vivo-like epithelial layer around the stromal-cell populated collagen gel. Uterine endothelial cells (HUtMECs) colonizing the channels of the HUMIMIC Chip2 were therefore also included in the model and co-cultured with the 3D endometrial model. Co-culture was successfully established and an effect of the hormone treatment on all three cell types could be observed. Moreover, a dose-dependent antagonistic effect of ulipristal acetate (UPA) could be seen. Looking at the secretion of the decidualization protein IGFBP1, a dose-dependent effect of the UPA could be observed and the standard condition (5µM) showed a comparable reduction on the protein secretion. ZBTB16, a PGR (progesterone receptor) transcription factor, was upregulated upon hormone treatment and dose-dependent downregulation when pre-treated with UPA was observed for all culture conditions.

In conclusion these *in vitro* models of endometrial tissue, whether in static or dynamic conditions hold promise for future enhancements and are fundamental for the study of multiple diseases. The

addition of key cell types, specifically those associated with immune system, may be crucial to fully mimic the implantation window. This approach has the potential to deepen our understanding of the intricate interactions at the implantation site, leading to more accurate simulation of endometrial dynamics and providing valuable insights into reproductive health and related conditions. In the future the integration of single-cell RNA sequencing (scRNA-seq) technology into the exploration of cellular dynamics within complex biological systems promises transformative insights into various fields, including endometrium biology. Looking ahead, leveraging scRNA-seq to analyze the transcriptional profiles of cellular components across different stages and conditions offers a compelling avenue for uncovering the nuanced heterogeneity within endometrial tissues, provides a high-resolution molecular and cellular characterization of human endometrial transformation across the menstrual cycle, providing insights into this essential physiological process (Wang *et al*., 2020). One promising future perspective is the elucidation of distinct cellular subpopulations within the endometrium, each potentially exhibiting unique susceptibilities to pharmacological interventions. By discerning these subpopulations and their transcriptional signatures, researchers can tailor pharmacological treatments with greater precision, potentially leading to more effective therapeutic strategies for endometrial disorders such as endometriosis or infertility. Moreover, the identification of transdifferentiation events between different cellular populations represents another intriguing frontier in endometrium biology. Understanding the molecular mechanisms underlying such transitions could provide invaluable insights into tissue regeneration, repair processes, and pathological conditions within the endometrium. As scRNA-seq methodologies continue to evolve and become more accessible, the future holds great promise for refining our understanding of endometrial biology at a cellular level. This deeper understanding not only enhances our knowledge of normal endometrial physiology but also holds significant implications for the development of novel diagnostic tools and targeted therapeutic interventions. Furthermore, the appropriateness of utilizing scRNA-seq in endometrial research extends beyond its immediate applications. By establishing robust cellular models and characterizing their transcriptional profiles across various physiological and pathological states, this approach lays the groundwork for a broad spectrum of future investigations. These may include the elucidation of intricate signaling pathways, the identification of novel therapeutic targets, and the development of innovative regenerative medicine strategies for treating endometrial-related disorders.

In summary, the integration of scRNA-seq into the study of endometrium biology holds immense promise for unraveling the complexities of cellular heterogeneity, pharmacological susceptibilities, and transdifferentiation events within this critical tissue. By embracing this cutting-edge technology, researchers can pave the way for a deeper understanding of endometrial physiology and the development of more precise and effective therapeutic interventions.

BIBLIOGRAPHY

Achache, H. and Revel, A. (2006) 'Endometrial receptivity markers, the journey to successful embryo implantation', *Human Reproduction Update*, 12(6), pp. 731–746. Available at: https://doi.org/10.1093/humupd/dml004.

Acosta, A.A. *et al.* (2000) 'Endometrial dating and determination of the window of implantation in healthy fertile women', *Fertility and Sterility*, 73(4), pp. 788–798. Available at: https://doi.org/10.1016/S0015-0282(99)00605-6.

Ahn, J. *et al.* (2021) 'Three-dimensional microengineered vascularised endometrium-on-a-chip', *Human Reproduction*, 36(10), pp. 2720–2731. Available at: https://doi.org/10.1093/humrep/deab186.

Aplin, J.D. (2000) 'The cell biological basis of human implantation', *Best Practice & Research Clinical Obstetrics & Gynaecology*, 14(5), pp. 757–764. Available at: https://doi.org/10.1053/beog.2000.0116.

Aplin, J.D., Charlton, A.K. and Ayad, S. (1988) 'An immunohistochemical study of human endometrial extracellular matrix during the menstrual cycle and first trimester of pregnancy', *Cell and Tissue Research*, 253(1). Available at: https://doi.org/10.1007/BF00221758.

Aplin, J.D. and Ruane, P.T. (2017) 'Embryo–epithelium interactions during implantation at a glance', *Journal of Cell Science*. Edited by A. Ewald, 130(1), pp. 15–22. Available at: https://doi.org/10.1242/jcs.175943.

Apparao, K.B.C. *et al.* (2002) 'Elevated Endometrial Androgen Receptor Expression in Women with Polycystic Ovarian Syndrome1', *Biology of Reproduction*, 66(2), pp. 297–304. Available at: https://doi.org/10.1095/biolreprod66.2.297.

Arnold, J.T. *et al.* (2001) 'Endometrial stromal cells regulate epithelial cell growth in vitro: a new co-culture model', *Human Reproduction*, 16(5), pp. 836–845. Available at: https://doi.org/10.1093/humrep/16.5.836.

Arnold, J.T. *et al.* (2002) 'Effect of normal endometrial stroma on growth and differentiation in Ishikawa endometrial adenocarcinoma cells', *Cancer Research*, 62(1), pp. 79–88.

Bali, U. *et al.* (2016) 'FKBP5 mRNA Expression Is a Biomarker for GR Antagonism', *The Journal of Clinical Endocrinology & Metabolism*, 101(11), pp. 4305–4312. Available at: https://doi.org/10.1210/jc.2016-1624.

Bell, S.C. *et al.* (1991) 'Regulation of Insulin-Like Growth Factor-Binding Protein-1 Synthesis and Secretion by Progestin and Relaxin in Long Term Cultures of Human Endometrial Stromal Cells*', *The Journal of Clinical Endocrinology & Metabolism*, 72(5), pp. 1014–1024. Available at: https://doi.org/10.1210/jcem-72-5-1014.

Boretto, M. *et al.* (2017) 'Development of organoids from mouse and human endometrium showing endometrial epithelium physiology and long-term expandability', *Development*, p. dev.148478. Available at: https://doi.org/10.1242/dev.148478.

Cabral-Pacheco, G.A. *et al.* (2020) 'The Roles of Matrix Metalloproteinases and Their Inhibitors in Human Diseases', *International Journal of Molecular Sciences*, 21(24), p. 9739. Available at: https://doi.org/10.3390/ijms21249739.

Cakmak, H. and Taylor, H.S. (2011) 'Implantation failure: molecular mechanisms and clinical treatment', *Human Reproduction Update*, 17(2), pp. 242–253. Available at: https://doi.org/10.1093/humupd/dmq037.

Campo, H. *et al.* (2020) 'Microphysiological Modeling of the Human Endometrium', *Tissue Engineering Part A*, 26(13–14), pp. 759–768. Available at: https://doi.org/10.1089/ten.tea.2020.0022.

Cindrova-Davies, T. *et al.* (2021) 'Menstrual flow as a non-invasive source of endometrial organoids', *Communications Biology*, 4(1), p. 651. Available at: https://doi.org/10.1038/s42003-021-02194-y.

Classen-Linke, I. *et al.* (1996a) 'Establishment of a human endometrial cell culture system and characterization of its polarized hormone responsive epithelial cells', *Cell and Tissue Research*, 287(1), pp. 171–185. Available at: https://doi.org/10.1007/s004410050743.

Classen-Linke, I. *et al.* (1996b) 'Establishment of a human endometrial cell culture system and characterization of its polarized hormone responsive epithelial cells', *Cell and Tissue Research*, 287(1), pp. 171–185. Available at: https://doi.org/10.1007/s004410050743.

Critchley, H.O.D. *et al.* (2020) 'Physiology of the Endometrium and Regulation of Menstruation', *Physiological Reviews*, 100(3), pp. 1149–1179. Available at: https://doi.org/10.1152/physrev.00031.2019.

Cui, Y. *et al.* (2020) 'Human Female Reproductive System Organoids: Applications in Developmental Biology, Disease Modelling, and Drug Discovery', *Stem Cell Reviews and Reports*, 16(6), pp. 1173–1184. Available at: https://doi.org/10.1007/s12015-020-10039-0.

De Los Santos, M.J. *et al.* (2003) 'Implantation Rates after Two, Three, or Five Days of Embryo Culture', *Placenta*, 24, pp. S13–S19. Available at: https://doi.org/10.1016/S0143-4004(03)00172-3.

Deryabin, P. *et al.* (2020) 'The link between endometrial stromal cell senescence and decidualization in female fertility: the art of balance', *Cellular and Molecular Life Sciences*, 77(7), pp. 1357–1370. Available at: https://doi.org/10.1007/s00018-019-03374-0.

Desai, N.N. *et al.* (1994) 'Novel human endometrial cell line promotes blastocyst development', *Fertility and Sterility*, 61(4), pp. 760–766.

Díaz-Gimeno, P. *et al.* (2011) 'A genomic diagnostic tool for human endometrial receptivity based on the transcriptomic signature', *Fertility and Sterility*, 95(1), pp. 50-60.e15. Available at: https://doi.org/10.1016/j.fertnstert.2010.04.063.

Dunn, C.L., Kelly, R.W. and Critchley, H.O. (2003) 'Decidualization of the human endometrial stromal cell: an enigmatic transformation', *Reproductive BioMedicine Online*, 7(2), pp. 151–161. Available at: https://doi.org/10.1016/S1472-6483(10)61745-2.

Eremichev, R. *et al.* (2021) 'Scar-Free Healing of Endometrium: Tissue-Specific Program of Stromal Cells and Its Induction by Soluble Factors Produced After Damage', *Frontiers in Cell and Developmental Biology*, 9, p. 616893. Available at: https://doi.org/10.3389/fcell.2021.616893.

Evans, J. *et al.* (2016) 'Fertile ground: human endometrial programming and lessons in health and disease', *Nature Reviews Endocrinology*, 12(11), pp. 654–667. Available at: https://doi.org/10.1038/nrendo.2016.116.

Finn, C.A. and Martin, L. (1974) 'THE CONTROL OF IMPLANTATION', *Reproduction*, 39(1), pp. 195–206. Available at: https://doi.org/10.1530/jrf.0.0390195.

Fitzgerald, H.C., Schust, D.J. and Spencer, T.E. (2021) 'In vitro models of the human endometrium: evolution and application for women's health+', *Biology of Reproduction*, 104(2), pp. 282–293. Available at: https://doi.org/10.1093/biolre/ioaa183.

Focarelli, R. *et al.* (2018) 'Dysregulation of GdA Expression in Endometrium of Women With Endometriosis: Implication for Endometrial Receptivity', *Reproductive Sciences*, 25(4), pp. 579–586. Available at: https://doi.org/10.1177/1933719117718276.

Gargett, C. and Rogers, P. (2001) 'Human endometrial angiogenesis', *Reproduction*, 121(2), pp. 181–186. Available at: https://doi.org/10.1530/rep.0.1210181.

Gargett, C.E. and Masuda, H. (2010) 'Adult stem cells in the endometrium', *Molecular Human Reproduction*, 16(11), pp. 818–834. Available at: https://doi.org/10.1093/molehr/gaq061.

Gill, S.E. and Parks, W.C. (2011) 'Matrix Metalloproteinases and Their Inhibitors in Turnover and Degradation of Extracellular Matrix', in W.C. Parks and R.P. Mecham (eds) *Extracellular Matrix Degradation*. Berlin, Heidelberg: Springer Berlin Heidelberg, pp. 1–22. Available at: https://doi.org/10.1007/978-3-642-16861-1_1.

Gnecco, J.S. *et al.* (2017) 'Compartmentalized Culture of Perivascular Stroma and Endothelial Cells in a Microfluidic Model of the Human Endometrium', *Annals of Biomedical Engineering*, 45(7), pp. 1758–1769. Available at: https://doi.org/10.1007/s10439-017-1797-5.

Governini, L. *et al.* (2021) 'Main actors behind the endometrial receptivity and successful implantation', *Tissue and Cell*, 73, p. 101656. Available at: https://doi.org/10.1016/j.tice.2021.101656.

Hannan, N.J. *et al.* (2010) 'Models for Study of Human Embryo Implantation: Choice of Cell Lines?1', *Biology of Reproduction*, 82(2), pp. 235–245. Available at: https://doi.org/10.1095/biolreprod.109.077800.

Helmestam, M. *et al.* (2014) 'Mifepristone-exposured human endometrial endothelial cells in vitro', *Reproductive Sciences (Thousand Oaks, Calif.)*, 21(3), pp. 408–414. Available at: https://doi.org/10.1177/1933719113497284.

Herrler, A., Von Rango, U. and Beier, H.M. (2003) 'Embryo-maternal signalling: how the embryo starts talking to its mother to accomplish implantation', *Reproductive BioMedicine Online*, 6(2), pp. 244–256. Available at: https://doi.org/10.1016/S1472-6483(10)61717-8.

Huang, X., Liu, H. and Li, R. (2017) 'Prostaglandin E $_2$ promotes BeWo spheroids implantation in RL95-2 cell monolayers', *Gynecological Endocrinology*, 33(7), pp. 548–552. Available at: https://doi.org/10.1080/09513590.2017.1296125.

Iruela-Arispe, M.L., Rodriguez-Manzaneque, J.C. and Abu-Jawdeh, G. (1999) 'Endometrial endothelial cells express estrogen and progesterone receptors and exhibit a tissue specific response to angiogenic growth factors', *Microcirculation (New York, N.Y.: 1994)*, 6(2), pp. 127–140.

Jabbour, H. and Critchley, H. (2001) 'Potential roles of decidual prolactin in early pregnancy', *Reproduction*, 121(2), pp. 197–205. Available at: https://doi.org/10.1530/rep.0.1210197.

Jensen, C. and Teng, Y. (2020) 'Is It Time to Start Transitioning From 2D to 3D Cell Culture?', *Frontiers in Molecular Biosciences*, 7, p. 33. Available at: https://doi.org/10.3389/fmolb.2020.00033.

Kane, N.M. *et al.* (2010) 'TGFβ1 Attenuates Expression of Prolactin and IGFBP-1 in Decidualized Endometrial Stromal Cells by Both SMAD-Dependent and SMAD-Independent Pathways', *PLoS ONE*. Edited by S.K. Dey, 5(9), p. e12970. Available at: https://doi.org/10.1371/journal.pone.0012970.

Kao, L.C. *et al.* (2002) 'Global Gene Profiling in Human Endometrium during the Window of Implantation', *Endocrinology*, 143(6), pp. 2119–2138. Available at: https://doi.org/10.1210/endo.143.6.8885.

Kirk, D. *et al.* (1978) 'Normal human endometrium in cell culture: I. Separation and characterization of epithelial and stromal components in vitro', *In Vitro*, 14(8), pp. 651–662. Available at: https://doi.org/10.1007/BF02616162.

Lalitkumar, P.G.L. *et al.* (2007) 'Mifepristone, but not levonorgestrel, inhibits human blastocyst attachment to an in vitro endometrial three-dimensional cell culture model', *Human Reproduction*, 22(11), pp. 3031–3037. Available at: https://doi.org/10.1093/humrep/dem297.

Ledee-Bataille, N. (2002) 'Concentration of leukaemia inhibitory factor (LIF) in uterine flushing fluid is highly predictive of embryo implantation', *Human Reproduction*, 17(1), pp. 213–218. Available at: https://doi.org/10.1093/humrep/17.1.213.

Lee, C. *et al.* (2016) 'The Pleiotropic Effect of Glycodelin-A in Early Pregnancy', *American Journal of Reproductive Immunology*, 75(3), pp. 290–297. Available at: https://doi.org/10.1111/aji.12471.

Lee, Y.-L. *et al.* (2015) 'Establishment of a novel human embryonic stem cell-derived trophoblastic spheroid implantation model', *Human Reproduction*, 30(11), pp. 2614–2626. Available at: https://doi.org/10.1093/humrep/dev223.

Li, Q. *et al.* (2011) 'The Antiproliferative Action of Progesterone in Uterine Epithelium Is Mediated by Hand2', *Science*, 331(6019), pp. 912–916. Available at: https://doi.org/10.1126/science.1197454.

Li, X. *et al.* (2022) 'Three-dimensional culture models of human endometrium for studying trophoblast-endometrium interaction during implantation', *Reproductive Biology and Endocrinology*, 20(1), p. 120. Available at: https://doi.org/10.1186/s12958-022-00973-8.

Lilley, E. *et al.* (2021) 'Integrating 3Rs approaches in WHO guidelines for the batch release testing of biologicals', *Biologicals*, 74, pp. 24–27. Available at: https://doi.org/10.1016/j.biologicals.2021.10.002.

Lindenberg, S., Nielsen, M.H. and Lenz, S. (1985) '*In Vitro* Studies of Human Blastocyst Implantation [a]', *Annals of the New York Academy of Sciences*, 442(1), pp. 368–374. Available at: https://doi.org/10.1111/j.1749-6632.1985.tb37541.x.

Liszczak, T.M. *et al.* (1977) 'Ultrastructure of human endometrial epithelium in monolayer culture with and without steroid hormones', *In Vitro*, 13(6), pp. 344–356. Available at: https://doi.org/10.1007/BF02615094.

Luddi, A. *et al.* (2018) 'Matrix metalloproteinases and their inhibitors in human cumulus and granulosa cells as biomarkers for oocyte quality estimation', *Fertility and Sterility*, 109(5), pp. 930-939.e3. Available at: https://doi.org/10.1016/j.fertnstert.2018.01.030.

Luddi, A., Marrocco, C., *et al.* (2020) 'Expression of Matrix Metalloproteinases and Their Inhibitors in Endometrium: High Levels in Endometriotic Lesions', *International Journal of Molecular Sciences*, 21(8), p. 2840. Available at: https://doi.org/10.3390/ijms21082840.

Luddi, A., Pavone, V., *et al.* (2020) 'Organoids of Human Endometrium: A Powerful In Vitro Model for the Endometrium-Embryo Cross-Talk at the Implantation Site', *Cells*, 9(5), p. 1121. Available at: https://doi.org/10.3390/cells9051121.

Lv, H. *et al.* (2022) 'Deciphering the endometrial niche of human thin endometrium at single-cell resolution', *Proceedings of the National Academy of Sciences*, 119(8), p. e2115912119. Available at: https://doi.org/10.1073/pnas.2115912119.

Macklon, N.S. and Brosens, J.J. (2014) 'The Human Endometrium as a Sensor of Embryo Quality1', *Biology of Reproduction*, 91(4). Available at: https://doi.org/10.1095/biolreprod.114.122846.

Majorova, D. *et al.* (2021) 'Use of Precision-Cut Tissue Slices as a Translational Model to Study Host-Pathogen Interaction', *Frontiers in Veterinary Science*, 8, p. 686088. Available at: https://doi.org/10.3389/fvets.2021.686088.

Makker, V. *et al.* (2021) 'Endometrial cancer', *Nature Reviews Disease Primers*, 7(1), p. 88. Available at: https://doi.org/10.1038/s41572-021-00324-8.

Mandalà, M. (2020) 'Influence of Estrogens on Uterine Vascular Adaptation in Normal and Preeclamptic Pregnancies', *International Journal of Molecular Sciences*, 21(7), p. 2592. Available at: https://doi.org/10.3390/ijms21072592.

Marx, U. *et al.* (2016) 'Biology-inspired microphysiological system approaches to solve the prediction dilemma of substance testing', *Altex*, 33(3), pp. 272–321. Available at: https://doi.org/10.14573/altex.1603161.

Marx, U. (2020) 'Biology-inspired microphysiological systems to advance medicines for patient benefit and animal welfare', *ALTEX* [Preprint]. Available at: https://doi.org/10.14573/altex.2001241.

Melkozerova, O.A. *et al.* (2019) 'Ultrastructural markers of tissue endometrial receptivity in patients with recurrent implantation failure', *Gynecological Endocrinology*, 35(sup1), pp. 45–48. Available at: https://doi.org/10.1080/09513590.2019.1653562.

Mihm, M., Gangooly, S. and Muttukrishna, S. (2011) 'The normal menstrual cycle in women', *Animal Reproduction Science*, 124(3–4), pp. 229–236. Available at: https://doi.org/10.1016/j.anireprosci.2010.08.030.

Muruganandan, S. *et al.* (2020) 'Development of A 3D Tissue Slice Culture Model for the Study of Human Endometrial Repair and Regeneration', *Biomolecules*, 10(1), p. 136. Available at: https://doi.org/10.3390/biom10010136.

Negami, A.I. and Tominaga, T. (1989) 'Gland and epithelium formation in vitro from epithelial cells of the human endometrium', *Human Reproduction*, 4(6), pp. 620–624. Available at: https://doi.org/10.1093/oxfordjournals.humrep.a136954.

Nikolakopoulou, K. and Turco, M.Y. (2021) 'Investigation of infertility using endometrial organoids', *Reproduction*, 161(5), pp. R113–R127. Available at: https://doi.org/10.1530/REP-20-0428.

Niswender, G.D. *et al.* (2000) 'Mechanisms Controlling the Function and Life Span of the Corpus Luteum', *Physiological Reviews*, 80(1), pp. 1–29. Available at: https://doi.org/10.1152/physrev.2000.80.1.1.

Norwitz, E.R., Schust, D.J. and Fisher, S.J. (2001) 'Implantation and the Survival of Early Pregnancy', *New England Journal of Medicine*, 345(19), pp. 1400–1408. Available at: https://doi.org/10.1056/NEJMra000763.

Noyes, R.W., Hertig, A.T. and Rock, J. (2019) 'Reprint of: Dating the Endometrial Biopsy', *Fertility and Sterility*, 112(4), pp. e93–e115. Available at: https://doi.org/10.1016/j.fertnstert.2019.08.079.

Osteen, K.G. *et al.* (1989) 'Development of a method to isolate and culture highly purified populations of stromal and epithelial cells from human endometrial biopsy specimens', *Fertility and Sterility*, 52(6), pp. 965–972. Available at: https://doi.org/10.1016/S0015-0282(16)53160-4.

Papp, C. *et al.* (2000) 'Biological mechanisms underlying the clinical effects of mifepristone (RU 486) on the endometrium', *Early Pregnancy*, 4(4), pp. 230–239.

Park, S.-R. *et al.* (2021) 'Development of a novel dual reproductive organ on a chip: recapitulating bidirectional endocrine crosstalk between the uterine endometrium and the ovary', *Biofabrication*, 13(1), p. 015001. Available at: https://doi.org/10.1088/1758-5090/abbd29.

Parks, W.C. (2006) 'MATRIX METALLOPROTEINASES', in *Encyclopedia of Respiratory Medicine*. Elsevier, pp. 18–25. Available at: https://doi.org/10.1016/B0-12-370879-6/00234-9.

Ponandai-Srinivasan, S. *et al.* (2019) 'Mifepristone mediates anti-proliferative effect on ovarian mesenchymal stem/stromal cells from female *BRCA* $^{1-/2-}$ carriers', *Acta Obstetricia et Gynecologica Scandinavica*, 98(2), pp. 250–261. Available at: https://doi.org/10.1111/aogs.13485.

Psychoyos, A. (1974) 'Hormonal Control of Ovoimplantation', in *Vitamins & Hormones*. Elsevier, pp. 201–256. Available at: https://doi.org/10.1016/S0083-6729(08)60999-1.

Rawlings, T.M. *et al.* (2021) 'Modelling the impact of decidual senescence on embryo implantation in human endometrial assembloids', *eLife*, 10, p. e69603. Available at: https://doi.org/10.7554/eLife.69603.

Rinehart, C.A., Lyn-Cook, B.D. and Kaufman, D.G. (1988) 'Gland formation from human endometrial epithelial cells in vitro', *In Vitro Cellular & Developmental Biology*, 24(10), pp. 1037–1041. Available at: https://doi.org/10.1007/BF02620878.

Rock, J. (1937) 'BIOPSY STUDIES OF HUMAN ENDOMETRIUM: CRITERIA OF DATING AND INFORMATION ABOUT AMENORRHEA, MENORRHAGIA AND TIME OF OVULATION', *Journal of the American Medical Association*, 108(24), p. 2022. Available at: https://doi.org/10.1001/jama.1937.02780240014006.

Rosenfield, R.L. and Ehrmann, D.A. (2016) 'The Pathogenesis of Polycystic Ovary Syndrome (PCOS): The Hypothesis of PCOS as Functional Ovarian Hyperandrogenism Revisited', *Endocrine Reviews*, 37(5), pp. 467–520. Available at: https://doi.org/10.1210/er.2015-1104.

Rosner, M. *et al.* (2021) 'Human Embryo Models and Drug Discovery', *International Journal of Molecular Sciences*, 22(2), p. 637. Available at: https://doi.org/10.3390/ijms22020637.

Rossi, G., Manfrin, A. and Lutolf, M.P. (2018) 'Progress and potential in organoid research', *Nature Reviews Genetics*, 19(11), pp. 671–687. Available at: https://doi.org/10.1038/s41576-018-0051-9.

Russell, WMS; Burch, RL (1959) *The principles of humane experimental technique*. Methuen.

Schatz, F. *et al.* (1990) 'Culture of human endometrial cells under polarizing conditions', *Differentiation*, 42(3), pp. 184–190. Available at: https://doi.org/10.1111/j.1432-0436.1990.tb00760.x.

Schimek, K. *et al.* (2013a) 'Integrating biological vasculature into a multi-organ-chip microsystem', *Lab on a Chip*, 13(18), p. 3588. Available at: https://doi.org/10.1039/c3lc50217a.

Schimek, K. *et al.* (2013b) 'Integrating biological vasculature into a multi-organ-chip microsystem', *Lab on a Chip*, 13(18), p. 3588. Available at: https://doi.org/10.1039/c3lc50217a.

Seppälä, M. *et al.* (2002) 'Glycodelin: A Major Lipocalin Protein of the Reproductive Axis with Diverse Actions in Cell Recognition and Differentiation', *Endocrine Reviews*, 23(4), pp. 401–430. Available at: https://doi.org/10.1210/er.2001-0026.

Spencer, T.E. *et al.* (2005) 'Comparative Developmental Biology of the Mammalian Uterus', in *Current Topics in Developmental Biology*. Elsevier, pp. 85–122. Available at: https://doi.org/10.1016/S0070-2153(05)68004-0.

Stern-Tal, D. *et al.* (2020) 'Novel 3D embryo implantation model within macroporous alginate scaffolds', *Journal of Biological Engineering*, 14(1), p. 18. Available at: https://doi.org/10.1186/s13036-020-00240-7.

Strowitzki, T. *et al.* (2006) 'The human endometrium as a fertility-determining factor', *Human Reproduction Update*, 12(5), pp. 617–630. Available at: https://doi.org/10.1093/humupd/dml033.

Talbi, S. *et al.* (2006) 'Molecular Phenotyping of Human Endometrium Distinguishes Menstrual Cycle Phases and Underlying Biological Processes in Normo-Ovulatory Women', *Endocrinology*, 147(3), pp. 1097–1121. Available at: https://doi.org/10.1210/en.2005-1076.

Teklenburg, G. *et al.* (2010) 'Natural Selection of Human Embryos: Decidualizing Endometrial Stromal Cells Serve as Sensors of Embryo Quality upon Implantation', *PLoS ONE*. Edited by V.J. Vitzthum, 5(4), p. e10258. Available at: https://doi.org/10.1371/journal.pone.0010258.

Timeva, T., Shterev, A. and Kyurkchiev, S. (2014) 'Recurrent implantation failure: the role of the endometrium', *Journal of Reproduction & Infertility*, 15(4), pp. 173–183.

Turco, M.Y., Gardner, L., Hughes, J., Cindrova-Davies, T., Gomez, M.J., Farrell, L., Hollinshead, M., Marsh, S.G.E., Brosens, J.J., Critchley, H.O., Simons, Benjamin D., *et al.* (2017) 'Long-term, hormone-responsive organoid cultures of human endometrium in a chemically defined medium', *Nature Cell Biology*, 19(5), pp. 568–577. Available at: https://doi.org/10.1038/ncb3516.

Turco, M.Y., Gardner, L., Hughes, J., Cindrova-Davies, T., Gomez, M.J., Farrell, L., Hollinshead, M., Marsh, S.G.E., Brosens, J.J., Critchley, H.O., Simons, Benjamin D., *et al.* (2017) 'Long-term, hormone-responsive organoid

cultures of human endometrium in a chemically defined medium', *Nature Cell Biology*, 19(5), pp. 568–577. Available at: https://doi.org/10.1038/ncb3516.

'US Congress. H.R.2565: FDA Modernization Act of 2021' (2021).

Vangala, S., Saxena, U. and Satish Chandran, C. (2022) 'Building Human In Vitro 3D Models to Replace Animal Studies During Drug Discovery Research: Scientific, Ethical and Regulatory Considerations', in P.V. Mohanan (ed.) *Microfluidics and Multi Organs on Chip*. Singapore: Springer Nature Singapore, pp. 695–717. Available at: https://doi.org/10.1007/978-981-19-1379-2_29.

Varma, V.A. *et al.* (1982) 'Monolayer culture of human endometrium: Methods of culture and identification of cell types', *In Vitro*, 18(11), pp. 911–918. Available at: https://doi.org/10.1007/BF02796347.

Vinketova, K., Mourdjeva, M. and Oreshkova, T. (2016) 'Human Decidual Stromal Cells as a Component of the Implantation Niche and a Modulator of Maternal Immunity', *Journal of Pregnancy*, 2016, pp. 1–17. Available at: https://doi.org/10.1155/2016/8689436.

Wang, H. *et al.* (2012) 'A novel model of human implantation: 3D endometrium-like culture system to study attachment of human trophoblast (Jar) cell spheroids', *Molecular Human Reproduction*, 18(1), pp. 33–43. Available at: https://doi.org/10.1093/molehr/gar064.

Wang, W. *et al.* (2020) 'Single-cell transcriptomic atlas of the human endometrium during the menstrual cycle', *Nature Medicine*, 26(10), pp. 1644–1653. Available at: https://doi.org/10.1038/s41591-020-1040-z.

Weimar, C.H.E. *et al.* (2013) 'In-vitro model systems for the study of human embryo–endometrium interactions', *Reproductive BioMedicine Online*, 27(5), pp. 461–476. Available at: https://doi.org/10.1016/j.rbmo.2013.08.002.

White, T.E.K., Sant'agnese, P.A. and Miller, R.K. (1990) 'Human endometrial cells grown on an extracellular matrix form simple columnar epithelia and glands', *In Vitro Cellular & Developmental Biology*, 26(6), pp. 636–642. Available at: https://doi.org/10.1007/BF02624214.

Xiao, S. *et al.* (2017) 'A microfluidic culture model of the human reproductive tract and 28-day menstrual cycle', *Nature Communications*, 8(1), p. 14584. Available at: https://doi.org/10.1038/ncomms14584.

Yanaihara, A. *et al.* (2005) 'Differences in gene expression in the proliferative human endometrium', *Fertility and Sterility*, 83(4), pp. 1206–1215. Available at: https://doi.org/10.1016/j.fertnstert.2004.11.032.

Zhang, Y. *et al.* (2023) *Human receptive endometrial organoid for deciphering the implantation window*. preprint. Cell Biology. Available at: https://doi.org/10.1101/2023.07.27.550771.